

République Algérienne Démocratique et Populaire

Ministère de l'Enseignement Supérieur et de la Recherche Scientifique

Université Hassiba Benbouali de Chlef

Faculté des Sciences Exactes & Informatique



THESE DE DOCTORAT EN SCIENCES

Spécialité: Physique

Option: Physique des matériaux

Présentée par: **Noureddine BOUTELDJA**

Intitulée

Etude ab-initio des propriétés électroniques et magnétiques de GaX dopé par Mn (X=N, P et As) dans le cadre de la spintronique

Soutenue le **05/06/2024**

Devant le jury composé de:

Abdelaali BOUDJEMAA

Mohamed BELABBAS

Habib RACHED

Ahmed BOUHEKKA

Sofiane HAIRECHE

Youcef GHERMIT

Rachid TALEB

Professeur/ Univ-Chlef

Professeur/ Univ-Chlef

Professeur/ Univ-Chlef

Professeur/ Univ-Tessemsilt

MCA/Univ-Médéa

MCA/Univ-Relizane

Professeur /Univ-Chlef

Président

Encadreur

Examineur

Examineur

Examineur

Examineur

Invité

Année Universitaire: 2023-2024

ACKNOWLEDGEMENTS

The research endeavors delineated within this thesis were conducted at the Laboratory for Theoretical Physics and Materials Physics (LTPM), Faculty of exact sciences and informatics, Hassiba Benbouali of Chlef University, under the esteemed tutelage of Professor **Mohammed HADJ MELIANI**. I am deeply indebted to him for his invaluable guidance and unwavering support throughout this endeavor.

My heartfelt appreciation is extended to Professor (**رحمة الله عليه**) **Abdelkader ALI BENAMARA** for offering me this exceptional dissertation topic and affording me the opportunity to pursue this endeavor. Despite his struggle with illness, he continued to supervise my thesis, albeit remotely, until his eventual passing. I am deeply indebted to him, more so than words can convey and I offer my profound gratitude for his guidance in shaping the direction of my research. Thank you sincerely for your kindness and accessibility. Your advice has been, and will always remain, invaluable.

I extend my profound gratitude and sincere appreciation to Professor **Mohamed BELABBAS** at Chlef University, for graciously agreeing to serve as the supervisor for this thesis. His willingness to undertake this responsibility is deeply appreciated. Our collaboration has been profoundly rewarding, offering new perspectives and enhancing the quality of my research. I am grateful for his ongoing support, thoughtful discussions and willingness to grapple with the complexities of my work. I am deeply thankful for his dedication and guidance throughout this journey.

I would like to express my sincere gratitude to Professor **Abdelaali BOUDJEMAA** at Chlef University, who graciously accepted the invitation to preside over the jury for this thesis.

I extend my sincere gratitude to Professor **Habib RACHED** at Chlef University, for graciously agreeing to serve as a member of the jury for my thesis. I am appreciative of his consistent hospitality in welcoming me to his office on numerous occasions, his assistance in installing the simulation tool on the computer and his valuable and stimulating scientific contributions and perspectives. All interactions were highly constructive and greatly appreciated.

I express my sincere gratitude to Mr. **Ahmed BOUHEKKA**, Professor at the Tissemsilet University, for his participation in the jury of my thesis. I am thankful for his constructive feedback and valuable assistance throughout the evaluation process. His contributions have been greatly appreciated.

I would like to take advantage of these few lines to warmly thank to **Sofiane HAIRECHE**, Lecturer at the Medea University, and **Youcef GUERMIT**, Lecturer at the Relizane University, to serve as members of my thesis jury. Their willingness to participate is deeply appreciated.

I would also like to take this opportunity to express my heartfelt appreciation to Professor **Rachid TALEB** at Chlef University, for his invaluable guidance, effective assistance and exchange of opinions on knowledge and scientific insights. Our discussions have been immensely beneficial, and I am grateful for his consensus in viewpoints. I thank him for accepting to serve as an invited member of my jury to discuss the thesis.

I express my profound gratitude to my colleagues from the Theoretical Physics and Materials Physics Laboratory for fostering an enriching atmosphere within the laboratory and for engaging in interesting discussions. Their support and availability have been invaluable throughout this journey. Additionally, I extend my sincere thanks to everyone who contributed directly or indirectly to the completion of this thesis.

Finally, a big thank you to my parents for their constant encouragement and support during my studies, and to my wife, children, brothers and sisters who spared no time or energy to help me. Your unwavering support means everything to me.

Thank you all again.....

Table of Contents

| | |
|----------------------------|------|
| Table of Contents | i |
| Summary | v |
| List of Figures | vi |
| List of Tables | viii |
| Abbreviations List | xi |
| General Introduction | 1 |
| References | 5 |

Chapter I: Spintronics Semiconductors

| | |
|--|----|
| I.1. Introduction | 7 |
| I.2. Spintronics: Definition and Characteristics | 7 |
| I.2.1. Spin Injection and Detection | 8 |
| I.2.2. Spin-Dependent Transport | 8 |
| I.2.3. Spin-Orbit Coupling | 9 |
| I.2.4. Spin Lifetime and Relaxation | 9 |
| I.3. Spintronics: Technologies and Devices | 9 |
| I.3.1. Giant Magnetoresistance (GMR) | 10 |
| I.3.2. Tunnel Magnetoresistance (TMR) | 10 |
| I.3.3. Magnetoresistive Random Access Memory (MRAM)..... | 10 |
| I.3.4. Spin Transfer Torque (STT) Devices | 11 |
| I.3.5. Spin Hall Effect (SHE) | 12 |
| I.3.6. Spin-FET (Spin Field-Effect Transistor)..... | 12 |
| I.3.7. Spin Wave Devices | 13 |
| I.3.8. Skyrmion-Based Devices | 13 |
| I.4. Magnetism: Types and Materials | 13 |
| I.4.1. Ferromagnetism | 14 |
| I.4.2. Antiferromagnetism | 14 |
| I.4.3. Ferrimagnetism | 14 |
| I.4.4. Paramagnetism | 15 |

Table of Contents

| | |
|--|----|
| I.4.5. Diamagnetism | 15 |
| I.4.6. Superparamagnetism | 15 |
| I.4.7. Magnetic Semiconductor Material | 16 |
| I.4.8. Hard Magnetic Material | 17 |
| I.4.9. Soft Magnetic Material | 17 |
| I.4.10 Ferrofluid Material | 17 |
| I.5. Magnetic Interaction | 17 |
| I.5.1. Heisenberg Exchange Interaction | 18 |
| I.5.2. RKKY Interaction (Ruderman-Kittel-Kasuya-Yosida)..... | 18 |
| I.5.3. Dzyaloshinsky-Moriya Interaction..... | 18 |
| I.5.4. Kondo Interaction | 19 |
| I.5.5. Anisotropic Magnetic Interaction | 19 |
| I.6. Diluted Magnetic Semiconductors III-V Based on GaX..... | 19 |
| I.6.1. Binary GaN Properties | 20 |
| I.6.2. Binary GaP Properties | 22 |
| I.6.3. Binary GaAs Properties | 25 |
| I.6.4. Types of Doping | 27 |
| I.6.5. Mn - Doped III-V Semiconductors..... | 28 |
| I.6.6. Crystallographic Characteristics of Mn..... | 29 |
| I.7. Conclusion | 30 |
| References | 31 |

Chapter II: Ab-initio Study

| | |
|---|----|
| II.1. Introduction | 34 |
| II.2. Ab-initio Theories | 34 |
| II.2.1. Hartree-Fock theory | 34 |
| II.2.1.1. Douglas Rayner Hartree Approach | 35 |
| II.2.1.2. Born-Oppenheimer Approximation | 36 |

Table of Contents

| | | |
|-------------|---|----|
| II.2.1.3. | Vladimir Aleksandrovich Fock Approach | 37 |
| II.2.1.4. | Combination of Hartree and Fock | 37 |
| II.2.1.4. | Development of Computational Techniques | 38 |
| II.2.1.5. | Expansion and Extensions | 42 |
| II.2.2. | Configuration Interaction Theory | 42 |
| II.2.3. | Coupled Cluster Theory | 43 |
| II.2.4. | Møller-Plesset Perturbation Theory | 44 |
| II.2.5. | Quasi-Degenerate Perturbation Theory | 45 |
| II.2.6. | Multi-Configurational Self-Consistent Field Theory | 46 |
| II.2.7. | Density Functional Theory | 47 |
| II.2.7.1. | Hohenberg-Kohn Theorem | 47 |
| II.2.7.2. | Kohn-Sham Formulation | 48 |
| II.2.7.3. | Exchange-Correlation Functional | 50 |
| II.2.7.3.1. | Local Density Approximation | 50 |
| II.2.7.3.2. | Generalized Gradient Approximation | 51 |
| II.2.7.3.3. | Hybrid Functionals | 52 |
| II.3. | Computational Method | 53 |
| II.3.1. | Full-Potential Linearized Augmented Plane Wave Method | 53 |
| II.3.1.1. | Introduction of Plane Waves | 53 |
| II.3.1.2. | Augmented Plane Wave | 54 |
| II.3.1.3. | Linear Augmented Plane Wave | 55 |
| II.3.1.4. | Full-Potential Approach | 56 |
| II.4. | Representative Code of Calculation | 57 |
| II.4.1. | Wien2k Code | 58 |
| II.5. | Conclusion | 61 |
| References | | 62 |

Chapter III: Results and Discussions

| | | |
|--------|--------------------------|----|
| III.1. | Introduction | 65 |
| III.2. | Calculation Details..... | 65 |

Table of Contents

| | |
|--|------------|
| III.3. Magnetic Configurations | 67 |
| III.4. Stable Crystal Structure of GaN, GaP and GaAs | 67 |
| III.5. Properties of GaN, GaP and GaAs | 68 |
| III.5.1. Structural Properties | 68 |
| III.5.2. Electronic Properties | 72 |
| III.6. Magnetic Supercell | 75 |
| III.7. Properties of $\text{Ga}_{1-x}\text{Mn}_x\text{N(P, As)}$ | 76 |
| III.7.1. Structural Properties | 76 |
| III.7.2. Electronic Properties..... | 82 |
| III.7.2.1. Band Structure..... | 82 |
| III.7.2.2. Density of States..... | 88 |
| III.7.3. Magnetic Properties..... | 93 |
| III.8. Effect of Exchange and Correlation Interactions..... | 94 |
| III.8.1. Lattice Parameter and Volume..... | 94 |
| III.8.2. Total Energy..... | 96 |
| III.8.3. Band Gap Energy..... | 97 |
| III.8.4. Magnetic Moment..... | 98 |
| III.8.5. Spin Polarized Band Structures..... | 98 |
| III.9. Conclusion..... | 103 |
| References..... | 104 |
| General Conclusion | 107 |

Abstract:

Dilute magnetic semiconductors (DMS) based on III-V compounds doped with manganese are highly promising for spintronic applications. The electronic and magnetic properties of Mn-doped III-V DMS, including $Ga_{1-x}Mn_xN$, $Ga_{1-x}Mn_xP$, and $Ga_{1-x}Mn_xAs$, are investigated using ab-initio simulation tools, specifically the Full-Potential Linear Augmented Plane Wave (FP-LAPW) method based on Density Functional Theory (DFT). The objective of this study is to analyze the magnetic properties of these alloys and compare them to determine which alloy holds potential for spintronic applications.

Keywords: Ab-initio, electronic, magnetic, doping, GaN/GaP/GaAs, Mn, spintronics.

Résumé:

Des semi-conducteurs magnétiques dilués (DMS) à base de III-V dopés par manganèse sont très intéressants pour les applications spintroniques. Les propriétés électroniques et magnétiques de DMS à base de III-V dopé par manganèse $Ga_{1-x}Mn_xN$, $Ga_{1-x}Mn_xP$ et $Ga_{1-x}Mn_xAs$ sont déterminées en utilisant un outil de simulation de type ab-initio (FP-LAPW) méthode des ondes planes augmentées et linéarisées à potentiel total basé sur la théorie de la densité fonctionnelle (DFT). L'objectif de ce travail est d'étudier les propriétés magnétiques de ces alliages pour déterminer lesquels présentent un intérêt dans les applications à la spintronique.

Mots clés: Ab-initio, électroniques, magnétiques, dopage, GaN/GaP/GaAs, Mn, spintronique.

المخلص:

تعتبر المواد شبه الموصلية المغناطيسية المخففة والمعززة بالمنغنيز (DMS) المستندة إلى III-V المشوبة بالمنغنيز مثيرة للاهتمام في مجال التطبيقات السبينترونية. تحدد الخصائص الإلكترونية والمغناطيسية لكل من $Ga_{1-x}Mn_xP$ ، $Ga_{1-x}Mn_xAs$ و $Ga_{1-x}Mn_xN$ باستخدام أداة محاكاة من نوع FP-LAPW وهي تقنية الموجات الكثيفة الموسعة والمنطقة بقاعدة الطاقة الكلية المستندة إلى نظرية الكثافة الوظيفية DFT. يهدف هذا العمل إلى دراسة الخصائص المغناطيسية لهذه السبائك ومن ثم إجراء مقارنة بين هذه الخصائص لتحديد أي من هذه السبائك يظهر اهتماماً لتطبيقات محتملة في مجال السبينترونيات. **الكلمات المفتاحية:** حسابات المبادئ الأولى، إلكترونية، مغناطيسية، شائبة، GaAs/GaP/GaN، Mn، السبينترونيك.

List of Figures

| | | |
|-------------------|--|-----------|
| Fig. I.1 | Intrinsic angular momentum and spin states..... | 5 |
| Fig. I.2 | Effects from spin-orbit coupling on electron..... | 7 |
| Fig. I.3 | Schematics of Magnetic Random Access Memory (MRAM)..... | 9 |
| Fig. I.4 | Illustration of current-induced torques..... | 10 |
| Fig. I.5 | Schematic of the skyrmion racetrack memory..... | 11 |
| Fig. I.6 | Magnetic varieties..... | 14 |
| Fig. I.7 | Symmetry-Breaking effects on magnetic interactions in crystals: RKKY and Dzyaloshinsky-Moriya interactions..... | 17 |
| | | |
| Fig. II.1 | Simplified algorithmic flowchart for the HF SCF (Hartree-Fock Self-Consistent Field) method..... | 39 |
| Fig. II.2 | Schematic representation of interstitial and muffin-tin regions in crystallographic structure..... | 52 |
| Fig. II.3 | Organization chart of programs in WIEN2k..... | 58 |
| | | |
| Fig. III.1 | Representation of magnetic configurations, (a) nm, (b) fm, (c) afmI, (d) afmII and (e) afmIII..... | 67 |
| Fig. III.2 | The unit cell of GaX (X = N, P, As) in the zinc blende structure..... | 68 |
| Fig. III.3 | Variation of the total energy as a function of volume calculated using the PBE method for different magnetic configurations..... | 69 |
| Fig. III.4 | Variation of the total energy as a function of volume calculated using the PBE+E method for different magnetic configurations..... | 70 |
| Fig. III.5 | Band structure and density of state of binary compound GaN calculated by the PBE+E ($\alpha=0.03$) method..... | 72 |
| Fig. III.6 | Band structure and density of state of binary compound GaP calculated by the PBE+E ($\alpha=0.04$) method..... | 73 |
| Fig. III.7 | Band structure and density of state of binary compound GaAs calculated by the PBE+E ($\alpha=0.05$) method..... | 73 |
| Fig. III.8 | Representation of the supercell with (a) 25%, (b) 50% and (c) 75% Mn substitution in GaX (X = As, N, P)..... | 76 |

List of Figures

| | | |
|--------------------|---|------------|
| Fig. III.9 | Variation of the total energy as a function of volume calculated using the PBE+E method of $Ga_{1-x}Mn_xN$ | 77 |
| Fig. III.10 | Variation of the total energy as a function of volume calculated using the PBE+E method of $Ga_{1-x}Mn_xP$ | 78 |
| Fig. III.11 | Variation of the total energy as a function of volume calculated using the PBE+E method of $Ga_{1-x}Mn_xAs$ | 79 |
| Fig. III.12 | Calculated spin polarized band structure of (a) $Ga_{0.75}Mn_{0.25}N$, (b) $Ga_{0.50}Mn_{0.50}N$ and (c) $Ga_{0.25}Mn_{0.75}N$ with the PBE + E ($\alpha=0.05$)..... | 83 |
| Fig. III.13 | Calculated spin polarized band structure of (a) $Ga_{0.75}Mn_{0.25}P$, (b) $Ga_{0.50}Mn_{0.50}P$ and (c) $Ga_{0.25}Mn_{0.75}P$ with the PBE + E ($\alpha=0.04$)..... | 84 |
| Fig. III.14 | Calculated spin polarized band structure of (a) $Ga_{0.75}Mn_{0.25}As$, (b) $Ga_{0.50}Mn_{0.50}As$ and (c) $Ga_{0.25}Mn_{0.75}As$ with the PBE + E ($\alpha=0.05$)..... | 85 |
| Fig. III.15 | Calculated spin polarized total and partial density of states of (a) $Ga_{0.75}Mn_{0.25}N$, (b) $Ga_{0.50}Mn_{0.50}N$ and (c) $Ga_{0.25}Mn_{0.75}N$ with the PBE + E ($\alpha=0.03$)..... | 89 |
| Fig. III.16 | Calculated spin polarized total and partial density of states of (a) $Ga_{0.75}Mn_{0.25}P$, (b) $Ga_{0.50}Mn_{0.50}P$ and (c) $Ga_{0.25}Mn_{0.75}P$ with the PBE + E ($\alpha=0.04$)..... | 90 |
| Fig. III.17 | Calculated spin polarized total and partial density of states of (a) $Ga_{0.75}Mn_{0.25}As$, (b) $Ga_{0.50}Mn_{0.50}As$ and (c) $Ga_{0.25}Mn_{0.75}As$ with the PBE + E ($\alpha=0.05$)..... | 91 |
| Fig. III.18 | Influence of exchange and correlation interactions on lattice parameter (LP) and volume (V) of (a) $Ga_{0.75}Mn_{0.25}P$, (b) $Ga_{0.75}Mn_{0.25}As$ and (c) $Ga_{0.50}Mn_{0.50}As$ | 95 |
| Fig. III.19 | Influence of exchange and correlation interactions on total energy (E_{Tot}) of (a) $Ga_{0.75}Mn_{0.25}P$, (b) $Ga_{0.75}Mn_{0.25}As$ and (c) $Ga_{0.50}Mn_{0.50}As$ | 96 |
| Fig. III.20 | Influence of exchange and correlation interactions on band gap energy (E_g) of (a) $Ga_{0.75}Mn_{0.25}P$, (b) $Ga_{0.75}Mn_{0.25}As$ and (c) $Ga_{0.50}Mn_{0.50}As$ | 97 |
| Fig. III.21 | : Influence of exchange and correlation interactions on magnetic moment μ_{Tot} , μ_{Mn} , μ_{Ga} and $\mu_{N/P/As}$ of (a) $Ga_{0.75}Mn_{0.25}P$, (b) $Ga_{0.75}Mn_{0.25}As$ and (c) $Ga_{0.50}Mn_{0.50}As$ | 99 |
| Fig. III.22 | Influence of exchange and correlation interactions on spin polarized band structures of (a) $Ga_{0.75}Mn_{0.25}P$, (b) $Ga_{0.75}Mn_{0.25}As$ and (c) $Ga_{0.50}Mn_{0.50}As$ | 100 |

List of Tables

| | | |
|-------------------|--|------------|
| Tab. I.1 | Various parameters of Wurtzite and Zinc Blende GaN structure..... | 18 |
| Tab. I.2 | Various parameters of Zinc Blende GaP structure..... | 21 |
| Tab. I.3 | Various parameters of Zinc Blende GaN structure..... | 23 |
| Tab. I.4 | Crystallographic characteristics of Mn..... | 27 |
| | | |
| Tab II.1 | Overview of ab-initio theories and computational methods in materials science..... | 56 |
| | | |
| Tab. III.1 | Electronic configurations and atomic spheres radii of Ga, Mn, N, P and As atoms..... | 66 |
| Tab. III.2 | Structural properties of GaN, GaP and GaAs with the PBE+E method..... | 71 |
| Tab. III.3 | Electronic properties of GaN, GaP and GaAs calculated with PBE+E method. | 75 |
| Tab. III.4 | Structural properties of Ga _{1-x} Mn _x N, Ga _{1-x} Mn _x P and Ga _{1-x} Mn _x As with PBE+E method..... | 81 |
| Tab. III.5 | Electronic properties of Ga _{1-x} Mn _x N, Ga _{1-x} Mn _x P and Ga _{1-x} Mn _x As with PBE+E method..... | 87 |
| Tab. III.6 | Magnetic properties of Ga _{1-x} Mn _x N, Ga _{1-x} Mn _x P and Ga _{1-x} Mn _x As with PBE+E method..... | 93 |
| Tab. III.7 | Structural, electronic and magnetic properties of Ga _{0.75} Mn _{0.25} P compound at different values of HF exchange parameter (α)..... | 101 |
| Tab. III.8 | Structural, electronic and magnetic properties of Ga _{0.75} Mn _{0.25} As compound at different values of HF exchange parameter (α)..... | 102 |
| Tab. III.9 | Structural, electronic and magnetic properties of Ga _{0.50} Mn _{0.50} As compound at different values of HF exchange parameter (α)..... | 102 |

Abbreviations List

DMS: Diluted Magnetic Semiconductors

MRAM: Magnetic Random Access Memory

TMR: Tunnel Magneto-Resistance

GMR: Giant Magneto-Resistance

IoT: Internet of Things

STT: Spin Transfer Torque

SHE: Spin Hall Effect

FET: Field-Effect Transistor

RKKY: Ruderman-Kittel-Kasuya-Yosida

GaN: Gallium Nitride

GaP: Gallium Phosphide

GaAs: Gallium Arsenide

RF: Radio Frequency

LED: Light-Emitting Diodes

BCC: Body-Centered Cubic

FCC: Face-Centered Cubic

HF: Hartree-Fock

Abbreviations List

DFT: Density Functional Theory

SCF: Self-Consistent Field

HOMO: Highest Occupied Molecular orbital

LUMO: Lowest Unoccupied Molecular Orbital

NBO: Natural Bond Orbital

UV: Ultra-Violet

CC: Coupled Cluster

CCSD: Coupled Cluster with Singles and Doubles

MP: Møller-Plesset Perturbation

QDPT: Quasi-Degenerate Perturbation Theory

MCSCF: Multi-Configurational Self-Consistent Field

LDA: Local Density Approximation

GGA: Generalized Gradient Approximation

PBE: Perdew, Burke and Ernzerhof

BLYP: Becke, Lee, Yang, and Parr

LAPW: Linearized Augmented Plane Wave

FP: Full-Potential

IR: Interstitial Region

MTA: Muffin-Tin Approximation

Abbreviations List

BZ: Brillouin Zone

TB: Tight-Binding

BSE: Bethe-Salpeter Equation

NEGF: Non-Equilibrium Green's Function

EHT: Extended Hueckel Theory

CAS: Complete Active Space

ELF: Electron Localization Function

LSDA: Local Spin Density Approximation

ZB: Zinc-Blende

NM: Non-Magnetic

FM: Ferro-Magnetic

AFM: Anti-Ferromagnetic

HM: Half-Metallic

CBM: Conduction Band Minimum

VBM: Valence Band Maximum

PDOS: Partial Density of States

LP: Lattice Parameter

Introduction

Dilute Magnetic Semiconductors (DMS) constitute a compelling arena within condensed-matter physics, where the fusion of semiconductor properties with magnetism unveils a rich tapestry of phenomena. Specifically, DMS materials, categorized as type III-V or II-VI semiconductors, undergo intentional doping with magnetic ions carrying 3d or 4f layers of transition metals or rare earths. This deliberate introduction of magnetic elements, even in minute concentrations, imparts ferromagnetic characteristics to the semiconductor, thereby creating a paradigm shift in materials science [1,2].

The genesis of Dilute Magnetic Semiconductors dates back to the late 1970s [3], with seminal work in introducing local magnetic moments into well understood semiconductors. Notably, the (III,Mn)V compounds, such as GaAs and InAs, have been at the forefront of this exploration. These materials exhibit ferromagnetic behavior when heavily doped with manganese (Mn), with ferromagnetic transition temperatures surpassing 100 K [4,5]. Such systems represent a subclass of ferromagnetic semiconductors, where the magnetic order originates from the coupling between local magnetic moments mediated by conduction-band electrons or valence-band holes [6].

Addressing the challenges inherent in DMS materials, researchers strive to achieve three critical objectives. First, the ferromagnetic transition temperature must exceed room temperature for practical applications [7]. Second, mobile charge carriers should exhibit a strong response to changes in the ordered magnetic state [8]. Third, DMS materials must retain fundamental semiconductor characteristics, remaining sensitive to doping, light, and electric fields induced by gate charges [9]. This triad of criteria sets the stage for the development of DMS materials suitable for spintronics applications.

In the vast landscape of spintronics, two standout phenomena, Giant Magneto Resistance (GMR) and Tunnel Magneto Resistance (TMR), have taken center stage [10]. The implications of these effects are already substantial, with Tunnel Magneto Resistance (TMR) serving as the foundation for reading hard disks and finding application in Magnetic Random Access Memories (MRAM) [11]. The significance of these studies has paved the way for a

new generation of electronic and optoelectronic components that seamlessly integrate memory functions.

Despite notable impacts, progress in this area has been constrained due to the challenge of efficiently injecting spins from metal into semiconductor, a difficulty arising from substantial differences in carrier densities between the two materials [12]. This hurdle presents formidable obstacles for research teams working on advancing DMS for practical applications.

The interplay between metals and semiconductors in spintronics represents a broader effort to harness DMS materials for technological innovation. The gradual progress in addressing carrier density differences underscores the complexity of this task [13-15]. Researchers in DMS development aim to overcome these challenges, envisioning a new class of electronic components seamlessly integrating memory functions. GaMnAs, a lightly doped semiconductor with magnetic ions like GaMn(N, P), is particularly intriguing, it can exist in the ground state at room temperature.

GaMn(N, P and As) materials have evolved into some of the most extensively employed semiconductors, drawing significant attention due to their potential for ushering in a new era of microelectronics device applications. The exploration of ferromagnetism in these materials has been a focal point of both experimental and theoretical research, with the anticipation that meeting specific criteria could unlock transformative possibilities in electronic and magnetic device technologies.

The practical utilization of GaMn(N, P and As) materials in microelectronics hinges on two critical criteria. Firstly, achieving a ferromagnetic transition temperature well above room temperature is imperative for device stability and functionality. Significant strides made over the last decade underscore the promising advances in meeting this temperature criterion [16]. Secondly, the responsiveness of mobile charge carriers within GaMn(N, P and As) materials to changes in the ordered magnetic state is crucial. This responsiveness lays the foundation for dynamic control of the magnetic state, unlocking advanced functionalities in microelectronics [17]. Additionally, the materials must retain fundamental semiconductor characteristics, ensuring sensitivity to doping, responsiveness to light, and susceptibility to electric fields

generated by gate charges. Preserving these semiconductor traits is essential for seamless integration into existing semiconductor technologies.

The study of GaMn(N, P and As) materials relies on Density-Functional Theory (DFT), a method known for its parameter-free approach. However, practical applications often involve approximations, particularly for the exchange-correlation energy. One common strategy is using onsite exact exchange for correlated electrons, based on microscopic calculations of electron-electron interactions [18]. This blend of theory and approximation helps us understand the electronic properties of GaMn(N, P and As) materials.

In the realm of DMS, the concept of exact exchange-correlation energy is crucial. This term combines exchange and correlation energies, reflecting electron-electron interactions [19,20]. Precise exact exchange-correlation energy calculations are vital for predicting the electronic and magnetic properties of DMS, providing insights into how exchanges and correlations shape the material's behavior. Delving into exact exchange-correlation energy in DMS is essential for advancing spintronic devices and uncovering the fundamental principles governing their magnetic properties [21].

The objective of this thesis is to examine the structural, electronic and magnetic properties, as well as the exchange mechanism associated with ferromagnetism in three systems: GaMnN, GaMnP and GaMnAs. A crucial aspect of our analysis involves the application of ab initio methods in simulation tools. The subsequent chapters offer a more detailed presentation of the theoretical findings related to the three systems, which will be the focus of the modeling presented in this thesis.

The structure of this manuscript is as follows.

The first chapter provides an overview of the most common applications of spintronics and the primary families of diluted magnetic semiconductors. Specifically, it delves into the theoretical and experimental examination of the diluted magnetic semiconductor based GaX (X= N, P and As), which is doped with transition metal (Mn).

In the second chapter, we delve into the theoretical tools employed in our study Full Potential Linearized Augmented Plane Wave (FP-LAPW) method. Our calculations are grounded in the

DFT combined with onsite exact exchange for correlated electrons treatment, which is instrumental in handling the interaction between exchange and correlations energy.

The third chapter presents the obtained results, along with a discussion of the structural, electronic, and magnetic properties of pure GaN, GaP and GaAs and the diluted magnetic semiconductors $\text{Ga}_{1-x}\text{Mn}_x\text{N(P/As)}$, considering different concentrations of Mn atoms, with varying the exchange portion (α).

Finally, we conclude our thesis with a general summary of our findings and discuss the broader implications and future directions of our research. This concluding section provides insights into the significance of our study and outlines potential avenues for further exploration in the field of diluted magnetic semiconductors and spintronics.

References

- [1] K. Burch, D. Basov. "Optical properties of III-Mn-V ferromagnetic semiconductors". *Journal of Magnetism and Magnetic Materials*. 320.23, 3207-3228, (2008).
- [2] H. Munekata, H. Ohno, S. V. Molnar, A. Segmüller, L. L. Chang, L. Esaki. "Diluted magnetic III-V semiconductors". *Physical Review Letters*. 63.1849, (1989).
- [3] A. Hoffman. "The origins and evolution of controlled drug delivery systems". *Official journal of the Controlled Release Society*. 132 3, 153-63 (2008).
- [4] H. Ohno. "Properties of ferromagnetic III–V semiconductors". *Journal of Magnetism and Magnetic Materials*. 200, 110-129(1999).
- [5] M. Tanaka and K. Takahashi. "Ferromagnet (MnAs)/semiconductor (GaAs, AlAs, InAs)/ferromagnet (MnAs) trilayer heterostructures: Epitaxial growth and magnetotransport properties". *Journal of Crystal Growth*. 227, 847-851(2001).
- [6] J. Wang, H.Mao, J. Yu, Q. Zhao, H. Zhang, P. Yang, Z. Zhu, and J. Chu. "Electrically tunable electron g factors in coupled InAs/GaAs pyramid quantum dots". *Applied Physics Letters*. 96, 062108(2010).
- [7] T.Jungwirth, J. Sinova, J. Kuvcera, and A. MacDonald. "Theoretical models of ferromagnetic III-V semiconductors". *Current Applied Physics*.(2003).
- [8] J. Tang, S. Cao, Y. Gao, Y. Sun, W. Geng, D. Williams, K. Jin, and X. Xu. "Charge state control in single InAs/GaAs quantum dots by external electric and magnetic fields". *Applied Physics Letters*, 105, 041109 (2014).
- [9] N. Samarth, and J. Furdyna. "Diluted Magnetic Semiconductors". *MRS Bulletin*, 13, 32-36 (1988).
- [10] W. Lin, M. Hehn, L. Chaput, B. Negulescu, S. Andrieu, F. Montaigne, and S. Mangin. "Giant spin-dependent thermoelectric effect in magnetic tunnel junctions". *Nature Communications*, 3(2011).
- [11] J. Zhu, and C. Park. "Magnetic tunnel junctions". *Materials Today*, 9, 36-45(2006).
- [12] A. Hanbicki, B. Jonker, G. Itkos, G. Kioseoglou, and S. Buffalo. "Efficient electrical spin injection from a magnetic metal/tunnel barrier contact into a semiconductor". *Applied Physics Letters*, 80, 1240-1242 (2001).
- [13] T. Dietl and H. Ohno. "Dilute ferromagnetic semiconductors: Physics and spintronic structures". *Reviews of Modern Physics*, 86, 187-251 (2013).
- [14] N. Nagaosa. "Spin Currents in Semiconductors, Metals, and Insulators". *Journal of the Physical Society of Japan*, 77, 031010(2008).
- [15] J. George, M. Elsen, V. Garcia, H. Jaffrès, and R. Mattana. "Spintronic with semiconductors". *Comptes Rendus Physique*, 6, 966-976(2005).
- [16] F. Matsukura, H. Ohno, A. Shen, and Y. Sugawara. "Transport properties and origin of ferromagnetism in (Ga,Mn)As". *Physical Review B*, 57 (1998).
- [17] H. Ohno. "Making nonmagnetic semiconductors ferromagnetic". *Science*, 281 5379, 951-5 (1998).

- [18] F. Tran, P. Blaha, K. Schwarz, and P. Novák. "Hybrid exchange-correlation energy functionals for strongly correlated electrons: Applications to transition-metal monoxides". *Physical Review B*, 74, 155108(2006).
- [19] S. Vosko and L. Wilk "A comparison of self-interaction-corrected local correlation energy functionals". *Journal of Physics B*, 16, 3687-3702(1983).
- [20] K. Burke, F. Cruz, and K. Lam. "Unambiguous exchange-correlation energy density". *Journal of Chemical Physics*, 109, 8161-8167(1998).
- [21] S. Hong, K. Yi and J. Quinn. "Self-consistent electronic structure of spin-polarized dilute magnetic semiconductor quantum wells". *Physical Review B*. 61, 13745-13752(2000).

Chapter I: Spintronics Semiconductors

I.1. Introduction

I.2. Spintronics: Definition and Characteristics

I.3. Spintronics: Technologies and Devices

I.4. Magnetism: Types and Materials

I.5. Magnetic Interaction

I.6. Diluted Magnetic Semiconductors III-V Based on GaX

I.7. Conclusion

I.1. Introduction

Diluted Magnetic Semiconductors (DMS) exhibit key properties essential for conventional spintronics. Operating as ferromagnetic semiconductors, they enable the modification of magnetic and other characteristics through standard semiconductor engineering. The introduction of a small percentage of manganese (Mn) into a III-V semiconductor demonstrates the profound influence of doping on magnetic properties [1-3]. Significantly, annealing processes post-growth offer a means to grossly change doping profiles and magnetic attributes, highlighting the inherent adaptability of DMS for dynamic spintronic applications.

I.2. Spintronics: Definition and Properties

a) **Definition:** Spintronics, short for spin transport electronics, is a field of study in condensed matter physics and electrical engineering that explores the intrinsic spin of electrons as well as their fundamental electronic charge. Traditional electronics relies on the manipulation of the electrical charge of electrons to carry and process information. Spintronics, on the other hand, exploits the intrinsic spin of electrons for information storage and transport [4-6].

The key quantity in spintronics is the electron's spin, which is a fundamental property akin to its charge. The spin of an electron can be thought of as an intrinsic angular momentum, and it has two possible states: "up" or "down" (**Figure I.1**). These spin states can be manipulated and used to represent binary information (analogous to the "0" and "1" states in conventional electronics).

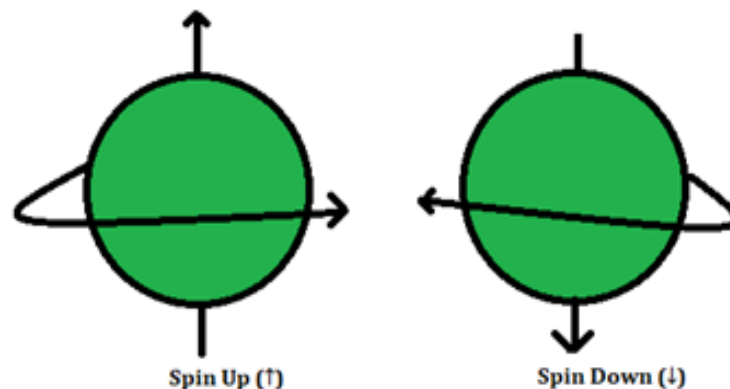


Fig. I.1: Intrinsic angular momentum and spin states.

b) Characteristics: here are some spintronics-related characteristics of DMS:

I.2.1. Spin Injection and Detection

Spin injection and detection are crucial aspects of spintronics, and DMS play a pivotal role in these processes. In spintronic devices, DMS materials are employed to introduce magnetic impurities into semiconductors, enabling the manipulation and control of electron spin orientation. This capability facilitates the generation of spin-polarized currents.

For spin injection, the process involves injecting spin-polarized electrons from a ferromagnetic material into the semiconductor. The introduction of magnetic impurities in the DMS semiconductor allows for the alignment and control of electron spins, contributing to the creation of spin-polarized electron currents [7,8].

On the other hand, spin detection involves sensing and measuring the spin state of electrons in the semiconductor. This detection process is essential for understanding and utilizing the spin information encoded in the electron currents. The unique magnetic properties of DMS materials make them valuable for both injecting and detecting spins, providing a foundation for the development of efficient spintronic devices.

I.2.2. Spin-Dependent Transport

Spin-dependent transport is a fundamental aspect of spintronics, and DMS play a crucial role in this domain. The conductivity of DMS materials is intricately linked to the spin orientation of charge carriers, presenting an avenue for manipulating and harnessing electron spins for functional purposes in spintronic devices.

In spin-dependent transport, the spin state of charge carriers, such as electrons, significantly influences the material's electrical conductivity. DMS materials, where magnetic impurities are intentionally introduced into semiconductors, exhibit a unique sensitivity to the spin orientation of electrons. This distinctive property is harnessed to control the flow of spin-polarized electrons through the material.

I.2.3. Spin-Orbit Coupling

Spin-orbit coupling is a phenomenon that arises from the interaction between the spin and orbital motion of electrons. In DMS materials, this interaction becomes particularly intriguing when combined with the intentional introduction of magnetic impurities. The interplay between spin-orbit coupling and magnetic impurities leads to the emergence of unique electronic band structures, adding a distinctive dimension to the properties of DMS materials and making them highly relevant for spintronic applications.

Figure I.2 illustrates the influence of spin-orbit coupling on electron spin states, highlighting changes in energy levels and spin orientations resulting from the interaction between intrinsic spin and orbital motion.

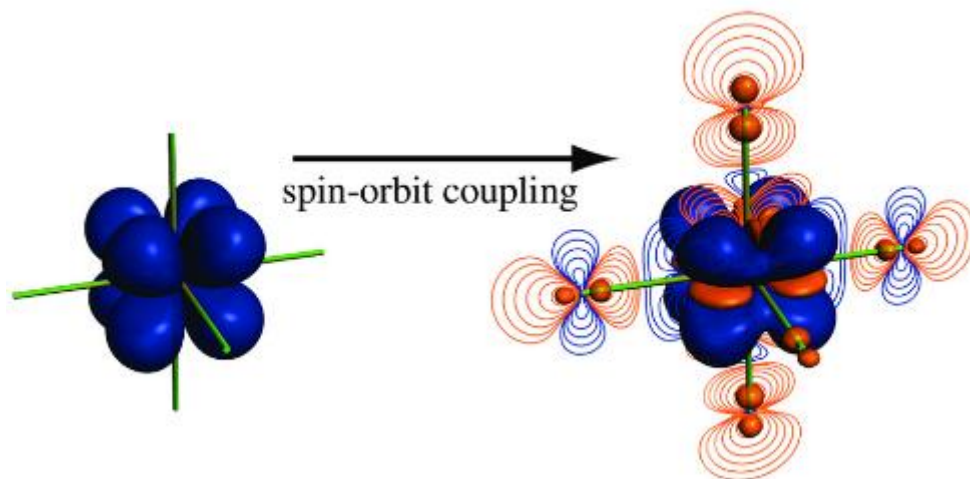


Fig. I.2: Effects from spin-orbit coupling on electron [9].

I.2.4. Spin Lifetime and Relaxation

Spin lifetime and relaxation times in DMS are critical parameters. Understanding and controlling these times are essential for maintaining the integrity of spin information over distances, influencing the efficiency of spintronic devices.

I.3. Spintronics: Technologies and Devices

a) **Technologies:** Spintronic is a groundbreaking field at the intersection of research and technology. It harnesses not only the fundamental electronic charge of electrons but also

their intrinsic spin for innovative applications. Several pivotal spintronic technologies have surfaced, each contributing to the evolution of electronic devices. Here, we delve deeper into the expansion of three noteworthy spintronic technologies: Giant Magneto-Resistance (GMR), Tunnel Magneto-Resistance (TMR), and Magnetic Random-Access Memory (MRAM).

I.3.1. Giant Magneto-Resistance (GMR)

GMR is a revolutionary spintronic effect discovered by Albert Fert and Peter Grünberg in 1988 [10-12]. It exploits the quantum mechanical alignment or misalignment of electron spins in ferromagnetic layers separated by a non-magnetic spacer. The remarkable feature of GMR is the substantial change in electrical resistance based on the relative orientation of the magnetic layers. This technology has transformed data storage, enabling the development of more sensitive read heads in hard disk drives and contributing to the significant increase in storage capacities.

I.3.2. Tunnel Magneto-Resistance (TMR)

TMR is another vital spintronic technology observed in magnetic tunnel junctions. It relies on the principle of electron tunnelling through an insulating barrier. TMR is characterized by a dramatic change in electrical resistance depending on the alignment of magnetic layers. This effect finds applications in magnetic sensors, spin valves, where information is stored based on the orientation of electron spins [13-15].

I.3.3. Magnetic Random-Access Memory (MRAM)

MRAM is a non-volatile memory technology that utilizes the magnetic orientation of electron spins to store information. Unlike traditional RAM, MRAM combines high-speed operation with non-volatility. This spintronic memory technology has the potential for low power consumption and rapid data access, making it suitable for a range of applications, including embedded systems, Internet of Things (IoT) devices, and various data storage solutions. **Figure I.3** provides a schematic representation of Magnetic Random Access Memory (MRAM).

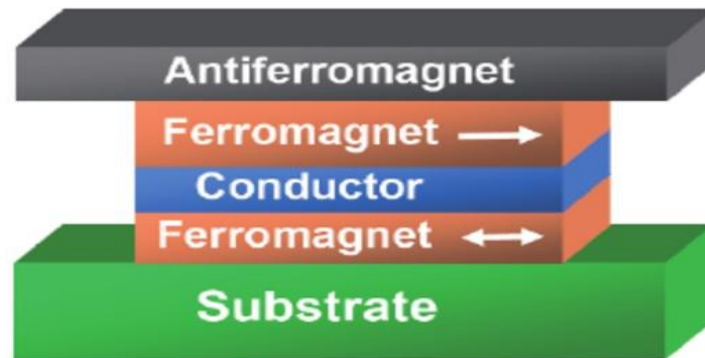


Fig. I.3: Schematics of Magnetic Random Access Memory (MRAM) [16].

Two ferromagnetic thin films, separated by a non-ferromagnetic conducting layer, exhibit distinct resistances (low/high) when their magnetizations are either parallel ($R_{\uparrow\uparrow}$) or antiparallel ($R_{\uparrow\downarrow}$). To establish '0' and '1' states, an antiferromagnetic over layer is used to pin one layer, creating exchange bias for well-defined switching.

b) Devices: Spintronics has spurred the development of various devices that harness the spin of electrons for information processing and storage. Here's an overview of some spintronic devices:

I.3.4. Spin Transfer Torque (STT) Devices

STT devices utilize the transfer of angular momentum from a spin-polarized current to a magnetic layer, influencing the magnetization direction. This torque can be employed to switch the magnetic state of the device, enabling the creation of non-volatile magnetic memories and magnetic tunnel junctions. STT devices have potential applications in spintronic memory and logic devices. **Figure I.4** visually presents an illustration of current-induced torques. This likely includes depictions of spin-transfer torque or other phenomena where an electric current influences the orientation of magnetic spins. The figure helps convey the principles behind current-driven effects on magnetic systems, providing insight into applications such as spintronics and magnetic data storage.

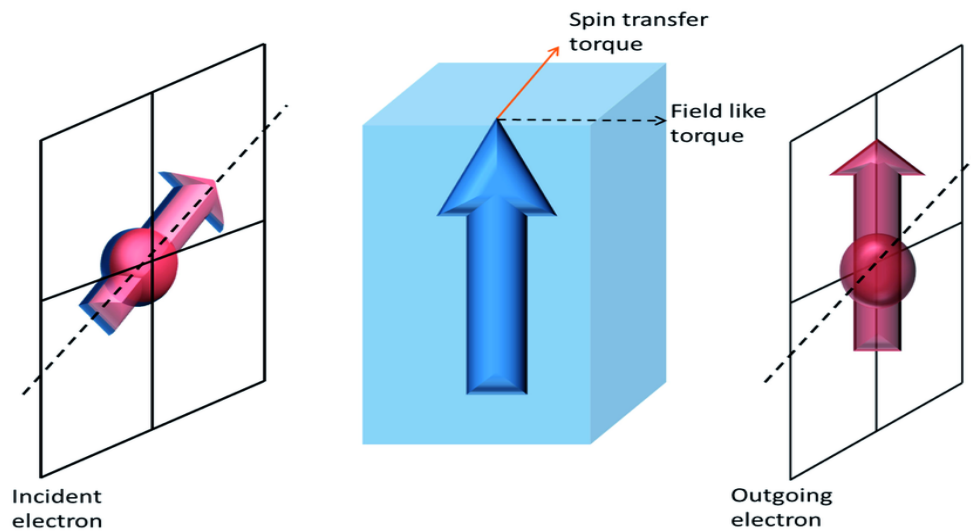


Fig. I.4: Illustration of current-induced torques [17].

Spin-polarized electrons interact with ferromagnetic materials, causing spin-transfer torque (in-plane) and field-like torque (perpendicular). This torque plays a key role in manipulating magnetization for spintronics applications and non-volatile memory devices [17].

I.3.5. Spin Hall Effect (SHE) Devices

Devices based on the Spin Hall Effect leverage the generation of a transverse spin current induced by an electric field. These devices include spin current generators and detectors. The SHE is utilized in spintronic applications such as spin-logic devices and spintronic memory elements. It provides a means to control and manipulate spin information using electric fields.

I.3.6. Spin-FET (Spin Field-Effect Transistor)

Spin-FET is a type of transistor designed to utilize the spin of electrons in addition to their charge. By controlling the spin orientation in a semiconductor channel, Spin-FETs offer potential advantages in terms of low power consumption and high-speed operation. Research in this area focuses on developing efficient spin-based transistors for future computing architectures.

I.3.7. Spin Wave Devices

Spin wave devices exploit spin waves, collective excitations of electron spins, for information transmission and processing. Spin waves can be manipulated by magnetic fields, and devices based on spin waves include spin wave waveguides and logic elements. Spin wave devices have potential applications in magnonic circuits and spintronic signal processing.

I.3.8. Skyrmion-Based Devices

Skyrmions are topologically stable magnetic structures that can be manipulated and moved within a material. Devices based on skyrmions include skyrmion racetrack memories and logic devices. Skyrmion-based devices offer advantages in terms of stability and low power consumption and are explored for future spintronic applications [18,19].

Figure I.5 presents a schematic representation of the skyrmion racetrack memory as discussed by S. Luo and L. Youin [20].

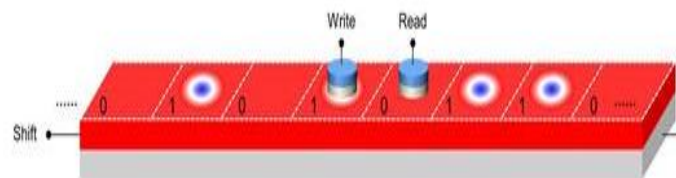


Fig. I.5: Schematic of the skyrmion racetrack memory.

Racetrack Memory (RM) leverages magnetic nanowires with storage bits, write ports for magnetization state switching, read ports using magneto-resistance for reading, and shift ports to move storage bits for operations. Binary data is represented by magnetization states, with or without a skyrmion. The concept resembles racing cars on a track, making RM a promising application for skyrmions in data storage.

I.4. Magnetism : Types and Materials

Magnetism is a phenomenon associated with the motion of electric charge, which results in attractive and repulsive forces between objects.

a) **Types:** Understanding the different types of magnetism is essential for various applications, including the development of magnetic materials for technological use, such as in electronics, data storage, and medical devices. There are several types of magnetism exhibit varying degrees of magnetic behaviour, the total magnetic field in an external magnetic field is:

$$\vec{B} = \vec{B}_0 + (1 + \chi_m)\mu_0\vec{M}, \quad (1)$$

Where:

\vec{B}_0 is the external field.

\vec{M} is the magnetic moment per unit volume.

μ_0 is the relative permeability.

χ_m is the magnetic susceptibility.

I.4.1. Ferromagnetism

Ferromagnetism is the strongest type of magnetism and is exhibited by materials that can be permanently magnetized. In ferromagnetic materials, the magnetic moments of individual atoms align parallel to each other, creating strong magnetic domains. When these domains are aligned, the material becomes magnetized. Example: Iron, cobalt, nickel, and certain alloys are common ferromagnetic materials.

I.4.2. Antiferromagnetism

Antiferromagnetism is characterized by adjacent magnetic moments in a material aligning in opposite directions. The magnetic moments in antiferromagnetic materials tend to cancel each other out, resulting in a net magnetic moment of zero. However, there is an ordering of magnetic moments in opposite directions. Example: Manganese oxide (MnO) is an example of an antiferromagnetic material.

I.4.3. Ferrimagnetism

Ferrimagnetism is similar to antiferromagnetism, but there is a net magnetic moment due to unequal magnetic strengths of opposing moments. In ferrimagnetic materials, there is a partial

cancellation of magnetic moments, leading to a residual magnetic moment. Example: Magnetite (Fe_3O_4) is an example of a ferrimagnetic material.

I.4.4. Paramagnetism

Paramagnetism is exhibited by materials with unpaired electrons, which have magnetic moments that align with an external magnetic field. Paramagnetic materials are weakly attracted to an external magnetic field and do not retain magnetization once the field is removed. Example: Aluminium, Platinum, and some rare-earth ions show paramagnetic behavior.

I.4.5. Diamagnetism

Diamagnetism occurs in materials where all the electron spins are paired, leading to a weak repulsion from an applied magnetic field. Diamagnetic materials are repelled by an external magnetic field, and the effect is usually very small.

Example: Most materials exhibit some degree of diamagnetism, but it is generally weak.

I.4.6. Superparamagnetism

Superparamagnetism is a phenomenon observed in small magnetic particles or nanoparticles. At certain sizes, these particles may not have a stable magnetic moment at zero applied field, but they can align with an external magnetic field. Example: Nanoparticles of ferromagnetic or ferrimagnetic materials can exhibit superparamagnetic behavior.

Figure I.6 provides an illustrative overview of different magnetic varieties found in materials.

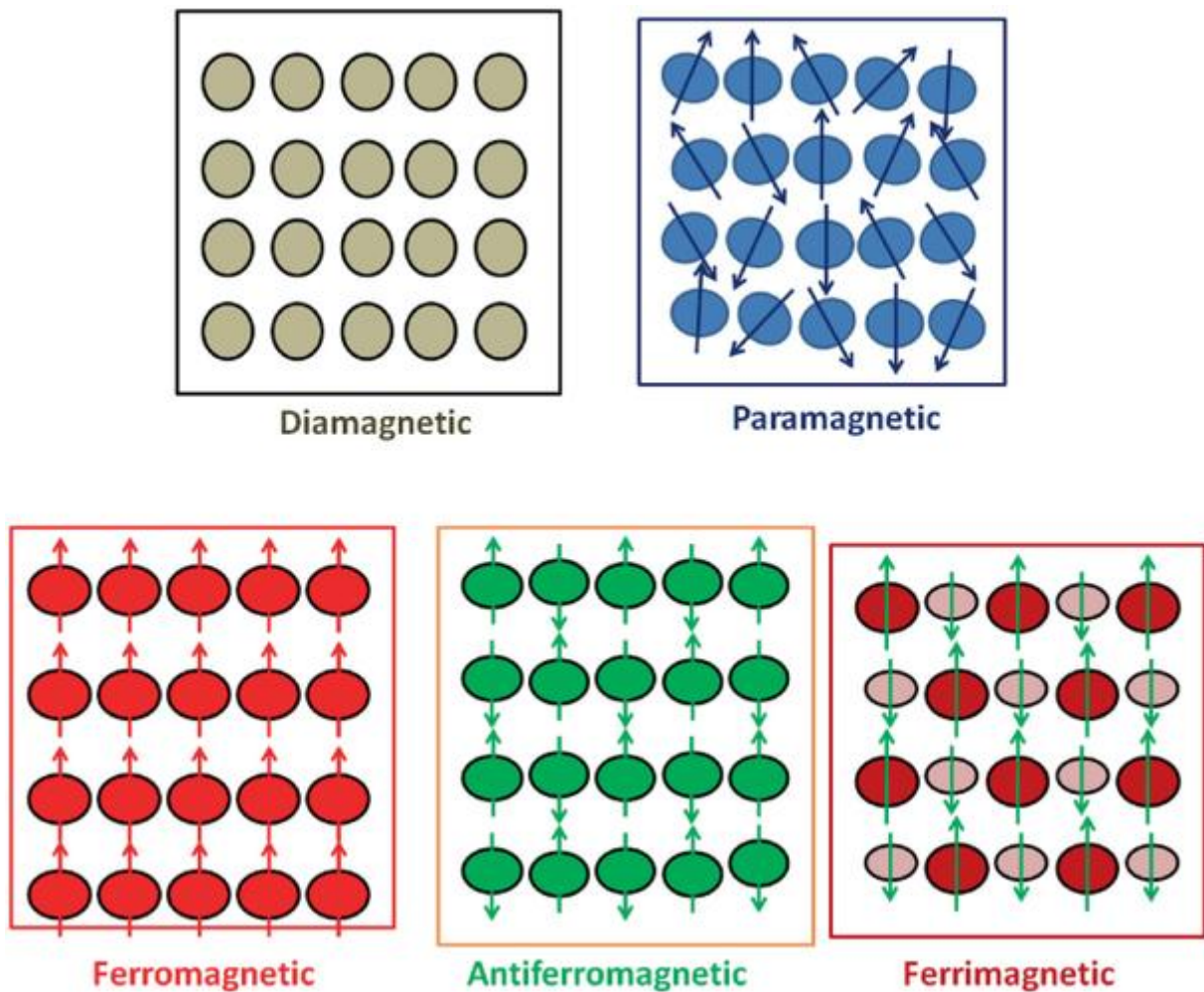


Fig. I.6: Magnetic varieties.

b) Materials: Understanding the magnetic properties of materials is crucial for designing electronic devices, sensors, medical equipment, and various industrial applications. Different types of magnetic materials are chosen based on their specific properties and suitability for a given application:

I.4.7. Magnetic Semiconductor Material

A magnetic semiconductor material is a substance that exhibits both magnetic and semiconducting properties. These materials are capable of carrying an electric charge while also displaying magnetic behavior. Magnetic semiconductors are crucial in spintronics, a field that exploits both the spin and charge of electrons. They find applications in information storage, quantum computing, and electronic devices where the control of both electronic and magnetic properties is essential.

I.4.8. Hard Magnetic Material

Hard magnetic materials often referred to as permanent magnets, retain their magnetization once they are magnetized. They have high coercivity, meaning a strong magnetic field is required to demagnetize them [21]. Hard magnetic materials are used in various applications such as refrigerator magnets, electric motors, generators, and magnetic data storage (hard disk drives). Common examples include Alnico (aluminium, nickel, cobalt) and rare-earth magnets (neodymium-iron-boron).

I.4.9. Soft Magnetic Material

Soft magnetic materials have low coercivity, meaning they can be easily magnetized and demagnetized [21]. They are used in applications where rapid changes in magnetic fields are necessary. Soft magnetic materials are employed in transformers, inductors, electric motors, and other devices where efficient energy transfer between magnetic fields is required. Examples include electrical steels and ferrites.

I.4.10. Ferrofluid Material

Ferrofluids are colloidal liquids containing magnetic nanoparticles. These nanoparticles become magnetized in the presence of an external magnetic field, giving the fluid unique properties. Ferrofluids find applications in seals for rotating shafts in vacuum systems, loudspeakers to dampen resonance, and as a contrast agent in medical imaging. Their ability to change viscosity in the presence of a magnetic field makes them useful in various engineering applications [22].

I.5. Magnetic Interaction

Comprehending the magnetic interactions is fundamental to explaining the magnetic properties of materials and is essential in the design and development of magnetic materials for various applications. The interplay of these interactions contributes to the rich and diverse behaviors observed in magnetic materials, influencing their magnetic ordering, stability, and response to external magnetic fields:

I.5.1. Heisenberg Exchange Interaction

The Heisenberg Exchange Interaction is a quantum mechanical phenomenon that describes the interaction between localized electron spins within a magnetic material. This interaction arises due to the exchange of virtual excitations between neighboring spins [23]. In ferromagnetic materials, it favors parallel alignment of spins, leading to a net magnetic moment. In antiferromagnetic materials, it favors antiparallel alignment, resulting in a cancellation of net magnetic moments [24].

I.5.2. RKKY Interaction (Ruderman-Kittel-Kasuya-Yosida)

The RKKY Interaction is an indirect magnetic interaction between localized magnetic moments mediated by conduction electrons in a nonmagnetic material. This interaction depends on the separation distance between the magnetic moments and oscillates in sign as a function of distance [25-27]. The RKKY interaction can lead to the formation of magnetic order or affect the behavior of magnetic impurities in metals.

I.5.3. Dzyaloshinsky-Moriya Interaction

The Dzyaloshinsky-Moriya interaction is another type of magnetic interaction that can occur in crystals with broken inversion symmetry [28]. Unlike the RKKY interaction, which is associated with the indirect exchange interaction mediated by itinerant electrons, the Dzyaloshinsky-Moriya interaction involves a direct exchange between neighboring magnetic moments due to spin-orbit coupling in the presence of broken inversion symmetry [28]. Mathematically, the Dzyaloshinsky-Moriya interaction term (D) can be expressed as:

$$H_{DM} = D \cdot (S_1 \times S_2) \quad (2)$$

Here, S_1 and S_2 are the spins of the neighboring magnetic moments, and D is the Dzyaloshinsky-Moriya vector.

In the **Figure I.7**, the interaction between two magnetic moments mediated by the host electrons in the crystal, which leads to the well known RKKY interaction, However, if the host crystal has broken symmetry, then additional interaction terms appear, known as the Dzyaloshinsky-Moriya interaction [29].

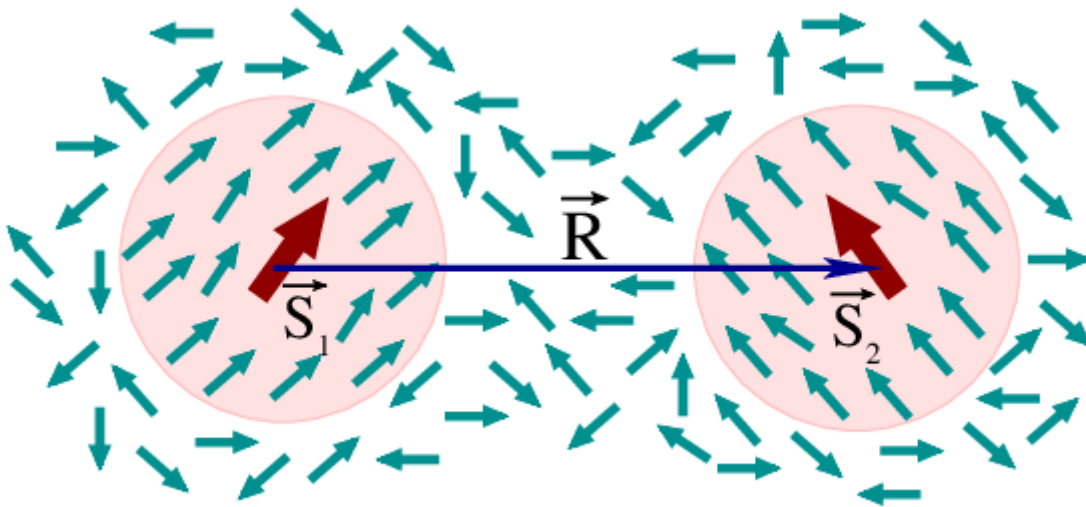


Fig. I.7: Symmetry-Breaking effects on magnetic interactions in crystals: RKKY and Dzyaloshinsky-Moriya Interactions [29].

I.5.4. Kondo Interaction

The Kondo Interaction is a magnetic interaction that occurs between localized magnetic impurities and conduction electrons in metals. At low temperatures, the localized magnetic moment forms a spin singlet with the conduction electrons, leading to an increase in electrical resistance [30]. This phenomenon is known as the Kondo effect and is crucial in understanding the behavior of magnetic impurities in metals.

I.5.5. Anisotropic Magnetic Interaction

Anisotropic Magnetic Interaction refers to the directional dependence of the magnetic properties of a material. It influences the preferred orientation of magnetic moments in a material, leading to anisotropy in its magnetic behavior. This interaction is crucial in determining the magnetic properties of ferromagnetic materials and can result in phenomena such as magnetic anisotropy energy and magnetic domain anisotropy.

I.6. Diluted Magnetic Semiconductors III-V Based on GaX

Research on DMS III-V materials, which are doped with Mn has experienced a surge in publications, reflecting the growing interest in their unique properties. The comparison

between DMS III-Mn-V and II-Mn-VI systems arises from the challenges posed by the solubility limits of Mn within crystalline matrices, a factor that significantly influences their structural and magnetic properties. In DMS III-V compounds incorporating Mn, the introduction of divalent magnetic ions serves as acceptors, altering the electronic structure and contributing to the emergence of ferromagnetic coupling mechanisms. This ferromagnetic coupling, primarily carried by the charge carriers within the material, plays a pivotal role in determining their overall magnetic behavior. However, it's important to highlight the intrinsic link between the magnetic character and the doping levels in these systems. This interdependence presents a substantial obstacle in fully understanding and manipulating their magnetic properties, thereby warranting further investigation and a nuanced approach in future studies. In this thesis, our research is centered on employing GaX (X= N, P and As) semiconductor materials doped with Mn for our studies.

I.6.1. Binary GaN Properties

Gallium Nitride (GaN) is a wide direct bandgap material (3.457eV) widely used for power applications due to the numerous advantages it presents. The various parameters of GaN at room temperature are gathered in **Table I.1**.

| Properties | GaN (Zinc Blende) | GaN (Wurtzite) |
|--|--|--|
| Stability | Metastable | Stable |
| Symmetry Group [31] | T_d^2 (F43m) | C_{6v}^4 (P6 ₃ mc) |
| Lattice Parameter (Å) [32] | a= 4.50 | a = 3.189 c = 5.185 c/a = 1.626 |
| Band Gap E_g (eV)[32] | 3.299 | 3.457 |
| Spin-Orbit Splitting Δ_{so} (eV) [32] | 0.017 | 0.014 |
| Electron Affinity χ (eV) [33] | 4.1 | 4.1 |
| Effective Mass [31], [33,34] | $m_e=0.13$ $m_{lh}=0.19$, $m_{hh}=1.3$ $m_{so}=0.33$ | $m_e=0.171$ $m_{lh}=0.30$ $m_{hh}=1.41$ $m_{so}=0.62$ |
| Density (g/cm ³) [31] | 6.10 | 6.095 |

Table I.1: Various parameters of Wurtzite and Zinc Blende of GaN structure.

a) The advantages of GaN include [35]:

- ✓ Good Thermal Conductivity: GaN efficiently dissipates heat, crucial for device longevity and performance in high-power applications.
- ✓ High Power Output: GaN ability to handle high power levels makes it ideal for power electronics, amplifiers, and converters.
- ✓ Significant reduction in size and weight: GaN compact design enhances portability and efficiency in electronic systems.
- ✓ Very High Switching Speed: GaN rapid switching capabilities improve system efficiency and performance in power converters and Radio Frequency (RF) amplifiers.
- ✓ Reduced Electrical Noise: GaN smaller packages and reduced stray elements result in cleaner electronic signals with less interference.
- ✓ High Temperature of Resistance: GaN resilience to high temperatures suits applications in automotive and power electronics.
- ✓ Radiation Resistance: GaN robustness against radiation effects makes it suitable for space and military applications.
- ✓ High Efficiency: GaN devices boast high electrical efficiency, converting power with minimal losses in various applications.
- ✓ High breakdown voltage: GaN devices often exhibit high breakdown voltages, enhancing their robustness in power applications.
- ✓ Compact size: GaN ability to handle high power in a small form factor contributes to the development of compact and lightweight electronic systems.
- ✓ Long device lifespan: GaN devices can have a longer lifespan compared to some other materials, contributing to increased reliability.
- ✓ Compatibility with high frequencies: GaN is well-suited for high-frequency applications, making it valuable in RF and microwave devices.

b) Different Domains in the GaN Application [36]:

- ✓ Power Electronics: GaN excels in power electronic devices, ensuring high efficiency and compact design in applications like inverters and converters.
- ✓ Blu-Ray Technology: GaN-based semiconductors contribute to Blu-ray players, enhancing data storage and playback capabilities.

- ✓ Laser Printing: GaN in laser diodes ensures precision and reliability in laser printing technology.
- ✓ Photovoltaics: GaN plays a key role in photovoltaics, forming InGaN/GaN heterostructures for solar cells capturing multiple wavelengths.
- ✓ Aircraft Power Supplies (SPS Switcher Power Supply): GaN-based SPS switchers efficiently manage power in aircraft systems, crucial for aviation where size and weight matter.
- ✓ 5G Wireless Communication: GaN enables high-frequency, high-power amplifiers for faster data transfer and improved performance in 5G networks.
- ✓ Electric Vehicles: GaN technology contributes to efficient and compact electric drive trains in electric vehicles.
- ✓ Medical Imaging: GaN-based detectors enhance sensitivity and resolution in medical imaging devices, especially X-ray imaging.
- ✓ Radar Systems: GaN transistors enhance radar performance in defense and aerospace applications.
- ✓ High-Frequency RF Devices: GaN is vital for high-frequency RF devices, including power amplifiers and switches, in communication systems and radar technology.

I.6.2. Binary GaP Properties

Gallium Phosphide (GaP) is characterized by its wide indirect bandgap, measuring 2.35 eV. This semiconductor material is extensively employed in power applications, leveraging a multitude of advantages. The key parameters defining GaP at room temperature are consolidated in **Table I.2**.

| Properties | GaP (Zinc Blende) |
|--|--|
| Stability | Stable |
| Symmetry Group [37] | T_d^2 (F43m) |
| Lattice Parameter (\AA) [32] | $a= 5.45$ |
| Band Gap E_g (eV) [32] | 2.35 |
| Spin-Orbit Splitting Δ_{so} (eV) [32] | 0.08 |
| Electron Affinity $e\chi$ (eV) [37] | 3.8 |
| Effective Mass [32],[37] | $m_e= 0.13$ $m_{lh}=0.14$ $m_{hh}=0.79$ $m_{so}=0.25$ |
| Density (g/cm ³) [37] | 4.14 |

Tab. I.2: Various parameters of Zinc Blende GaP structure.

a) The Advantages of GaP include [38]:

- ✓ Tunable Bandgap: GaP bandgap can be adjusted to produce different colors of light, making it versatile for applications in displays and lighting technologies.
- ✓ High Thermal Conductivity: GaP has relatively high thermal conductivity, which helps in dissipating heat from electronic devices. This is crucial for maintaining the performance and longevity of devices, especially those operating at high power levels.
- ✓ Compatibility with Silicon Substrates: GaP can be grown on silicon substrates, facilitating integration into existing silicon-based technologies. This compatibility is advantageous for manufacturing processes and can help reduce costs.
- ✓ Varied Alloying Possibilities: GaP can be alloyed with other materials to tailor its properties for specific applications, providing flexibility in design and functionality.
- ✓ Radiation Hardness: GaP is known for its radiation-hard properties, making it suitable for applications in space and other environments where exposure to radiation is a concern.
- ✓ Compatibility with Silicon Technology: Researchers explore the integration of GaP with silicon technology, aiming to enhance the performance of electronic and optoelectronic devices.

- ✓ Low Noise Characteristics: GaP devices often exhibit low noise characteristics, making them suitable for applications where signal integrity is critical, such as in communication systems.
- ✓ Piezoelectric Properties: GaP exhibits piezoelectric properties, which means it can convert mechanical vibrations or stress into electrical signals. This property is valuable in sensors and actuators.

b) Different domains in the GaP application [39,40]:

- ✓ Optoelectronics: GaP is widely used in the production of light-emitting diodes (LEDs) and laser diodes, contributing to advancements in lighting technology and display systems.
- ✓ Solar Cells: GaP is employed in the development of solar cells, where its properties are harnessed for efficient photovoltaic energy conversion.
- ✓ Telecommunications: GaP plays a role in telecommunications, particularly in the development of components for optical communication systems.
- ✓ Electronic Components: GaP is utilized in various electronic components, benefiting from its semiconductor properties in the design of transistors and other semiconductor devices.
- ✓ Crystal Growth and Semiconductors: GaP crystal growth properties make it a material of interest for semiconductor applications, contributing to the advancement of semiconductor technology.
- ✓ Photoconductive Devices: GaP is utilized in the creation of photoconductive devices, including photo-detectors. These devices are sensitive to light and find applications in various optical and sensing systems.
- ✓ Terahertz Radiation Generation: GaP is explored for its potential in generating terahertz radiation, which has applications in imaging, communication, and spectroscopy.
- ✓ Nonlinear Optical Devices: GaP is employed in the development of nonlinear optical devices, contributing to applications in telecommunications and signal processing.
- ✓ Lighting Technology: GaP ability to emit light efficiently is leveraged in lighting technologies, including applications ranging from general lighting to specialized illumination systems.
- ✓ Imaging Devices: GaP is incorporated into imaging devices, contributing to the development of high-performance cameras and sensors.

- ✓ Medical Applications: In certain medical applications, GaP may be employed in the development of devices for imaging or diagnostic purposes.

I.6.3. Binary GaAs Properties

Gallium Arsenide (GaAs) is a semiconductor material known for its direct bandgap of 1.512eV, making it a valuable component in electronic and optoelectronic applications. GaAs exhibits distinct properties that contribute to its widespread use. It is extensively employed in various technological domains, and key parameters defining GaAs at room temperature are compiled in **Table I.3**.

| Properties | GaAs (Zinc Blende) |
|--|---|
| Stability | Stable |
| Symmetry Group [41] | T_d^2 (F43m) |
| Lattice Parameter (\AA) [32] | $a= 5.653$ |
| Band Gap E_g (eV) [32] | 1.512 |
| Spin-Orbit Splitting Δ_{so} (eV) [32] | 0.341 |
| Electron Affinity χ (eV) [41] | 4.07 |
| Effective Mass [32], [41] | $m_e= 0.067$ $m_{lh}=0.082$ $m_{hh}=0.51$ $m_{so}=0.172$ |
| Density (g/cm ³) [41] | 4.07 |

Table I.3: Various parameters of Zinc Blende GaAs structure.

a) The advantages of GaAs include [42,43]:

- ✓ Low Noise Figure: GaAs devices typically have low noise figures, making them valuable in applications such as low-noise amplifiers for communication systems.
- ✓ High Electron Mobility: GaAs exhibits high electron mobility, making it suitable for high-speed electronic devices, including field-effect transistors (FETs) and integrated circuits operating at microwave and radio frequencies.

- ✓ High Frequency Operation: GaAs devices can operate at high frequencies, making them suitable for applications in RF and microwave communication systems.
- ✓ Versatility: GaAs finds application in various domains, including telecommunications, aerospace, and defense technology, showcasing its versatility across different industries.
- ✓ Low Power Consumption: GaAs devices can offer lower power consumption compared to some other semiconductor materials, contributing to energy-efficient electronic systems.
- ✓ High Breakdown Voltage: GaAs devices often exhibit high breakdown voltages, enhancing their robustness in power applications.
- ✓ Harsh Environment Performance: GaAs demonstrates reliable performance in harsh environments, making it suitable for space and defense applications where extreme conditions may be encountered.
- ✓ High Temperature Performance: GaAs devices can operate at relatively high temperatures, making them suitable for applications where thermal stability is important.
- ✓ Excellent optical properties: GaAs has excellent optical properties, allowing for the efficient conversion of electrical signals to optical signals and vice versa. This is particularly useful in the development of optoelectronic devices.

b) Different domains in the GaAs application [44,45]:

- ✓ Optoelectronics: GaAs is extensively used in optoelectronic devices, including Light-Emitting Diodes (LEDs) and laser diodes, contributing to advancements in lighting technology and display systems.
- ✓ Telecommunications: GaAs plays a crucial role in telecommunications, particularly in the development of components for optical communication systems, such as optical fibers and detectors.
- ✓ Microwave and RF Applications: GaAs is vital in microwave and RF applications, where its high electron mobility is exploited for the design of high-frequency integrated circuits, amplifiers, and oscillators.
- ✓ Solar Cells: GaAs is employed in the production of solar cells, contributing to the development of high-efficiency photovoltaic devices for converting solar energy into electricity.

- ✓ **Space and Defense Technology:** GaAs is utilized in space and defense applications due to its reliability in harsh environments. It is used in the production of high-performance electronic components for satellites, communication systems, and radar technology.
- ✓ **Photovoltaics:** GaAs-based solar cells are highly efficient in converting sunlight into electricity. GaAs solar cells are commonly used in space applications due to their high efficiency and radiation resistance.
- ✓ **Satellite Technology:** GaAs is preferred in satellite technology for its ability to operate at high frequencies, making it suitable for satellite communication systems and space-based applications.
- ✓ **Fiber Optics:** GaAs-based devices are used in the production of components for fiber optic communication systems, such as modulators and detectors.
- ✓ **Quantum Dots:** GaAs quantum dots are employed in the development of quantum dot-based devices for applications in quantum computing and quantum information processing.
- ✓ **Consumer Electronics:** GaAs is used in various consumer electronic devices, including mobile phones, where its high-frequency capabilities contribute to improved performance.

I.6.4. Types of Doping

Doping in semiconductors involves introducing impurities into the crystal lattice to alter their electrical or magnetic properties. There are various doping mechanisms, including substitutional, interstitial and clustering of magnetic impurities:

- a) **Substitutional Doping:** In substitutional doping, foreign atoms replace some of the host atoms in the crystal lattice. This can lead to changes in the electronic structure and magnetic properties of the semiconductor [46]. For example, in the context of DMS, substituting certain host atoms with magnetic impurities like manganese (Mn) can induce ferromagnetism.
- b) **Interstitial Doping:** Interstitial doping involves inserting impurity atoms into the spaces between the host atoms in the crystal lattice. This can create defects and alter the electronic and magnetic behavior of the semiconductor. In the case of magnetic impurities, interstitial doping might involve placing additional magnetic atoms within the lattice, affecting the magnetic interactions and properties of the material [46].

c) **Clusters of Magnetic Impurity:** Clustering occurs when multiple magnetic impurities group together in the lattice. This clustering phenomenon can significantly influence the magnetic properties of the semiconductor. The interactions between the clustered impurities may lead to emergent magnetic behavior not present in individual impurities [46]. Understanding and controlling these clusters are crucial for tailoring the magnetic properties of materials for specific applications.

Recent research identifies substitutional defects as the sole contributors to ferromagnetism in III-V semiconductors [47]. Consequently, my calculations exclusively consider these impurities, aiming to unveil their pivotal role in shaping the semiconductor magnetic behavior.

I.6.5. Mn - Doped III-V Semiconductors

Manganese (Mn) is used as a dopant in III-V semiconductors (e.g. GaN, GaAs and GaP) to introduce magnetic properties, crucial for spintronics applications. With its magnetic moment from a five unpaired electrons in the 3d, Mn acts as a magnetic impurity, creating local magnetic moments in the crystal lattice. This imparts magnetic characteristics, useful for manipulating electron spins in spintronics, a field aiming to utilize both charge and spin for electronic devices.

Manganese is also commonly alloyed with metals like Co, Cr, Cu, Fe, Ni, Sc, Ti and V to enhance their magnetic properties, extending its application in electronic and optoelectronic devices.

Here are several factors contribute to the preference for manganese as a dopant in III-V [48]:

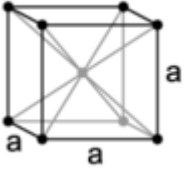
- ✓ **Solubility:** Manganese can have good solubility in III-V materials, allowing it to form a solid solution with the host material. This can lead to a homogeneous distribution of manganese atoms within the crystal lattice, influencing the magnetic behavior of the material.
- ✓ **Control of Atom Size:** The addition of manganese can influence the atom size of the material. Fine-atom structures often exhibit improved magnetic properties, as they can lead to better alignment of magnetic domains and reduced magnetic domain wall motion.

- ✓ **Stabilization of Crystal Structure:** Manganese may help stabilize the crystal structure of III-V materials. This stability can impact the magnetic properties by preventing phase transformations or crystal defects that could negatively affect magnetic behavior.
- ✓ **Enhancement of Magnetic Moments:** Manganese can contribute to the enhancement of magnetic moments within the material. This effect is crucial for improving the overall magnetic properties of the alloy, making it more suitable for magnetic applications.
- ✓ **Alloy Hardening:** The addition of manganese can contribute to the overall hardness and strength of the alloy. While this might not be the primary focus for magnetic properties, it can influence the material's mechanical and magnetic characteristics.
- ✓ **Magnetic Anisotropy:** Manganese can influence the magnetic anisotropy of the material, providing control over the directional dependence of its magnetic properties. This is important for applications where a specific magnetic orientation is desired.

I.6.6. Crystallographic Characteristics of Mn

Mn can exhibit various crystal structures depending on the temperature and pressure conditions. At room temperature, manganese is typically found in a Body-Centered Cubic (BCC) crystal structure (stable). However, it can also adopt other structures under different conditions, such as Face-Centered Cubic (FCC) structures.

Here are some key points regarding in **Table I.4**, the crystallography of Mn [49].

| Allotrope | Crystalline Structure | Crystal System | Coordination Number | Space Group | Lattice Parameter (a) (pm) | Atoms per Unit Cell | Theoretical Density (g/cm ³) |
|--------------------|---|----------------|---------------------|-------------|----------------------------|---------------------|--|
| Alpha (α) |  | Cubic | 8 | Im-3m | 308.1 | 2 | 6.238 |

Tab. I.4: Crystallographic characteristics of Mn.

I.7. Conclusion

In the fusion of spintronics with diluted magnetic semiconductors, GaMn(N, P, As) emerges as a key player, shedding light on the interplay between spin and charge in semiconductor devices. The crystal structure reveals intriguing interaction types, including the ones we studied, offering a versatile platform for spin manipulation. This opens avenues for designing efficient, low-power spintronic devices, marking a transformative impact on semiconductor technology. The study not only deepens fundamental physics understanding but also promises practical applications, emphasizing the need for meticulous material engineering. In sum, GaMn(N, P and As) propels us toward efficient and multifunctional spintronic devices in the foreseeable future.

References

- [1] K. Burch, D. Awschalom, D. Basov, "Optical properties of III-Mn-V ferromagnetic semiconductors", *Journal of Magnetism and Magnetic Materials*, 320.23, 3207-3228, (2008).
- [2] D. Chiba, F. Matsukura, M. Yamanouchi, H. Ohno, "Electrical magnetization reversal in ferromagnetic III–V semiconductors", *Journal of Physics D: Applied Physics*, International Conference on MEMS, NANO and Smart Systems (ICMENS'04), (2004).
- [3] H. Munekata, H. Ohno, S. V. Molnar, A. Segmüller, L. L. Chang, L. Esaki, "Diluted magnetic III-V semiconductors", *Physical Review Letters* 63.1849, (1989).
- [4] S. A. Wolf, R. A. Buhrman, J. M. Daughton, S. von Molnár, M. L. Roukes, A. Y. Chtchelkanova, and D. M. Treger. " Spintronics: a spin-based electronics vision for the future". *Science* 294, 1488, (2001).
- [5] J. De Boeck, W. Van Roy, J. Das, V. Motsnyi, Z. Liu, L. Lagae, H. Boeve, K. Dessen, and G. Borghs. " Technology and materials issues in semiconductor-based magnetoelectronics". *Semicond. Sci. Technol.* 17, 342, (2002).
- [6] I. Zutic, J. Fabian, and S. Das Sarma. "Spintronics: Fundamentals and applications". *Rev. Mod. Phys.* 76, 323, (2004).
- [7] M. Oestreich, J. Hübner, D. Hägele, P. Klar, W. Heimbrodt, W. Rühle, D. Ashenford, B. Lunn. " spin injection into semiconductors". *Appl. Phys. Lett.* 74, 1251–1253 (1999).
- [8] J. Kulkarni, O. Kazakova, J. Holmes. "Dilute magnetic semiconductor nanowires". *Applied Physics A*, Vol 85, pages 277–286, (2006).
- [9] K. Sharkas, B. Pritchard and J. Autschbach. "Effects from Spin–Orbit Coupling on Electron–Nucleus Hyperfine Coupling Calculated at the Restricted Active Space Level for Kramers Doublets". *J. Chem. Theory Comput.* 11, 2, 538–549, (2015).
- [10] E. Fullerton, I. Schuller. " The 2007 Nobel Prize in Physics: magnetism and transport at the nanoscale". *ACS Nano*, 1, 5, 384–389, (2007).
- [11] S. Thompson. "The discovery, development and future of GMR". *J. Phys. D: Appl. Phys.* 41 093001, (2008).
- [12] D. Samal, P. A. Anil Kumar. "Giant magnetoresistance". *Resonance*, Vol 13, pages 343–354, (2008).
- [13] N. Ryzhanova, G. Reiss, F. Kanjouri, A. Vedyayev. " Resonance magneto-resistance in double barrier structure with spin-valve". *Physics Letters A*, Vol 329, I 4–5, P 392-395, (2004).
- [14] Z. Xiong, D. Wu, Z. Vardeny, J. Shi. "Giant magnetoresistance in organic spin-valves". *Nature* volume 427, pages 821–824 (2004).
- [15] R. Roundy, M. Raikh. "Tunnel magnetoresistance in organic spin valves in the regime of multistep tunneling". *Phys. Rev. B* 88, 205206, (2013).

- [16] W. Kleemann and P. Borisov. "Multiferroic and Magnetoelectric Materials for Spintronics". NATO Security through Science Series B: Physics and Biophysics, pp.3-12, Chapter: I.1, (2008).
- [17] B. Kaviraj and J. Sinha. "Relativistic torques induced by currents in magnetic materials: physics and experiments". RSC Advances 8(44):25079-25093, (2018).
- [18] R. Tomasello, E. Martínez, R. Zivieri, L. Torres, M. Carpentieri, G. Finocchio. "A strategy for the design of skyrmion racetrack memories". Scientific Reports 4:06784-1-7, (2014).
- [19] W. Kang, C. Zheng, Y. Huang, X. Zhang, Y. Zhou, W. Lv, W. Zhao. "Complementary Skyrmion Racetrack Memory With Voltage Manipulation". IEEE Electron Device Letters 37(7):924, (2016).
- [20] S. Luo and L. You. "Skyrmion devices for memory and logic applications". APL Mater. 9, 050901 (2021).
- [21] D. Campos, M. Flávio. "Coercivity Mechanism in Hard and Soft Sintered Magnetic Materials". Materials Science Forum 802:563-568, (2014).
- [22] X. Zhang, L. Sun, Y. Yu, Y. Zhao. "Flexible Ferrofluids: Design and Applications". Advanced Materials 31(51):1903497, (2019).
- [23] V. Borisov, Y. Kvashnin, N. Ntallis, D. Thonig, P. Thunström, M. Pereiro, A. Bergman, E. Sjöqvist, A. Delin, L. Nordström, O. Eriksson. "Theory of Heisenberg and anisotropic exchange interactions in magnetic materials with correlated electronic structure and significant spin-orbit coupling". Phys. Rev. B 103, 174422, (2021).
- [24] N. Mermin, H. Wagner. "Absence of Ferromagnetism or Antiferromagnetism in One- or Two-Dimensional Isotropic Heisenberg Models". Phys. Rev. Lett. 17, 1307 (1966).
- [25] A. Kundu, Z. B. Siu, M. Jalil. "Ruderman–Kittel–Kasuya–Yosida (RKKY) interaction in Weyl semimetals with tilted energy dispersion". New J. Phys. 25 013037, (2022).
- [26] D. Aristov. "Indirect RKKY interaction in any dimensionality". Phys. Rev. B 55, 8064, (1997).
- [27] M. Fähnle. "Note on RKKY interactions in nearly-free electron systems". Journal of Magnetism and Magnetic Materials, 10 (1), 9-13, (1979).
- [28] J. H. Moon, S. Seo, K. J. Lee, K. W. Kim, J. Ryu, H. W. Lee, R. McMichael, M. Stiles. "Spin-wave propagation in the presence of interfacial Dzyaloshinskii-Moriya interaction". Physical Review B, 88(18), (2013).
- [29] M. Valizadeh, S. Satpathy. "RKKY Interaction for the Spin Polarized Electron Gas". International Journal of Modern Physics B, Vol. 29, No. 30, 1550219 (2015).
- [30] M. Maple, L. DeLong, B. Sales. "Chapter 11 Kondo effect: Alloys and compounds". Handbook on the Physics and Chemistry of Rare Earths, Vol 1, Pages 797-846, (1978).
- [31] H. Morkoç. "Handbook of Nitride Semiconductors and Devices Vol 1, Materials Properties". Physics and Growth, ISBN: 978-3-527-40837-5, (2008).
- [32] I. Vurgaftman, J. R. Meyer, L. R. Ram-Mohan. "Band parameters for III–V compound semiconductors and their alloys". J. Appl. Phys. Vol 89. N°11, (2001).

- [33] V. Bougrov, M. E. Levinshtein, S. L. Rumyantsev, A. Zubrilov "In Properties of Advanced Semiconductor Materials GaN, AlN, InN, BN, SiC, SiGe". New York, 1-30, (2001).
- [34] M. Leszczynski, T. Suski, H. Teisseyre, P. Perlin, I. Grzegory, J. Jun, S. Porowski, T.D. Moustakas. "Thermal expansion of gallium nitride", J. Appl. Phys. 76, 8, 4909-4911, (1994).
- [35] F. Medjdoub, K. Iniewski. "Gallium Nitride (GaN) Physics, Devices, and Technology". CRC Press Taylor & Francis Group, ISBN-13: 978-1-4822-2004-9, (2016).
- [36] K. Boomer, L. Scheick, and A. Hammoud. "Body of Knowledge (BOK): Gallium Nitride (GaN) Power Electronics for Space Applications". Electronics And Electrical Engineering, (2019).
- [37] http://www.matprop.ru/GaP_basic.
- [38] S. Pyshkin and J. Ballato. "Properties of GaP Studied over 50 Years. In: Optoelectronics - Advanced Device Structures". IntechOpen, (2017).
- [39] S. Adachi. "Gallium Phosphide (GaP). In: Optical Constants of Crystalline and Amorphous Semiconductors". Springer, Boston, MA. 198-212, (1999).
- [40] P.B. Hart. "Gallium Phosphide. In: Waller, W.F. (eds) Electronics Design Materials". Macmillan Engineering Evaluations. Palgrave Macmillan, London. (1971).
- [41] http://www.matprop.ru/GaAs_basic.
- [42] A. D. Kramer. "Gallium and Gallium Arsenide: Supply, Technology, and Uses". 9208, (2009).
- [43] M. Brozel. "Gallium Arsenide. In: Kasap, S., Capper, P. (eds) Springer Handbook of Electronic and Photonic Materials". Springer Handbooks. Springer, Boston, MA. 499–536 (2006).
- [44] P. R. Morris. "Appendix D: Characteristics and applications of gallium arsenide". (1990).
- [45] J. E. Fisher, I. Bahl. "Gallium Arsenide IC Applications Handbook", (1995).
- [46] Dietl, M. Kaminska, H. Ohno. "Semiconductors and Semimetals". academic press, Spintronics, Volume 82, (2008).
- [47] F. Máca and J. Mašek. "Electronic states in $\text{Ga}_{1-x}\text{Mn}_x\text{As}$: Substitutional versus interstitial position of Mn". Phys. Rev. B 65, 235209, (2002).
- [48] G. Semenova and T. Sushkova. "Defect formation in manganese-doped III–V compounds". Russian Journal of Inorganic Chemistry. 55, 1930-1934, (2010).
- [49] R. G. W. Wyckhoff. "Crystal structures – volume 1". 7–83, (1963).

Chapter II: Ab-initio Study

II.1. Introduction

II.2. Ab-initio Theories

II.3. Computational Method

II.4. Representative Code of Calculation

II.5. Conclusion

II.1. Introduction

In the realm of ab-initio theories within the field of materials science, two prominent methods employed for understanding the electronic structure of atoms, molecules, and materials are the Hartree-Fock (HF) theory and Density Functional Theory (DFT). While HF theory approximates the wave function of a quantum system using a single Slater determinant and treats electrons as independent entities within an average field, DFT takes a more computationally efficient approach by focusing on the electron density rather than the wave function. To perform accurate calculations using these theories, advanced computational methods are essential. The Full-Potential Linearized Augmented Plane Wave (FLAPW) method is a widely used approach that offers a balanced treatment of electronic structure with high precision. Within this framework, the Wien2k code stands out as a powerful tool, leveraging the FPLAPW method to perform ab-initio calculations on a variety of materials, providing researchers with valuable insights into the intricate details of their electronic and structural properties. This combination of theoretical frameworks and computational tools plays a pivotal role in advancing our understanding of materials at the quantum level, contributing to the design and discovery of novel materials with tailored properties for diverse applications.

II.2. Ab-initio Theories

Both the Hartree-Fock (HF) theory and Density Functional Theory (DFT) are widely used ab-initio methods in the field of materials science and quantum chemistry. These methods are employed to study the electronic structure and properties of atoms, molecules, and materials at the quantum level.

II.2.1. Hartree-Fock Theory

Hartree-Fock (HF) theory serves as a foundational framework for understanding the electronic structure of atoms and molecules, utilizing a single determinant wave function to approximate complex many-electron systems. This approach, treating electrons as indistinguishable particles subject to the Pauli Exclusion Principle, simplifies the quantum mechanics many-body problem through a mean-field approximation.

While successful as a starting point for predicting molecular properties, HF inherent approximations necessitate more advanced methods to address electron correlation intricacies and enhance accuracy. The theory expresses the total electronic wave function as a single Slater determinant, embodying the antisymmetrization principle to adhere to the Pauli Exclusion Principle. This elegant concept captures key electronic interactions and lays the groundwork for more sophisticated quantum chemistry techniques. These are the steps and equations used to solve the HF problem for a molecular system using the Born-Oppenheimer approximation.

II.2.1.1. Douglas Rayner Hartree Approach

Douglas Rayner Hartree groundbreaking work in 1927 marked the introduction of the Hartree method [1], a significant step toward solving the Schrödinger equation for many-electron systems [2]. At its core, the Hartree method aimed to establish a self-consistent field (ψ) approximation for electrons in atoms [3].

The governing equation took the form:

$$H\psi = E\psi, \quad (1)$$

Where:

H : is the total molecular Hamiltonian operator, encapsulating the kinetic and potential energy terms associated with electrons.

ψ : is the molecular wave function, expressing the quantum state of the system.

E : is the total energy of the molecular system.

The total molecular Hamiltonian can be expressed as the sum of various terms:

$$H_{total} = T_n + V_{n-n} + V_{e-n} + V_{e-e} + T_e, \quad (2)$$

Where:

T_n : is the operator of kinetic energy nuclei.

V_{n-n} : is the nuclear-nuclear repulsion energy.

V_{e-n} : is the interaction energy between electrons and nuclei.

V_{e-e} : is the electron-electron repulsion energy.

T_e : is the operator of kinetic energy electrons.

II.2.1.2. Born-Oppenheimer approximation

The Born-Oppenheimer approximation separates the nuclear and electronic motion [4]. This allows the total molecular wave function to be approximated as the product of nuclear and electronic wave functions:

$$\psi(R, r) = \chi_{nuc}(R) \cdot \phi(r; R), \quad (3)$$

Where:

R : represents nuclear coordinates,

r : represents electronic coordinates,

χ_{nuc} : is the nuclear wave function,

ϕ : is the electronic wave function that depends parametrically on nuclear coordinates R ,

Assuming that electronic motion is much faster than nuclear motion, the total molecular Hamiltonian is written as follows:

$$H_{total} = T_e + V_{e-n} + V_{e-e}, \quad (5)$$

Therefore nuclear motion can be eliminated. The Born-Oppenheimer approximation yields a system of interacting electrons, posing an unsolvable many-body problem. Hence, another approximation is required [4].

The independent electron approximation models interacting electrons as non-interacting electrons in an effective potential created by all N electrons.

The single-electron wave function (Orbital) is represented as follows:

$$\psi_i(r) = \sum_{j=1}^N \phi_j(r) C_{ji}, \quad (6)$$

Here, ψ_i represents the (i – th) molecular orbital, ϕ_j is the (j – th) atomic orbital, and C_{ji} are the coefficients that determine the expansion of the molecular orbitals in terms of atomic orbitals.

II.2.1.3. Vladimir Aleksandrovich Fock Approach

Around 1930, Vladimir Aleksandrovich Fock made a significant independent contribution by formulating a method that complemented Hartree's work. Fock's efforts were particularly notable for enhancing the mathematical formalism underlying quantum mechanics [5]. In his work, Fock introduced a crucial concept involving the many-electron wave function (ψ), which he expressed as a Slater determinant [6]. This representation addressed the necessity for antisymmetry, aligning with the Pauli Exclusion Principle governing indistinguishable electrons. The Slater determinant for a system of N electrons is denoted as:

$$\psi(r_1, r_2, r_3, \dots, r_N) = \frac{1}{\sqrt{N!}} \begin{vmatrix} \phi_1(r_1)\phi_2(r_1) \dots \phi_N(r_1) \\ \phi_1(r_2)\phi_2(r_2) \dots \phi_N(r_2) \\ \dots \dots \dots \\ \phi_1(r_N)\phi_2(r_N) \dots \phi_N(r_N) \end{vmatrix}, \quad (7)$$

II.2.1.4. Combination of Hartree and Fock

In the 1950s, the Hartree and Fock methods were combined into the Hartree-Fock method, utilizing Hartree's self-consistent field idea and Fock's mathematical formalism [7]. The spinorbitals ϕ_j functions of the position (r_i) are the solutions of a system of coupled differential equations called Hartree-Fock equations:

$$\hat{F}_i \phi_i(r_i) = \epsilon_i \phi_i(r_i), \quad (8)$$

Where:

\hat{F}_i : is the Fock operator,

ϵ_i : is the Fock operator in the physical direction of opposite of the ionization potential,

In the case of atoms and molecules, the Fock operator uses it to express:

$$\hat{F}_i = -\frac{\hbar^2}{2m} \nabla_{r_i}^2 + \hat{V}_{eN}(r_i) + \sum_j \hat{J}_j - \hat{K}_j, \quad (9)$$

Where:

$\frac{\hbar^2}{2m} \nabla_{r_i}^2$: is the operator corresponds to the kinetic energy of electron i,

$\hat{V}_{eN}(r_i)$: is the electrostatic potential between this electron and the nucleus,

\hat{J}_j : is the Coulomb operator represents the average potential created by the other electrons,

\hat{K}_j : is the exchange operator,

II.2.1.5. Development of Computational Techniques

The advent of computers in the 1950s and 1960s revolutionized quantum chemistry, rendering the HF method computationally viable. This marked a pivotal shift from analytical to numerical solutions. The Self-Consistent Field (SCF), crucial to the method, was determined through iterative processes involving the solution of the HF equations [8].

The HF method, operating as an independent particle mean-field approximation, hinges on the self-consistency of the field. In this framework, the Fock operator (\hat{F}) relies explicitly on its own solutions. The SCF method emerged as the predominant iterative approach during this era. This method continually refines the molecular orbitals and the electron density, minimizing the total electronic energy. The iterative SCF method entails the following steps:

a) Initial Guess:

- ✓ Begin with an estimate of molecular orbitals, crucial for electron distribution.
- ✓ Use atomic orbitals or heuristic methods for the initial guess.

- ✓ Quality impacts efficiency and convergence in the iterative process.
- ✓ Thoughtful initial guesses accelerate reaching a self-consistent solution.
- ✓ Subsequent steps refine the guess, converging towards accurate orbitals and electron density.

b) Build the Fock Matrix:

- ✓ Fock matrix (\hat{F}) is the one-electron operator in HF.
- ✓ Influenced by average electron density, iteratively updated.
- ✓ Constructed from electron-electron repulsion and exchange terms: $\hat{F} = \hat{H} + \hat{J} - \hat{K}$,
- ✓ Integration of electron density and molecular orbitals refines the matrix.
- ✓ Iteratively constructed and diagonalized in the HF process.
- ✓ Convergence reached when minimal changes indicate self-consistency.

c) Solve the Hartree-Fock Equations:

- ✓ Eigenvalue equations from the variational principle.
- ✓ Expressed as: $\hat{F}_i \phi_i = \epsilon_i \phi_i$,
- ✓ Diagonalizing the Fock matrix transforms it, revealing orbital energies.
- ✓ Eigenvectors represent improved molecular orbitals.
- ✓ Orbital energies determine stability and occupation.
- ✓ Occupancy follows Pauli Exclusion Principle.
- ✓ Part of an iterative process updating electron density.
- ✓ Convergence achieved with minimal changes in orbitals and Fock matrix.

d) Iterative Process:

- ✓ Begin with initial molecular orbital guess.
- ✓ Construct electron density reflecting electron distribution.
- ✓ Build Fock matrix using the electron density.
- ✓ Diagonalize the Fock matrix for refined orbitals and energies.
- ✓ Update electron density based on new orbitals.
- ✓ Evaluate changes in electron density and orbital energies.
- ✓ If not converged, iterate; else, proceed to self-consistency.

- ✓ Self-consistency reached when minimal changes occur.
- ✓ Define convergence criteria for termination.
- ✓ Final orbitals and density represent accurate electronic structure.

e) Calculate Properties:

✓ **Total Electronic Energy:**

- ✧ Computed using final molecular orbitals.
- ✧ Includes kinetic energy, electron-nucleus, and electron-electron repulsion terms.
- ✧ Mathematically: $E_{\text{total}} = T_e + V_{e-n} + V_{e-e}$,

✓ **Ionization Potentials:**

- ✧ Energy to remove an electron, determined by molecular orbital energies.
- ✧ Calculated as negative Highest Occupied Molecular orbital (HOMO) energy.

✓ **Electron Affinities:**

- ✧ Energy change adding an electron, based on molecular orbital energies.
- ✧ Affinity for adding electron to Lowest Unoccupied Molecular Orbital (LUMO).

✓ **Visualization of Molecular Orbitals:**

- ✧ Gain insights into electron distribution.
- ✧ Visualize orbitals like HOMO and LUMO.

✓ **Dipole Moment:**

- ✧ Quantifies charge separation in a molecule.
- ✧ Calculated from molecular coordinates and charge distribution.

✓ **Electron Density:**

- ✧ Obtained from final molecular orbitals.
- ✧ Reveals electron probability distribution.

✓ **Bond Orders:**

- ✧ Indicate strength of chemical bonds.
- ✧ Derived from final electronic wavefunction.

✓ **Mulliken Population Analysis:**

- ✧ Partitions electron density between atoms.
- ✧ Provides charge distribution information.

- ✓ **Natural Bond Orbital (NBO) Analysis:**
 - ✧ Localized representation of molecular orbitals.
 - ✧ Identifies donor-acceptor interactions.
- ✓ **Charge Distribution:**
 - ✧ Determines charge distribution within a molecule.
- ✓ **Spin Density:**
 - ✧ Reveals electron spin distribution.
 - ✧ Relevant for radicals and magnetic properties.
- ✓ **Excited States and UV-Vis Spectra:**
 - ✧ Extends to calculate excited states and predict spectra.
 - ✧ Analyzes transitions between molecular orbitals.

The flowchart labeled as **Figure II.1** outlines a simplified algorithmic flow for the Hartree-Fock Self-Consistent Field (HF SCF) method.

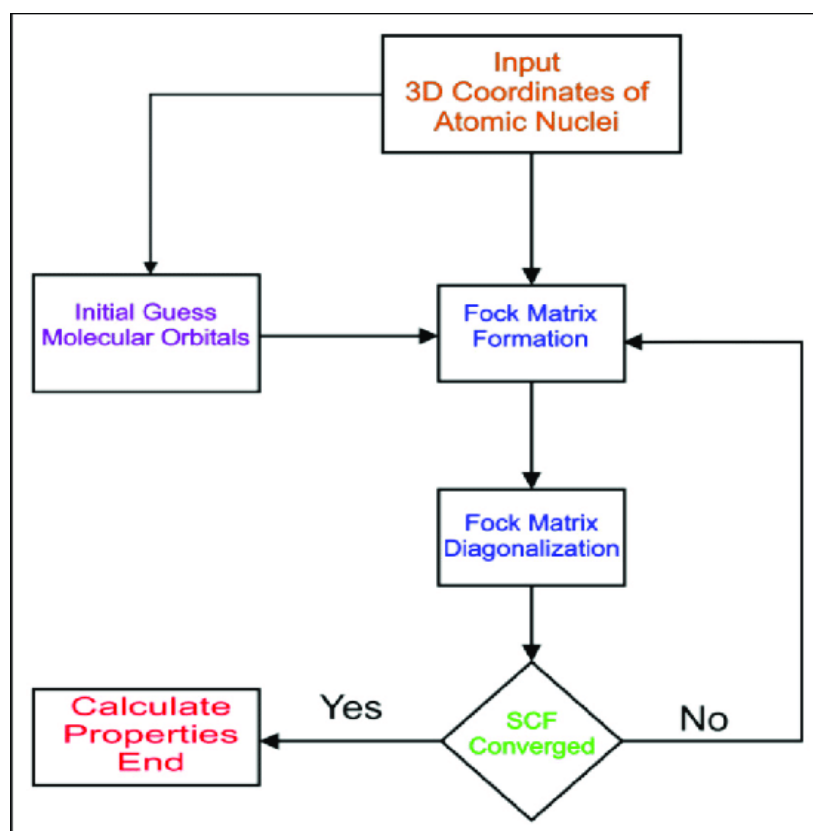


Fig. II.1: Simplified algorithmic flowchart for the HF SCF (Hartree-Fock Self-Consistent Field) method [9].

II.2.1.6. Expansion and Extensions

The HF method underwent a pivotal transformation, evolving from a foundational approach to a precursor for advanced post-HF techniques [10]. Recognizing the limitations of the mean-field approximation, these methods, including Configuration Interaction (CI), Coupled Cluster (CC), and Density Functional Theory (DFT), emerged to address electron correlation more accurately.

II.2.2. Configuration Interaction Theory

In the 1950s, Configuration Interaction (CI) methods emerged to overcome HF limitations in capturing electron correlation effects [11]. CI power lies in systematically incorporating electron correlation by expanding the wave function across multiple electronic configurations, leading to improved accuracy in electronic structure calculations.

The CI wave function, denoted as $|\psi_{CI}\rangle$, is expressed as a linear combination of Slater determinants, each representing a different electronic configuration:

$$|\psi_{CI}\rangle = \sum_i c_i |\phi_i\rangle, \quad (10)$$

Here:

$|\psi_{CI}\rangle$ is the CI wavefunction.

$|\phi_i\rangle$ represents the $(i - th)$ Slater determinant, corresponding to a specific electron configuration.

c_i are the coefficients (expansion weights) associated with each determinant, and they are determined by solving the CI eigenvalue problem.

The CI eigenvalue problem involves constructing and diagonalizing the Hamiltonian matrix within the chosen basis set of Slater determinants. The Hamiltonian matrix elements between different determinants represent the electronic energy contributions for those configurations.

The CI wave function aims to provide a more accurate representation of the true wave function by explicitly including contributions from different electron configurations. The accuracy of CI calculations improves as more determinants are included in the expansion. However, the computational cost increases rapidly with the size of the configuration space, making CI methods computationally demanding, especially for large systems.

CI methods have played a crucial role in quantum chemistry, serving as a foundation for many advanced electronic structure methods. While they are computationally expensive, they continue to be employed for accurate calculations of molecular properties, particularly in situations where strong electron correlation effects are significant.

II.2.3. Coupled Cluster Theory

In the 1960s, Fritz Coester and Herman Kümmel introduced Coupled Cluster (CC) theory, a transformative approach in quantum chemistry [12]. By expressing the correlated wave function as an exponential operator acting on a reference state, CC theory systematically addressed the limitations of the HF approximation, providing a powerful and accurate method for handling electron correlation effects. Its success in capturing strong correlation made CC theory widely adopted in quantum chemistry.

The CC wave function is represented as:

$$|\psi_{CC}\rangle = e^T |\phi_0\rangle, \quad (11)$$

Where: e^T is the cluster operator, and $|\phi_0\rangle$ is often the HF reference state. The exponential operator is expanded in a power series:

$$e^T = 1 + T + \frac{T^2}{2!} + \frac{T^3}{3!} + \dots, \quad (12)$$

The CC equations are obtained by projecting the Schrödinger equation onto the space spanned by these cluster operators, leading to a set of non-linear, coupled algebraic equations. For example, the CCSD (Coupled Cluster with Singles and Doubles) equations are:

$$\langle \phi_i^a | \hat{H} e^T | \phi_0 \rangle = 0, \quad (14)$$

$$\langle \phi_{ij}^{ab} | \hat{H} e^T | \phi_0 \rangle = 0 \quad (15)$$

Here, $|\phi_i^a\rangle$ and $|\phi_{ij}^{ab}\rangle$ represent singly and doubly excited determinants, respectively. The CC equations are typically solved iteratively to determine the cluster amplitudes (T).

The exponential Ansatz in CC theory allows for a systematic treatment of electron correlation, making it a powerful and widely used method for accurate quantum chemical calculations.

II.2.4. Møller-Plesset Perturbation Theory

Møller-Plesset Perturbation Theory (MPn) emerged in the 1930s and later developed in the 1950s as a perturbative approach to improve upon the limitations of the HF method. The method was named after its originators C. Møller and M. S. Plesset. MPn methods represent a significant milestone in the history of quantum chemistry, offering a systematic way to incorporate electron correlation beyond the HF level [13].

The MP2 correlation energy correction is given by:

$$E_{corr}^{(2)} = \sum_{ijab} \frac{\langle ij || ab \rangle \langle ab || ij \rangle}{(\varepsilon_i + \varepsilon_j) - (\varepsilon_a + \varepsilon_b)}, \quad (16)$$

The MP3 correction includes terms up to third order, introducing contributions from triple excitations. The MP3 correlation energy correction is expressed as follows:

$$E_{corr}^{(3)} = \sum_{ijkabc} \frac{\langle ijk || abc \rangle \langle abc || ijk \rangle}{(\varepsilon_i + \varepsilon_j + \varepsilon_k) - (\varepsilon_a + \varepsilon_b + \varepsilon_c)}, \quad (17)$$

Here:

i, j, k represent occupied orbitals.

a, b, c represent virtual (unoccupied) orbitals.

$\langle ijk || abc \rangle$ denotes three-electron integrals.

ε_i represents the orbital energy of orbital (i).

While MPn methods provide a systematic way to account for electron correlation effects, their computational cost increases with higher orders. The convergence of the series can be slow, particularly for systems with strong electron correlation. This limitation makes higher-order MPn calculations computationally demanding and impractical for large molecular systems.

MPn methods are part of the broader category of post-HF methods, and their historical development reflects a continuous effort to enhance the accuracy of electronic structure calculations.

II.2.5. Quasi-Degenerate Perturbation Theory (QDPT)

Quasi-Degenerate Perturbation Theory (QDPT) was developed as an extension of traditional perturbation theory to address challenges arising from nearly degenerate electronic states [14-16]. It emerged as a response to the limitations encountered when applying perturbation theory to systems with close-lying energy levels. QDPT allows for a more accurate treatment of near-degeneracies, making it particularly relevant in situations where standard perturbation theory may fail.

In perturbation theory, the energy correction ($E^{(n)}$) for the ($n - th$) order perturbation is given by:

$$E^{(n)} = \sum_i \frac{|\psi_i^{(0)} \langle \mathcal{V} | \psi \rangle|^2}{E_i^{(0)} - E}, \quad (18)$$

For quasi-degenerate systems, QDPT introduces a correction factor to address the near-degeneracy:

$$E_{QDPT}^{(n)} = \sum_i \frac{|\psi_i^{(0)} \langle \mathcal{V} | \psi \rangle|^2}{E_i^{(0)} - E} - \sum_{i \neq j} \frac{|\psi_i^{(0)} \langle \mathcal{V} | \psi_j^0 \rangle|^2}{E_j^{(0)} - E_i^{(0)}}, \quad (19)$$

Here:

$\psi_i^{(0)}$ and $E_i^{(0)}$ represent the unperturbed wavefunctions and energies.

$|\psi\rangle$ is the total wavefunction.

\hat{V} is the perturbing operator.

While QDPT provides improvements in handling near-degeneracies compared to standard perturbation theory, it may still face challenges in systems with very strong electron correlation. The method's effectiveness can be influenced by the nature and extent of correlation effects in the electronic structure.

The development of QDPT reflects ongoing efforts in quantum chemistry to refine perturbative approaches for a more accurate description of electronic states in various molecular systems.

II.2.6. Multi-Configurational Self-Consistent Field (MCSCF)

Multi-Configurational Self-Consistent Field (MCSCF) methods emerged in the mid-20th century as a response to the limitations of Configuration Interaction (CI) methods in handling electron correlation [17,18]. Pioneered by Robert Parr and coworkers, MCSCF allowed for a flexible treatment of electron correlation by incorporating multiple electronic configurations with variably weighted contributions [19]. This marked a significant step towards a more accurate and adaptable approach to quantum chemical calculations.

In MCSCF, the wave function is expressed as a linear combination of multiple configurations:

$$|\psi_{MCSCF}\rangle = \sum_i c_i |\phi_i\rangle, \quad (20)$$

Here:

$|\phi_i\rangle$ represents the (i - th) electronic configuration.

c_i are the coefficients determining the weight of each configuration, and are optimized self-consistently by variationally minimizing the energy.

The MCSCF energy is obtained by solving a generalized eigenvalue problem involving the Hamiltonian and overlap matrices. The optimization process involves adjusting the coefficients to find the combination of configurations that minimizes the total energy.

While MCSCF provides a more flexible treatment of electron correlation compared to CI, its limitation lies in the size of the configuration space. The number of configurations increases combinatorially with the number of electrons and orbitals, making the method computationally demanding and challenging for larger systems.

MCSCF methods laid the foundation for more advanced electronic structure methods, including Complete Active Space Self-Consistent Field (CASSCF) and its variants, where a specific subset of configurations is chosen to focus computational resources on the most relevant electronic correlations.

II.2.7. Density Functional Theory

DFT originated in the 1960s with pioneering contributions from Walter Kohn, Pierre Hohenberg, and Lu Sham [20,21]. However, it gained significant prominence in the 1980s with the development of the Kohn-Sham formulation [22,23]. Kohn and Sham's work, which earned them the Nobel Prize in Chemistry in 1998, provided a practical and powerful framework for applying DFT to real-world systems [24,25]. DFT has since become one of the most widely used methods in quantum chemistry and condensed matter physics.

II.2.7.1. Hohenberg-Kohn Theorem

In the 1960s, Pierre Hohenberg and Walter Kohn made groundbreaking contributions by formulating the Hohenberg-Kohn theorems, which laid the theoretical groundwork for DFT [26]. These theorems marked a significant departure from traditional many-body quantum mechanics by focusing on the electron density as the central variable.

The first theorem asserts that the external potential ($V_{ext}(r)$) acting on electrons is uniquely determined by the electron density ($n(r)$) in the system's ground state. Mathematically, this is expressed as:

$$(V_{ext}(r)) = V_{ext}[n(r)], \quad (21)$$

This theorem implies that if two different systems share the same ground-state electron density, they must also share the same external potential. The groundbreaking aspect is the

shift in focus from the wave function, a central concept in traditional quantum mechanics, to the electron density, making DFT a more practical and versatile method.

The second theorem states that the ground-state energy (E) of a quantum system is a unique functional of the electron density ($n(r)$). The energy functional is given by:

$$E[n] = \langle \psi | \hat{T} + \hat{V}_{ext} + \hat{V}_{ee} | \psi \rangle, \quad (22)$$

Here:

ψ represents the many-electron wavefunction.

\hat{T} is the kinetic energy operator.

\hat{V}_{ext} is the external potential.

\hat{V}_{ee} is the electron-electron interaction potential.

The second theorem establishes that the ground-state energy is uniquely determined by the electron density and, importantly, is a functional of this density. It provided a theoretical basis for the development of DFT, as it implied that all observable properties of a system are encoded in its electron density.

The Hohenberg-Kohn theorems opened the door to a new era in quantum chemistry, leading to the development of practical DFT methodologies, such as the Kohn-Sham formulation, which revolutionized computational quantum chemistry by offering an efficient and accurate approach to study the electronic structure of materials.

II.2.7.2. Kohn-Sham Formulation

In 1965, Walter Kohn and Lu Sham introduced the Kohn-Sham formulation, a monumental advancement in DFT following Hohenberg and Kohn's foundational theorems [27]. This formulation emerged as a response to the challenge of practically implementing DFT for real-world systems, offering a transformative solution to the complex many-body problem in quantum mechanics.

The Kohn-Sham formulation revolutionized computational quantum chemistry by transforming the intricate many-body problem into a set of single-electron equations. Its significance lies in its practicality, enabling accurate and efficient calculations of electronic structure for a broad range of materials.

At the core of the Kohn-Sham formulation are the Kohn-Sham equations, which are a set of single-electron equations. The central equation for a Kohn-Sham orbital (ψ_i) is given by:

$$\hat{H}_{KS}\psi_i = \varepsilon_i\psi_i, \quad (23)$$

Here:

\hat{H}_{KS} is the Kohn-Sham Hamiltonian.

ψ_i is a Kohn-Sham orbital.

ε_i is the orbital energy.

The Kohn-Sham Hamiltonian is composed of the kinetic energy, external potential, and an effective potential:

$$\hat{H}_{KS} = -\frac{1}{2}\nabla^2 + V_{ext}(r) + V_{eff}(r), \quad (24)$$

The effective potential (V_{eff}) is carefully designed to encapsulate the effects of electron-electron interactions, essentially simplifying the problem into a set of non-interacting electrons.

The Kohn-Sham formulation made DFT computationally feasible for a diverse array of systems. Its pragmatic approach allowed researchers to conduct accurate electronic structure calculations for molecules, solids, and materials. This method laid the groundwork for modern quantum chemistry simulations, influencing various scientific disciplines, including materials science, condensed matter physics, and computational chemistry. The Kohn-Sham formulation remains a cornerstone in the computational toolbox for understanding and predicting the properties of complex systems.

II.2.7.3. Exchange-Correlation Functional

The exchange-correlation functional in DFT approximates electron-electron interactions beyond the mean-field approximation. It combines exchange and correlation energies into a single mathematical expression, impacting the electronic structure calculation [28]. The choice of functional influences DFT's accuracy and efficiency, making it a critical component in diverse scientific applications.

The total energy E_{total} of a system within DFT can be expressed as the sum of the kinetic energy $T[n]$ of non-interacting electrons, the external potential V_{ext} from the atomic nuclei, and the exchange-correlation energy $E_{XC}[n]$:

$$E_{total} = T[n] + V_{ext}[n] + E_{XC}[n], \quad (25)$$

Here, n represents the electron density.

The accurate determination of $E_{XC}[n]$ is a challenging task due to the complexity of electron-electron interactions. Numerous exchange-correlation functionals have been developed to approximate $E_{XC}[n]$ and make DFT calculations practical. These functionals can be categorized into various types, including Local Density Approximation (LDA), Generalized Gradient Approximation (GGA), hybrid functional and more.

II.2.7.3.1. Local Density Approximation

In 1970, John Perdew and Alex Zunger made a significant contribution to DFT by proposing the Local Density Approximation (LDA) for the exchange-correlation energy. This marked a crucial step in the development of practical DFT methodologies and opened new possibilities for applying DFT to a wide range of real materials [29].

The LDA was a groundbreaking approximation that simplified the treatment of the exchange-correlation energy, a challenging component in DFT calculations. By introducing a local density-based approach, Perdew and Zunger provided a practical and computationally efficient way to apply DFT to real-world materials, making electronic structure calculations more accessible and applicable [30].

The LDA for the exchange-correlation energy is expressed as follows:

$$E_{XC}^{LDA}[n] = \int n(r) \varepsilon_{XC}^{LDA}(n(r)) dr, \quad (26)$$

Here:

$E_{XC}^{LDA}[n]$ is the exchange-correlation energy.

$n(r)$ is the electron density.

$\varepsilon_{XC}^{LDA}(n(r))$ is the exchange-correlation energy per particle at a given point in space.

In LDA, the exchange-correlation energy per particle is approximated as a function of the local electron density at each point in space, making the calculation computationally more feasible.

The introduction of LDA had a profound impact on the application of DFT to condensed matter physics and materials science. It provided a practical and efficient way to incorporate exchange-correlation effects into electronic structure calculations, enabling researchers to study the properties of materials, surfaces, and molecules with improved accuracy. The success of LDA spurred further developments in exchange-correlation approximations, contributing to the versatility and widespread adoption of DFT in the scientific community.

II.2.7.3.2. Generalized Gradient Approximation

In the 1980s, a significant stride in enhancing DFT was made by John Perdew, Jay P. Perdew and collaborators with the introduction of Generalized Gradient Approximation (GGA) for the exchange-correlation functional [31]. Building upon the foundations laid by LDA, GGA emerged to address the limitations of LDA in capturing spatial variations of electron density.

GGA significance lies in providing a more accurate description of exchange-correlation effects by considering spatial variations in electron density. This refinement enhances accuracy, especially for molecular systems and surfaces, where LDA may fall short. GGA represents a crucial step toward achieving better agreement between theoretical predictions and experimental observations.

GGA incorporates not just the electron density ($n(r)$) but also its gradient ($\nabla n(r)$) into the exchange-correlation energy density. The GGA exchange-correlation energy is expressed as:

$$E_{XC}^{GGA} = \int n(r) \varepsilon_{XC}^{GGA}(n, \nabla n) dr, \quad (27)$$

Common GGA functionals include PBE (Perdew, Burke and Ernzerhof) and BLYP [32] (Becke, Lee, Yang, and Parr).

The introduction of GGA has significantly improved the accuracy of DFT calculations, making it a standard choice for studying electronic structures of diverse materials. GGA functionals have become widely adopted in computational quantum chemistry and materials science, allowing researchers to make more reliable predictions and gain deeper insights into the behavior of molecular systems and surfaces.

II.2.7.3.3. Hybrid Functionals

Hybrid Functionals represent a further evolution in the development of exchange-correlation functionals within DFT. The concept of hybrid functionals was introduced independently by John P. Perdew, Alex Zunger (PBE0) [31], and Axel D. Becke (B3LYP) [33] in the 1990s. These functionals combine a fraction of Hartree-Fock (HF) exchange with the exchange-correlation functionals used in GGA, aiming to improve accuracy.

Hybrid functionals aim to balance the strengths of HF exchange, which accurately captures long-range interactions, with the efficiency of GGA functionals in describing short-range correlation. This results in improved accuracy for a wide range of molecular and material properties.

The general form of a hybrid functional is:

$$E_{XC}^{hybrid} = \alpha(E_X^{HF} - E_X^{GGA}) + E_X^{GGA}, \quad (28)$$

Here:

E_X^{HF} is the HF exchange energy.

E_X^{GGA} is the exchange energy from GGA.

E_{XC}^{GGA} is the exchange-correlation energy from GGA.

α is a parameter determining the fraction of HF exchange.

The development of hybrid functionals has significantly enhanced the accuracy of DFT calculations, making them a popular choice for studying molecular structures, electronic properties, and reaction mechanisms. The flexibility in adjusting the fraction of HF exchange allows researchers to tailor these functionals for specific systems or phenomena, expanding the utility of DFT in diverse scientific applications.

II.3. Computational Method

II.3.1. Full-Potential Linearized Augmented Plane Wave Method

The Full-Potential Linearized Augmented Plane Wave (FLAPW) method, a key player in density functional theory (DFT), excels in accurately describing the electronic structure of crystalline materials. Notably, it avoids the common muffin-tin approximation by treating the potential within a crystal as continuously varying, particularly beneficial in regions with significant electronic density variations near atomic cores. This deviation enhances accuracy and makes FLAPW a valuable computational tool for condensed matter physicists and materials scientists studying a diverse range of materials.

Here are the main components of the FLAPW method:

II.3.1.1. Introduction of Plane Waves

The use of plane waves gained prominence as a basis set for solving the Schrödinger equation in the context of solids [2]. This marked a shift in the approach to understanding the electronic structure of materials. Plane waves provide a natural basis for Fourier series expansion, allowing the representation of complex wavefunctions as a sum of simpler plane wave components. This expansion facilitates solving the Schrödinger equation for periodic systems [34].

The wave function (ψ) in the context of plane wave basis set can be expressed as a superposition of plane waves:

$$\psi(r) = \sum_G c_G e^{iGr}, \quad (29)$$

Where:

G represents reciprocal lattice vectors.

c_G are expansion coefficients determining the contribution of each plane wave.

This representation captures the periodic nature of the crystal lattice. The sum over reciprocal lattice vectors (G) allows for an efficient representation of the wave function, emphasizing the advantage of the plane wave basis set in dealing with periodic systems.

II.3.1.2. Augmented Plane Wave

In 1937, Slater introduced Augmented Plane Waves (APW) for solving single-electron equations, now synonymous with Kohn-Sham equations in DFT [7]. APW captures electron behavior in two regions: far from nuclei (described by plane waves) and near nuclei (described by spherical functions). The system is divided into non-overlapping spheres, each around centered an atomic nucleus, treating the region inside the sphere (muffin-tin region) differently from the Interstitial Region (IR). This allows for a more accurate representation of the potential near the atomic cores (**Figure II.2**).

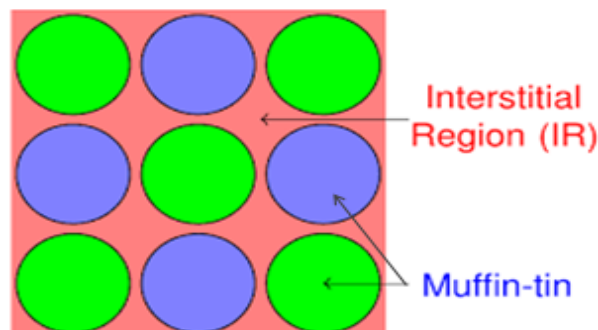


Fig. II.2: Schematic representation of interstitial and muffin-tin regions in crystallographic structure.

The Muffin-Tin Approximation (MTA) treats these potential and wave functions, assuming spherical symmetry and smoothness within spheres. The wave functions are expressed using radial solutions inside spheres and plane waves in the IR.

The wave function (ψ) is expressed as a combination of plane waves and augmented functions:

$$\psi(r) = \begin{cases} \sum_{LK} A_{LK} u_L(r) Y_{LK}(r) & r > R_{MT} \\ \frac{1}{\Omega^{1/2}} \sum_G c_G e^{i(G+K)r} & r < R_{MT} \end{cases}, \quad (30)$$

Here:

L represents quantum numbers.

Ω is the volume of the cell.

A_{LK} and c_G are the coefficients of the development in plane waves.

Y_{LK} is coefficients of the spherical harmonics.

$u_L(r)$ is the augmented wave function.

G are reciprocal lattice vectors.

The APW method, as initially formulated, faced challenges related to the radial function $u_L(r)$. To overcome these issues, several modifications were proposed, including those suggested by Koelling and Anderson [35]. The modification involves representing the wave function $\psi(r)$ inside the sphere as a linear combination of the radial functions $u_L(r)$ and their derivatives with respect to energy $u'_L(r)$, giving rise to the LAPW (Linear Augmented Plane Wave) method. This is called asymptote problem.

II.3.1.3. Linear Augmented Plane Wave

The LAPW (Linear Augmented Plane Wave) method, introduced by Anderson and Jepsen [36], to address non-linearity challenges in the APW method, introduces a linear

representation of the wave function (ψ) and its derivative with respect to energy ($\frac{d\psi}{dE}$) within the atomic sphere. This linearized approach, centered on the value of linearization energies $E_{L,i}$, enhances computational efficiency and stability compared to the APW method. The modification proposed by Koelling and Anderson, involving the Taylor series expansion of the radial function, has significantly improved the accuracy and flexibility of LAPW in describing electronic states near atoms, where the wave function undergoes notable variations[37]. The basis functions within muffin-tin spheres, combining radial functions ($U_L(r)$) and their energy derivatives $\frac{U_L(r)}{dE}$, contribute to a more accurate portrayal of electronic behaviors in crystalline materials. It's important to note that specific equations and implementation details may vary based on the chosen formulation of the LAPW method:

$$\psi(r) = \begin{cases} \sum_{LK} A_{LK} u_L(r, E_{L,1}) Y_{LK}(r) + B_{LK} w_L(r, E_{L,i}) Y_{LK}(r) & r > R_{MT} \\ \frac{1}{\Omega^{1/2}} \sum_G c_G e^{i(G+K)r} & r < R_{MT} \end{cases}, \quad (31)$$

B_{LK} is the same nature of A_{LK} which correspond to the function w_L .

Unlike the APW method, where the energy for each band needs to be calculated individually, the LAPW method achieves band energy determination with a single diagonalization step. This distinction highlights the computational efficiency of LAPW.

II.3.1.4. Full-Potential Approach

The Full Potential (FP) approach combines with the LAPW method to enhance the accuracy of electronic structure calculations. This integration allows for a comprehensive treatment of the potential, avoiding approximations in representing its shape, while also leveraging the benefits of LAPW methodology for efficient computations within atomic spheres and the interstitial region.

In the muffin-tin spheres, the potential is expanded using radial functions and spherical harmonics. This expansion allows for an accurate representation of the potential in the vicinity of atomic sites:

$$V_{eff}^{MT}(r) = \sum_{LK} V_{LK}(r) Y_{LK}(r), \quad (32)$$

In the interstitial region, a different treatment is applied to account for the smooth, periodic nature of the crystal lattice. The potential is typically expressed as a Fourier series:

$$V_{eff}^{inter}(r) = \sum_G V_G e^{iGr}, \quad (33)$$

This dual treatment ensures an accurate and efficient description of the potential throughout the crystal lattice, capturing both the localized effects near atomic sites and the periodic nature of the crystal lattice in the interstitial regions.

II.4. Representative Code of Calculation

Electronic structure calculations play a crucial role in understanding and predicting the properties of materials at the quantum level. Computational codes have become indispensable tools for researchers and scientists in the field of materials science, enabling them to simulate and analyze the behavior of electrons within solids. Several powerful codes have been developed, each employing diverse methodologies and algorithms. In this work, we used the FP-LAPW method, implemented in the Wien2k code.

Here's a **Table II.1** summarizing various ab initio theories and methods of calculation, along with some notable codes associated with each method:

| Ab Initio Theory | Method of Calculation | Codes of Calculation |
|---|--|--|
| Hartree-Fock (HF) | Gaussian Basis Sets | Gaussian, GAMESS, NWChem |
| Configuration Interaction (CI) | Gaussian Basis Sets | MOLPRO, GAMESS, NWChem |
| Coupled Cluster (CC) | Gaussian Basis Sets | PSI4, Molpro, CFOUR |
| Møller-Plesset Perturbation Theory (MP2) | Gaussian Basis Sets | Gaussian, GAMESS, NWChem |
| Quasi-Degenerate Perturbation Theory | Perturbation Expansion | MOLPRO, GAMESS, NWChem, DALTON |
| Multi-Configurational SCF (MCSCF) | Configuration Interaction with Multiple Configurations | Molpro, COLUMBUS, ORCA |
| Density Functional Theory (DFT) | Plane Waves, Pseudopotentials or All-electron | VASP, WIEN2k, Quantum ESPRESSO, GPAW, ABINIT |
| Exact Exchange (EXX) | Exchange-Only DFT Approximation | Octopus, WIEN2k, FHI-aims |
| Tight-Binding (TB) | Empirical Tight-Binding | DFTB+, ATK-DFTB, NEMO |
| Linear Scaling DFT | Divide and Conquer Approaches | BigDFT, ONETEP, PARSEC |
| Range-Separated Hybrid Functionals | Long-Range and Short-Range Corrections | NWChem, Gaussian, Orca |
| Bethe-Salpeter Equation (BSE) | Excitonic Effects in Materials | Yambo, BerkeleyGW, Quantum ESPRESSO |
| irac Equation Solvers | Relativistic Electronic Structure | DIRAC, YAMBO, ADF (with ZORA) |
| Non-Equilibrium Green's Function (NEGF) | Transport Properties | ATK, Nanocal, QuantumATK |
| Extended Hückel Theory (EHT) | Semi-Empirical Method | MOPAC, Hückel |
| Complete Active Space (CAS) | Multiconfigurational Wave Functions | MOLPRO, PySCF, COLUMBUS |
| Wannier Functionals | Construction of Tight-Binding Models | Wannier90, Quantum ESPRESSO (Wannier) |
| Electron Localization Function (ELF) | Analysis of Electron Pairing | AIMAll, Multiwfn, VASP (LOBSTER) |

Tab. II.1: Overview of ab-initio theories and computational methods in materials science.

II.4.1. Wien2k Code

The WIEN simulation code originated at the Institute of Materials Chemistry, Vienna University of Technology. First published in 1990 by P. Blaha, K. Schwarz, P. Sorantin and S. Tricky, it initially ran on UNIX or LINUX platforms [38]. Over the years, it underwent

revisions with version names like WIEN93, WIEN95, and WIEN97. The 2000 release became known as "Wien2k." Wien2k is based on FP-LAPW methods in DFT, featuring independent FORTRAN90 programs and C-shell scripts for program integration. Input files, starting with "case.struct," detail structural parameters, and subsequent commands generate necessary inputs for a SCF calculation.

The calculation procedure in WIEN2k involves a series of well-defined steps to determine the electronic structure of a material. Below is a general outline of the calculation procedure:

First Step: Preparation of the structure files:

This involves preparing the structure file (case.struct) based on ab-initio data, including lattice parameters, atomic positions, and the number of non-equivalent atoms.

Second Step: Initialization:

This step executes a series of auxiliary programs to produce inputs for the main programs:

- **NN:** Calculates distances between nearest neighbors and determines the atomic sphere radius, controlling sphere overlap.
- **SGROUP:** Determines the space group and point group of the given structure.
- **SYMMETRY:** Generates symmetry operations and expansion angular momentum quantum numbers for spherical harmonics.
- **LSTART:** Produces electron densities of free atoms, specifying how different orbitals are treated in band structure calculations.
- **KGEN:** Generates a mesh of k-points in the irreducible Brillouin Zone (BZ).
- **DSTART:** Produces an initial density for the SCF cycle.

Third Step: Execution of the SCF Cycle:

Once input files are prepared, the SCF calculation converges energy, density, and potential. Sub-programs in the SCF cycle include:

- **LAPW0:** Generates the potential from the density.
- **LAPW1:** Calculates valence bands through eigenvalue and eigenvector diagonalization.

- **LAPW2**: Computes valence densities from eigenvectors and Fermi energy.
- **LCORE**: Determines core energies and states.

Figure II.3 illustrates the organizational structure of programs within the WIEN2k package, a widely used code for performing electronic structure calculations based on the Full-Potential Linearized Augmented Plane Wave (FLAPW) method. The organization chart outlines the interconnections and dependencies between different programs within WIEN2k.

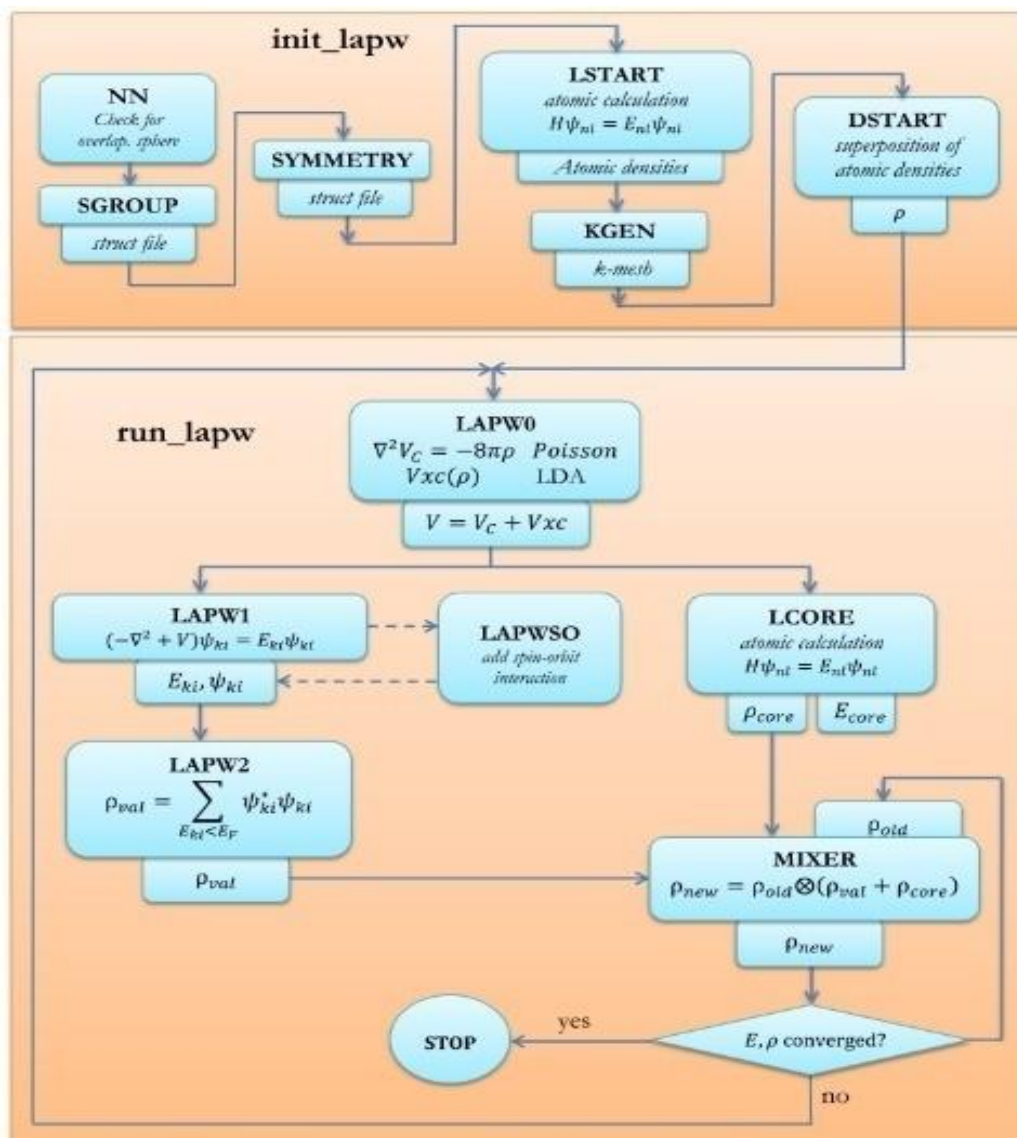


Fig. II.3: Organization chart of programs in WIEN2k [39].

II.5. Conclusion

The synergy of ab-initio theories like Hartree-Fock (HF) and Density Functional Theory (DFT) with the Full-Potential Linearized Augmented Plane Wave (FLAPW) method, implemented in the Wien2k code, has propelled materials science to new heights. This integrated approach achieves success by accurately predicting electronic structures and material properties. Its idealism lies in bridging theory and experiment, allowing for the design of novel materials. Credibility is bolstered by the robust mathematical foundations of HF, the efficiency of DFT, and the precision of FLAPW. In summary, this combination is a powerful and reliable tool shaping the exploration of advanced materials and their tailored functionalities.

References

- [1] D. R. Hartree. "The Wave Mechanics of an Atom with a Non-Coulomb Central Field". *Mathematical Proceedings of the Cambridge Philosophical Society*, 01(24), 89 – 110, (1928).
- [2] E. Schrödinger. "An Undulatory Theory of the Mechanics of Atoms and Molecules". *Phys. Rev.* 28, 1049-1070 (1926).
- [3] B. Swirles. "The Relativistic Self-Consistent Field". *Proceedings of the Royal Society of London. Series A, Mathematical and Physical Sciences*, 152(877), 625-649, 1935.
- [4] M. Born, J.R. Oppenheimer. "Zur Quantentheorie der Molekeln". *Annalen Physik*, 389, 457-484, (1927).
- [5] V. A. Fock, "Näherungsmethode zur Lösung des quantenmechanischen Mehrkörperproblems". *Zeitschrift für Physik*, 61, 126-148, (1930).
- [6] J. C. Slater. "Note on Hartree's Method". *Phys. Rev.* 35 (2), 210–211, (1930).
- [7] J. C. Slater, "A Simplification of the Hartree-Fock Method". *Physical Review*, 81 (3), 385–390, (1951).
- [8] J.C. Slater. "Quantum Theory of Molecules and Solids, Symmetry and energy bands in crystals ". Vol 2, (1965).
- [9] P. Auburger. "Ab-initio investigation of dissociative electron attachment to halogenated hydrocarbons on the ice surface". *Chemistry, Environmental Science*, (2020).
- [10] P. Piecuch, A. E. Kondo, V. Špirko, J. Paldus. "Molecular quadrupole moment functions of HF and N₂. I. Ab initio linear-response coupled-cluster results". 12, 4716-4727, (1996).
- [11] A. Bunge. "Electronic Wave functions for Atoms. III. Partition of Degenerate Spaces and Ground State of C". *Journal of Chemical Physics* (1970).
- [12] R. Bartlett. "Coupled-cluster theory and its equation-of-motion extensions". *Wiley Interdisciplinary Reviews: Computational Molecular Science*, 2(1), 126-138, (2012).
- [13] C. Møller and M.S. Plesset. "Note on an Approximation Treatment for Many-Electron Systems". *Phys. Rev.* 46, 618–622, (1934).
- [14] C. Angeli, R. Cimiraglia, S. Evangelisti, T. Leininger, J.P. Malrieu, "Introduction of n-electron valence states for multireference perturbation theory". *The Journal of Chemical Physics*. 114 (23), 10252, (2001).
- [15] C. Angeli, R. Cimiraglia, J.P. Malrieu. "N-electron valence state perturbation theory: A fast implementation of the strongly contracted variant". *Chemical Physics Letters*, 350 (3–4), 297, (2001).
- [16] C. Angeli, R. Cimiraglia, J.P. Malrieu, "N-electron valence state perturbation theory: A spinless formulation and an efficient implementation of the strongly contracted and of the partially contracted variants". *The Journal of Chemical Physics*. 117 (20), 9138, (2002).

- [17] G. P. Robert, D. P. Craig, I. G. Ross. "Molecular Orbital Calculations of the Lower Excited Electronic Levels of Benzene, Configuration Interaction included". *Journal of Chemical Physics*. 18 (12): 1561–1563, (1950).
- [18] J. Christopher and Cramer. "Essentials of Computational Chemistry". Chichester: John Wiley & Sons, Ltd, 191–232, (2002).
- [19] R. G. Parr. "On the genesis of a theory". *Int. J. Quantum Chem.* 37 (4): 327–347. (1990).
- [20] N. Argaman, G. Makov. "Density functional theory: An introduction". *American Journal of Physics* 68, 69-79, (2000).
- [21] S. Sousa, P. Fernandes, M. Ramos. "General performance of density functionals". *J. Phys. Chem. A*, 111, 42, 10439–10452, (2007).
- [22] P. Suryanarayana, V. Gavini, T. Blesgen, K. Bhattacharya, M. Ortiz. "Non-periodic finite-element formulation of Kohn–Sham density functional theory". *Journal of the Mechanics and Physics of Solids*. (2010).
- [23] N. Hadjisavvas, A. Theophilou. "Rigorous formulation of the Kohn and Sham theory". *Journal of the Mechanics and Physics of Solids*, 58(2), 256-280, (2010).
- [24] A. M. Sarry, M. F. Sarry. "On the density functional theory". *Physics of the Solid State*, 54, 1315-1322, (2012).
- [25] J. Sordo. "Computational contributions to chemistry, biological chemistry and biophysical chemistry: the 2013 Nobel Prize in Chemistry". *Analytical and Bioanalytical Chemistry*, 406(7), 1825-8, (2014).
- [26] P. Hohenberg and W. Kohn. "Inhomogeneous Electron Gas". *Phys. Rev.* 136, B864 (1964).
- [27] W. Kohn and L.J. Sham. "Self-Consistent Equations Including Exchange and Correlation Effects". *Phys. Rev.* 140, A1133, (1965).
- [28] R. Baer and D. Neuhauser. "Density functional theory with correct long-range asymptotic behavior". *Physical Review Letters*, 94(4), 043002, (2005).
- [29] J.P. Perdew and A. Zunger. "Self-Interaction Correction to Density-Functional Approximations for Many-Electron Systems". *Physical Review B*, 23, 5048-5079, (1981).
- [30] I. Y. Zhang, X. Xu. "A New-Generation Density Functional: Towards Chemical Accuracy for Chemistry of Main Group Elements". Part of the book series: SpringerBriefs in Molecular Science, (2014).
- [31] P. B. Ernzerhof. "Generalized Gradient Approximation Made Simple". *Phys. Rev. Lett.* 77, 3865, (1996).
- [32] M.W. Gill, Peter, G. B. Johnson, A. J. Pople, J. M. Frisch. "The performance of the Becke Lee Yang Parr (BLYP) density functional theory with various basis sets". *Chemical Physics Letters*, 197, 4–5, 499-505, (1992).
- [33] A. D. Becke. "Density-functional exchange-energy approximation with correct asymptotic behavior". *Phys. Rev. A*, 38(6), 3098-3100, (1988).
- [34] L. Dong. "Existence theorems for the 2D quasi-geostrophic equation with plane wave initial conditions". *Nonlinearity*, 22(7), 1639, (2009).

- [35] D.D. Koelling and J.S. Anderson. "Improved First-Principles Calculation of the Electronic Structure and Magnetic Properties of Ferromagnetic bcc Fe". *Journal of Physics C: Solid State Physics*, 10, 3107-3114, (1977).
- [36] O. K. Andersen and O. Jepsen. "Linear Methods in Band Theory". *Phys. Rev. Lett.* 53, 2571-2574, (1984).
- [37] R. Carbó-Dorca, E. Besalú. "Generalized quantum similarity and DFT-Molecular electron density functionals: foundations, current advances, and applications". *Journal of Mathematical Chemistry*, 49(4),836-842, (2011).
- [38] P. Blaha, K. Schwarz, P. Sorantin, and S. B. Tricky. "WIEN2k: An Augmented Plane Wave Plus Local Orbitals Program for Calculating Crystal Properties". *Computer Physics Communications*, 59, 399-415, (1990).
- [39] <https://cygutz.readthedocs.io/en/latest/overview.html>

Chapter III: Results and Discussions

III.1. Introduction

III.2. Calculation Details

III.3. Magnetic Configurations

III.4. Stable Crystal Structure of GaN, GaP and GaAs

III.5. Properties of GaN, GaP, GaAs

III.6. Magnetic Supercell

III.7. Properties of Ga_{1-x}MnxN(P, As)

III.8. Effect of Exchange and Correlation Interactions

III.9. Conclusion.

III.1. Introduction

In this chapter, we delve into the computational exploration of key properties in Dilute Magnetic Semiconductors (DMS), focusing on compounds such as GaMnN, GaMnP, and GaMnAs, all of which exhibit the zinc blende crystal structure. Our investigations utilize the LAPW method implemented in the Wien2k computational code for our calculations. To account for the exchange-correlation term, we employ both the standard PBE functional and hybrid functionals, denoted as PBE+E, where the "E" signifies exact exchange treatment to accurately capture the behavior of correlated electrons. We systematically vary the Hartree-Fock exchange (α) parameter to probe the intricate interplay between electronic structure and magnetic properties in these materials.

III.2. Calculation details

The calculations were conducted utilizing the WIEN2k computer package of Two-Dimensional Optimize [1], employing the FP-LAPW method (Full Potential Linearized Augmented Plane Wave). For addressing the exchange-correlation potential, hybrid functionals were chosen, bridging the gap between DFT theory and Hartree-Fock theory, renowned for yielding results in concordance with experimental findings, especially in strongly correlated systems. Hybrid methodologies, akin to the DFT+U method, adhere to the following approach: partition the system into two subsystems. One caters to weakly correlated electrons (s and p electrons) and is treated using the standard method (PBE in our case). The other accommodates strongly correlated electrons (d electrons) and is addressed through the Hartree-Fock approximation. Three functionals were utilized in this context: the standard PBE functional, parameterized by Perdew, Burke, and Ernzerhof, applied to weakly correlated electrons; and two hybrid functionals, one involving on-site exact exchange and the other being an on-site hybrid functional.

Given that hybrid functionals operate on the same principles as the PBE+U functional, it was deemed more fitting to designate them as PBE+E for the first and PBE+H for the second.

For spin polarized calculations, the PBE+E parameterization was used, which combines for the PBE (Perdew, Burke and Ernzerhof) method with an onsite exact-exchange treatment for

correlated electrons. This approximation effectively considered the exchange and correlation effect. The onsite exact-exchange energy expression as defined by Novák et al [2] can be represented as:

$$E_{XC}^{DFT} = E_{XC}^{DFT+E}[\rho] + (\alpha E_{XC}^{HF}[\varphi] - E_{XC}^{DFT}[\rho]), \quad (1)$$

Where (ρ) represents the electron density, (φ) denotes the wave function and (α) signifies the fraction of HF exchange, which can take on either a short-range or long-range value [3]. The long-range value of HF exchange up to 50% is required to obtain acceptable thermo chemistry for the Local Spin Density Approximation (LSDA) [4]. In the Generalized Gradient Approximation (GGA) of PBE, typically uses a short-range value of $\alpha=0.25$ it has been theoretically deduced and this choice has proven notable success [5,6].

The wave functions and potential are expanded using Muffin-tin approach with a cutoff $I_{\max} = 9$. For the Interstitial Region (IR), a cutoff $R_{\min} = 8$ is employed. The chosen cut-off energy is 10^{-3} Ryd which separates core states from valence states. For first-consistent results, 1000 k-points are used in the first Brillouin zone.

The atomic spheres radii and the electronic configurations of the Ga, Mn, N, P and As atoms are shown in **Table III.1**:

| Atoms | Electronic Configurations | Atomic Spheres Radii |
|-----------|---------------------------|----------------------|
| Ga | $4s^2 4p^1 3d^{10}$ | 1.95 |
| Mn | $4s^2 3d^5$ | 1.99 |
| N | $2s^2 2p^3$ | 1.45 |
| P | $3s^2 3p^3$ | 1.55 |
| As | $4s^2 4p^3 3d^{10}$ | 1.65 |

Tab. III.1: Electronic configurations and atomic spheres radii of Ga, Mn, N, P and As atoms.

III.3. Magnetic Configurations

The **Figure III.1** shows the different magnetic phases corresponding to the five magnetic configurations, nonmagnetic (nm), ferromagnetic (fm $\uparrow\uparrow\uparrow$), and three antiferromagnetic states afmI ($\uparrow\uparrow\downarrow\downarrow$), afmII ($\uparrow\downarrow\uparrow\downarrow$), and afmIII ($\uparrow\downarrow\downarrow\uparrow$) according to the configuration mentioned by Krause and Bechstedt [7].

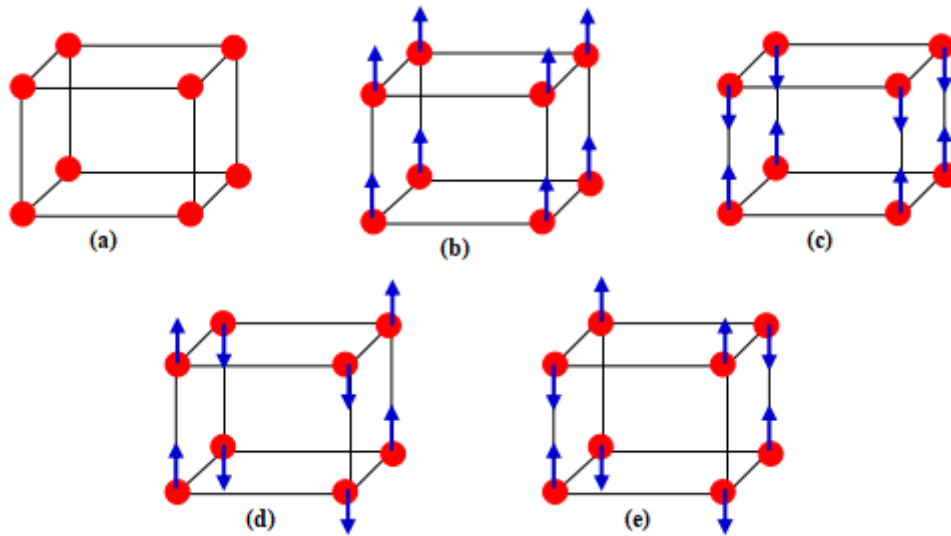


Fig. III.1: Representation of magnetic configurations, (a) nm, (b) fm, (c) afmI, (d) afmII and (e) afmIII.

III.4. Stable Crystal Structure of GaN, GaP and GaAs

GaAs and GaP are semiconductor materials that adopt the zinc blende crystal structure, whereas GaN crystallizes in the wurtzite structure. In our calculations, we focused on the zinc blende structure, also known as the sphalerite structure, to analyze their electronic properties.

The zinc blende structure is characterized by its arrangement of two interpenetrating Face-Centered Cubic (FCC) sub-lattices. One sub-lattice consists exclusively of Ga atoms, while the other sub-lattice comprises atoms labeled as X, which can be N in the case of GaN, P in the case of GaP or As in the case of GaAs. These two sub-lattices are offset from each other by a vector $(1/4, 1/4, 1/4)$ of the unit cell.

This crystal structure is illustrated in **Figure III.2**, where the FCC arrangement and the positioning of Ga and X atoms demonstrate the symmetry and periodicity of the zinc blende lattice. This arrangement is crucial for understanding the band structure and electronic behavior of these semiconductors, particularly in relation to their optical and electronic properties.

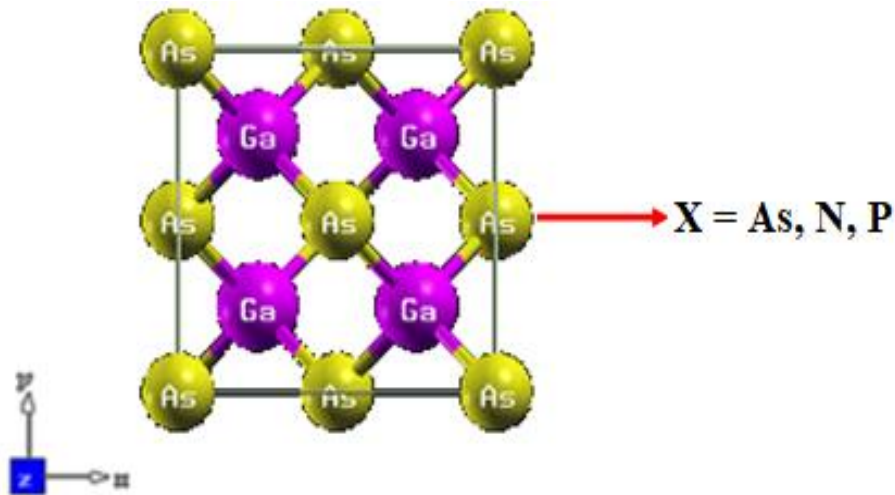


Fig. III.2: The unit cell of GaX (X = N, P, As) in the zinc blende structure.

III.5. Properties of GaN, GaP and GaAs

III.4.1. Structural Properties

Figure III.3 illustrates the total energy variation corresponding to the calculated volume using the PBE method for various magnetic configurations (nm, fm, afmI, afmII, afmIII) of GaN, GaP and GaAs. Notably, convergence is observed across all magnetic configurations, indicating that both non-magnetic and anti-ferromagnetic states converge towards the ferromagnetic state.

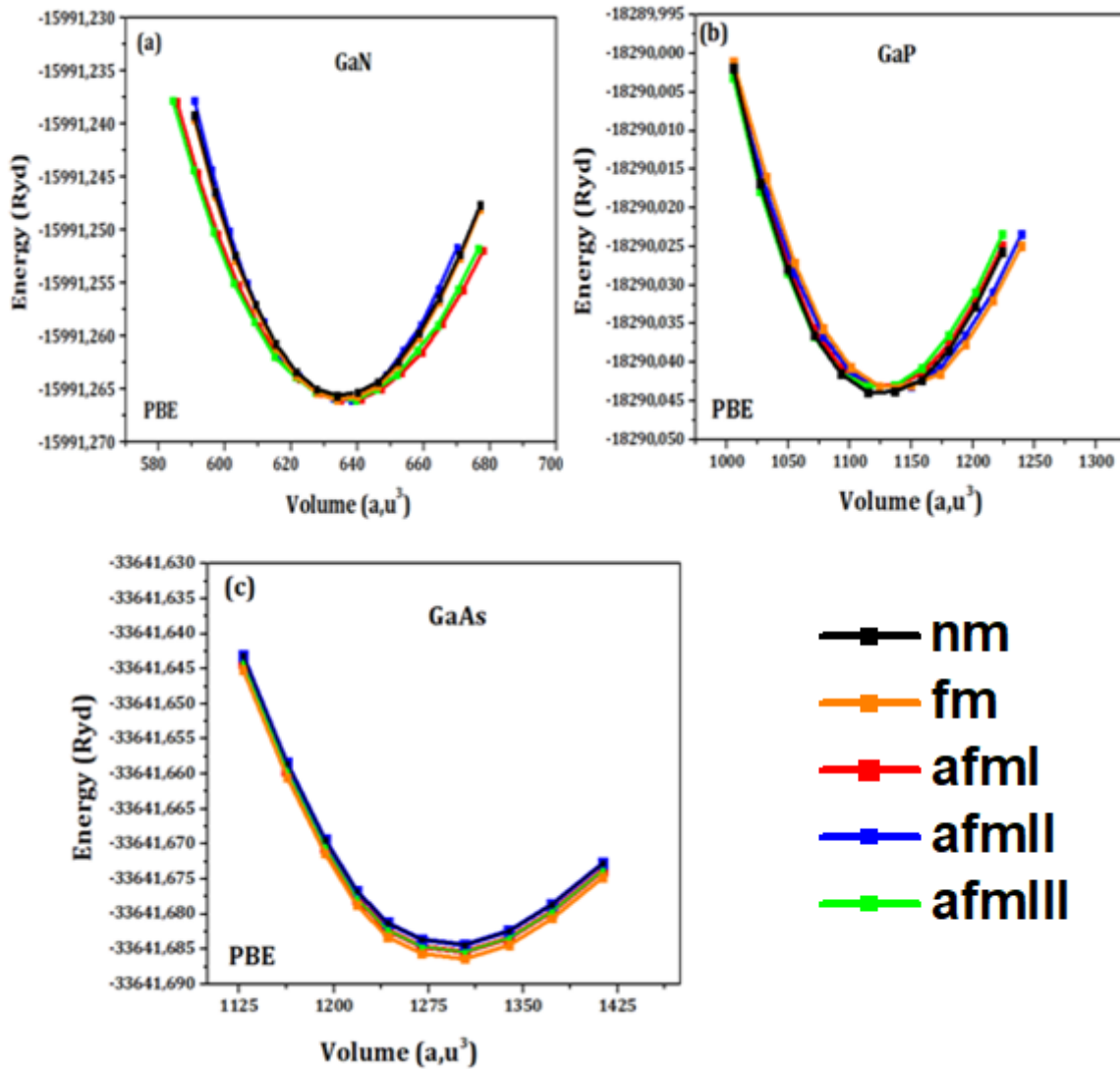


Fig. III.3: Variation of the total energy as a function of volume calculated using the PBE method for different magnetic configurations.

The precision of our calculations relies on selecting the right empirical parameter, denoted as α . The identification of an optimal α value, specifically set at 3% for GaN, 4% for GaP and 5% for GaAs, guarantees the accuracy of our results. It's worth noting that when α falls below these values, convergence is evident among the five magnetic configurations, aligning with the characteristics of the PBE method.

Figure III.4 illustrates the total energy variation across various magnetic configurations, computed using the PBE+E method and based on the calculated volume.

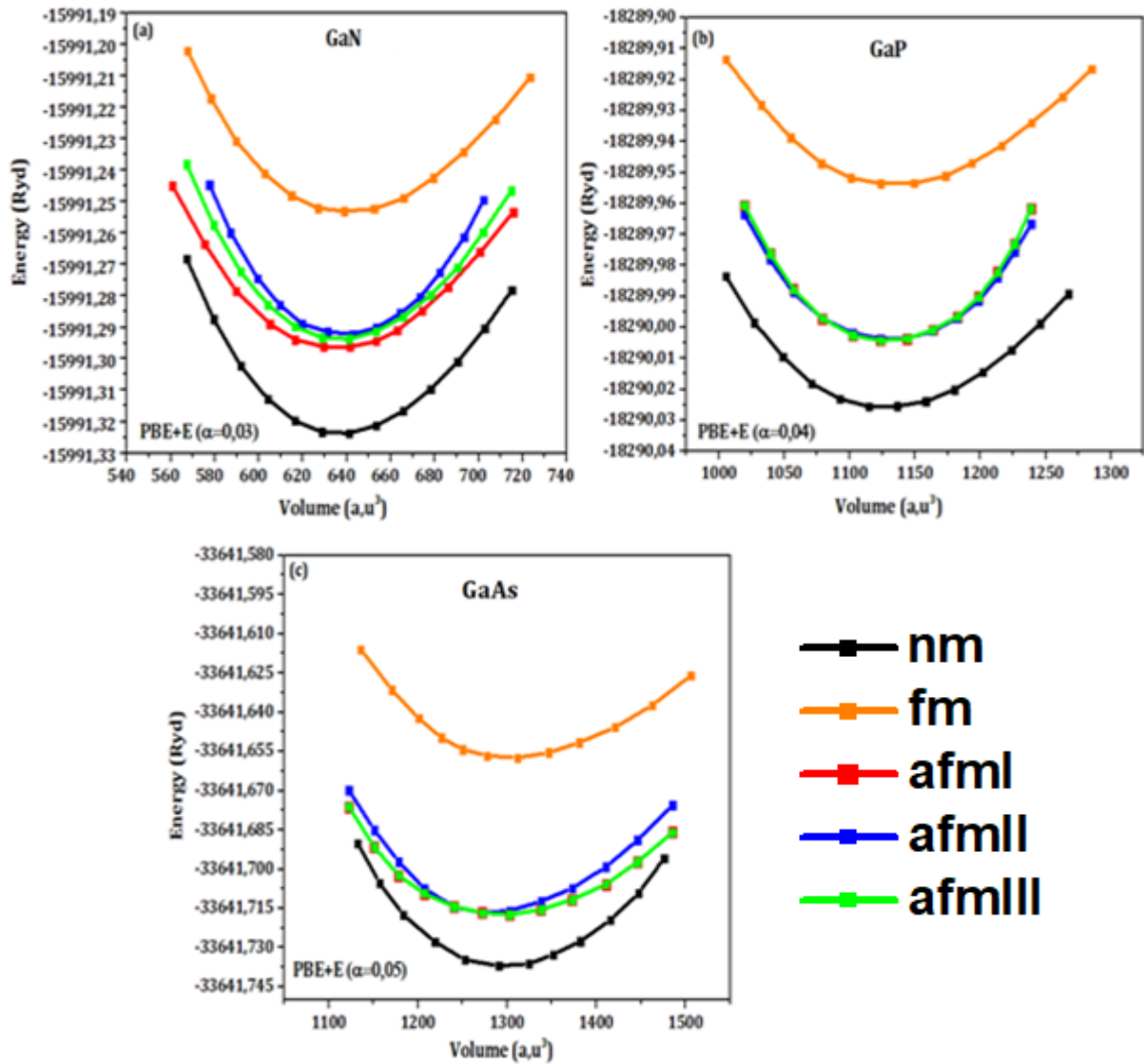


Fig. III.4: Variation of the total energy as a function of volume calculated using the PBE+E method for different magnetic configurations.

Upon analyzing the total energy variation computed using the PBE+E method, it becomes clear that the most stable magnetic state corresponds to the non-magnetic phase (nm). This particular phase displays the lowest total energy, signifying its stability. Consequently, for the GaX series, the ground state at room temperature demonstrates a non-magnetic behavior, with the exchange portion representing 3%, 4% and 5% of the exact exchange for GaN, GaP and GaAs respectively.

The variation of total energy with the change in the volume is fitted using the Birch-Murnaghan equation [8], given by Formula:

$$E(V) = E_0 + \frac{B_0 V_0}{B'} \left[\left(\frac{V_0}{V} \right)^{B'} - 1 \right], \quad (2)$$

Where:

E_0 is the energy of the ground state.

V_0 is the volume at the ground state.

B is the compressibility modulus, determined by $B = (B_0 V_0)^{B'}$

At the optimized volume, we have determined crucial structural parameters, including the lattice constant (a), bulk modulus (B), and the derivative of the bulk modulus (B'), as summarized in **Table III.2**.

| Materials | Parameter | This works | Other works | Exp [12-16] |
|----------------------------------|-----------------------------|--------------|-------------|----------------|
| | | PBE+E | PBE [9-11] | |
| GaN(nm) $\alpha=0.03$ | a (A°) | 4,56294 | 4.582 | 4.50 |
| | B (Gpa) | 179.333 | 162.2 | 203.7 |
| | B' | 4.357 | 4.29 | 4.3 |
| | E_{Tot}(Ryd) | -15991.32361 | / | / |
| GaP(nm) $\alpha=0.04$ | a (A°) | 5,48660 | 5.52 | 5.4505 |
| | B (Gpa) | 76.488 | 76.58 | 88.19 |
| | B' | 4.428 | 4.674 | 4.79 |
| | E_{Tot}(Ryd) | -18290.02659 | / | / |
| GaAs(nm) $\alpha=0.05$ | a (A°) | 5.76173 | 5.747 | 5.65325 |
| | B (Gpa) | 60.414 | 60.22 | 75.50 |
| | B' | 4.564 | 4.81 | 4.487 |
| | E_{Tot}(Ryd) | -33641.73723 | / | / |

Tab. III.2: Structural properties of GaN, GaP and GaAs with the PBE+E method.

Based on **Table III.2**, our results obtained with the PBE+E method exhibit favorable agreement with those from the PBE method and other available theoretical calculations, with

differences not exceeding 10%. However, in comparison with experimental results, we note an overestimation for the parameter (a), while the modulus of compressibility (B) is underestimated. Nevertheless, there is a noticeable convergence in results for the derivative of the modulus of compressibility (B').

III.4.2. Electronic Properties

The band structures and total density of states of GaN, GaP and GaAs obtained by the PBE+E method are illustrated in **Figures (III.5, III.6 and III.7)**.

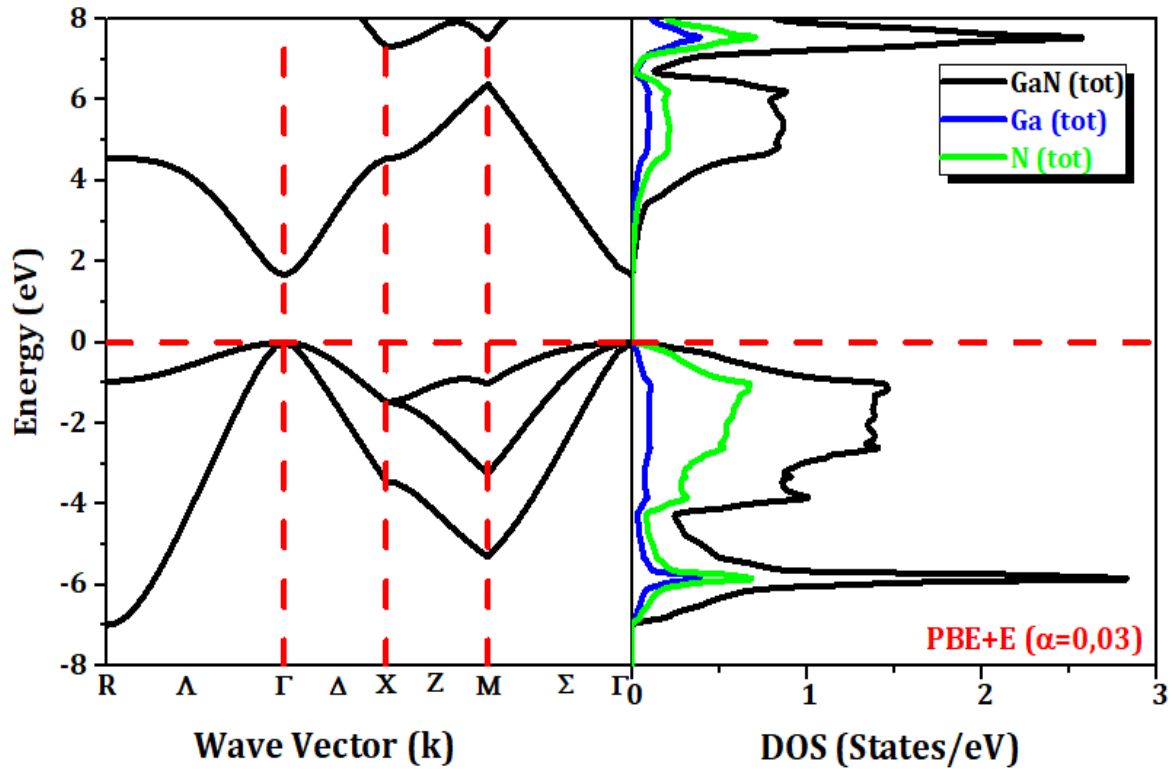


Fig. III.5: Band structure and density of state of binary compound GaN calculated by the PBE+E ($\alpha=0.03$) method.

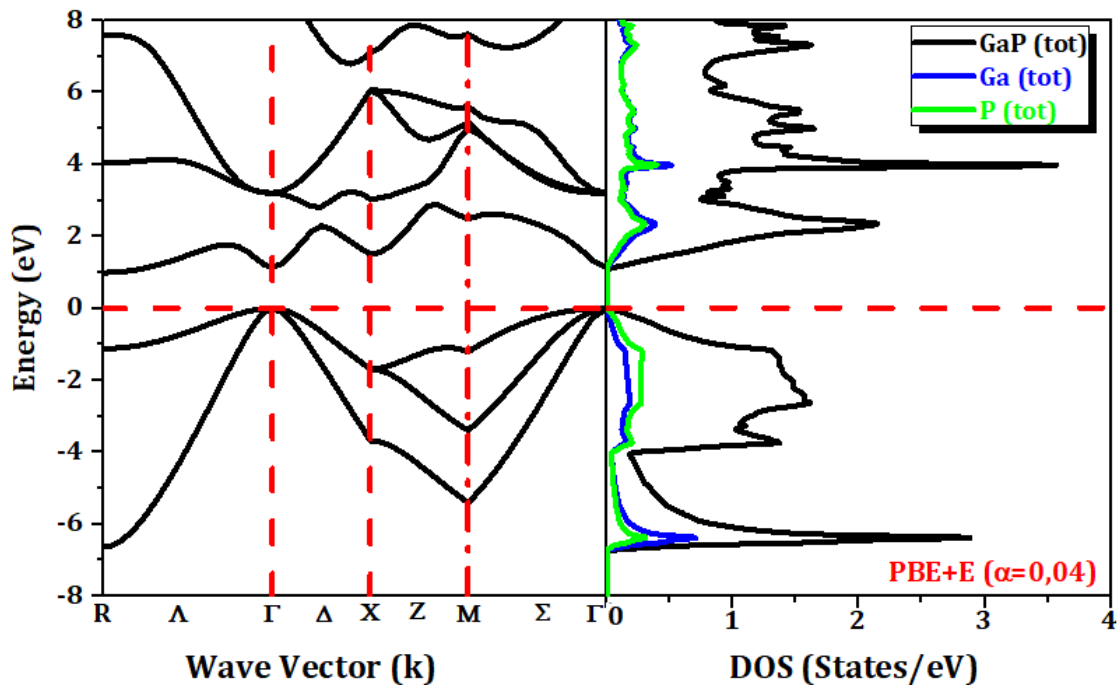


Fig. III.6: Band structure and density of state of binary compound GaP calculated by the PBE+E ($\alpha=0.04$) method.

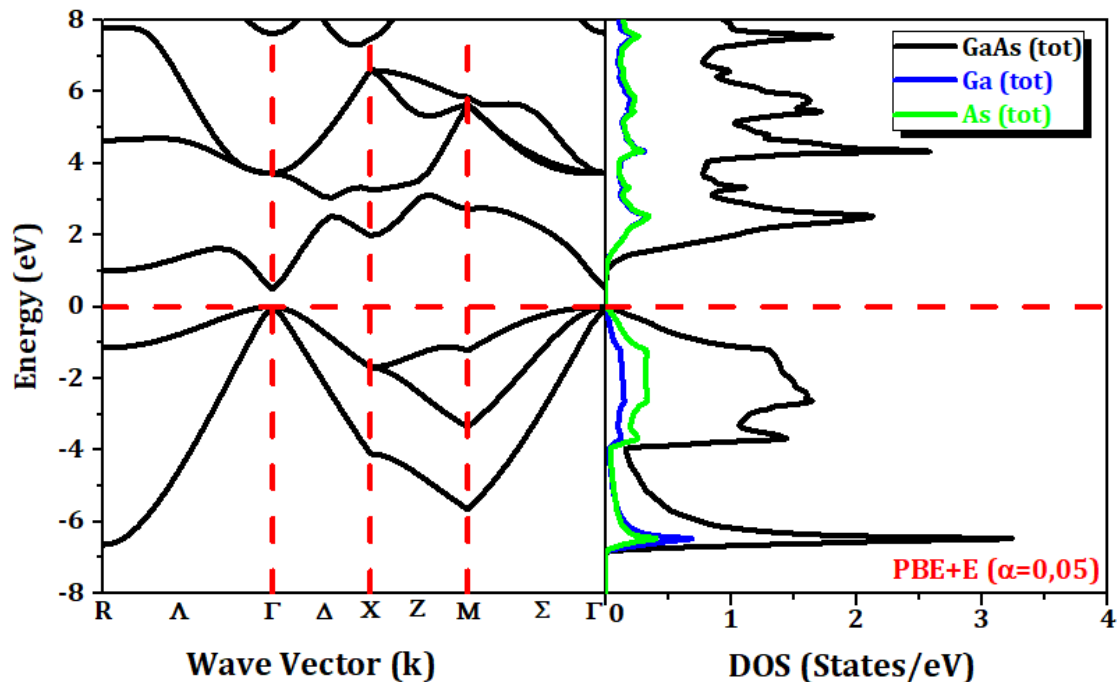


Fig. III.7: Band structure and density of state of binary compound GaAs calculated by the PBE+E ($\alpha=0.05$) method

According to the **Figures (III.5, III.6 and III.7)** and the band structures, we observe that GaN and GaAs have direct band gaps. This means that the minimum of the conduction band and the maximum of the valence band occur at the same point in k-space, specifically at the Γ (Gamma) point, which is at the center of the Brillouin zone. In other words, an electron can transition directly from the valence band to the conduction band (or vice versa) without any change in momentum, making these materials particularly efficient for optoelectronic applications .

In contrast, GaP exhibits an indirect band gap. This means that the minimum of the conduction band and the maximum of the valence band occur at different points in k-space. Specifically, for GaP, the minimum of the conduction band is located at the R point, while the maximum of the valence band is at the Γ point. In an indirect band gap semiconductor, an electron transition between the valence band and the conduction band requires a change in momentum, which typically involves a phonon to conserve momentum. This makes indirect band gap materials like GaP less efficient for light-emitting applications compared to direct band gap materials.

In the density of states (DOS) of GaP and GaAs, we observe that the states of the Ga atom and the states of the P (in GaP) or As (in GaAs) atom contribute similarly to the formation of the conduction bands. This indicates that both types of atoms have a significant presence in the conduction band states, suggesting a mixed character in these bands.

However, in the valence bands, there is a clearer distinction in the contributions from the different atoms. Specifically, certain regions of the valence bands are predominantly formed by the states of the Ga atom, while other regions are primarily formed by the states of the P (in GaP) or As (in GaAs) atom. This separation indicates that the valence band has distinct regions where the electronic states are largely influenced by one type of atom over the other.

In contrast, for GaN, both the conduction bands and the valence bands are mainly formed by the states of the N atom. This implies that the N atom plays a dominant role in the electronic structure of both bands, indicating a stronger localization of electronic states around the N atoms compared to Ga atoms. This difference can significantly influence the electronic and optical properties of GaN compared to GaP and GaAs.

The gap values are provided in **Table III.3** and are compared with experimental values and other values calculated using the PBE method.

| Materials | Parameter | This works | Other works | Exp [20] |
|---------------------------|-------------------|------------|-------------|----------|
| | | PBE+E | PBE [17-19] | |
| GaN(nm) $\alpha=0.03$ | E_c^Γ (eV) | 1,66684 | / | / |
| | E_v^Γ (eV) | -0,00161 | / | / |
| | E_g (eV) | 1.66845 | 1.517 | 3.299 |
| GaP(nm) $\alpha=0.04$ | E_c^R (eV) | 0,99166 | / | / |
| | E_v^Γ (eV) | -0.000039 | / | / |
| | E_g (eV) | 0.991699 | 0.91 | 2.35 |
| GaAs(nm) $\alpha=0.05$ | E_c^Γ (eV) | 0,49767 | / | / |
| | E_v^Γ (eV) | -0.000036 | / | / |
| | E_g (eV) | 0.4977 | 0.4 / 0.51 | 1.519 |

Tab. III.3: Electronic properties of GaN, GaP and GaAs calculated with PBE+E method.

According to the **Table III.3**, our findings show excellent consistency with theoretical results obtained through various methods, indicating strong agreement across different theoretical approaches. However, they appear to underestimate the values observed in experimental studies. This discrepancy suggests that while our theoretical calculations align well with predictions from other methodologies, experimental measurements indicate a slightly larger or different gap than what our theoretical framework predicts. This discrepancy between theory and experiment highlights the ongoing challenge in accurately predicting material properties and emphasizes the importance of experimental validation in confirming theoretical predictions.

III.6. Magnetic Supercell

To develop the magnetic structure from the zincblende structure, we need to increase the size of the cells. Starting with a 1x1x1 supercell, which contains 8 atoms: 4 atoms of Ga and 4 atoms of As, P or N, we obtain a cubic lattice (P) for this supercell.

The initial supercell is a simple cubic unit cell with the formula GaX (where X = As, P, or N). This cubic lattice can be visualized as having Ga and X atoms arranged alternately in a three-dimensional grid.

When we replace Ga atoms with Mn atoms in varying proportions, we can study the impact on the magnetic properties of the material. Specifically, we replace Ga atoms with Mn at 25%, 50%, and 75% substitution levels.

25% Mn Substitution: Replace 1 Ga atom with Mn. The resulting formula is $\text{Ga}_{0.75}\text{Mn}_{0.25}\text{X}$.

50% Mn Substitution: Replace 2 Ga atoms with Mn. The resulting formula is $\text{Ga}_{0.50}\text{Mn}_{0.50}\text{X}$.

75% Mn Substitution: Replace 3 Ga atoms with Mn. The resulting formula is $\text{Ga}_{0.25}\text{Mn}_{0.75}\text{X}$.

The **Figure III.8** below illustrates this process.

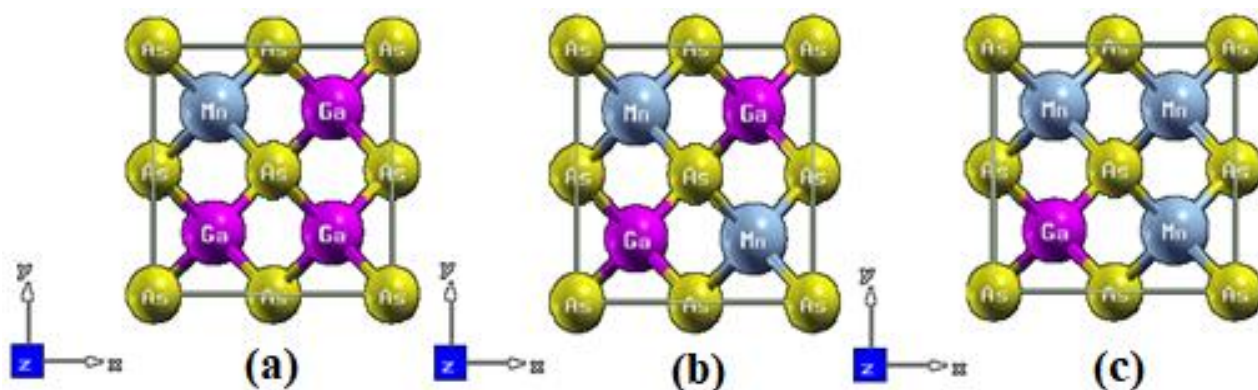


Fig. III.8: Representation of the supercell with (a) 25%, (b) 50% and (c) 75% Mn substitution in GaX (X = As, N, P).

III.7. Properties of $\text{Ga}_{1-x}\text{Mn}_x\text{N(P, As)}$

III.7.1. Structural Properties

To ascertain the ground state of GaMnX (X = N, P, and As), the total energy was optimized using the Birch-Murnaghan equation of state, applying both the PBE and PBE+E methods. This optimization process is critical for determining the magnetic states of alloy materials, as it enables a thorough exploration of the total energy-volume relationship, which is particularly important for magnetic alloy systems.

Figures (III.9, III.10, and III.11) illustrate this relationship for three specific alloys: $\text{Ga}_{0.75}\text{Mn}_{0.25}\text{X}$, $\text{Ga}_{0.50}\text{Mn}_{0.50}\text{X}$, and $\text{Ga}_{0.75}\text{Mn}_{0.25}\text{X}$. These figures consider both spin-polarized and non-spin-polarized configurations, highlighting the differences in total energy as a function of volume for each composition. The energy optimization results reveal the preferred magnetic states and the stability of these alloys, providing key insights into their electronic and magnetic properties.

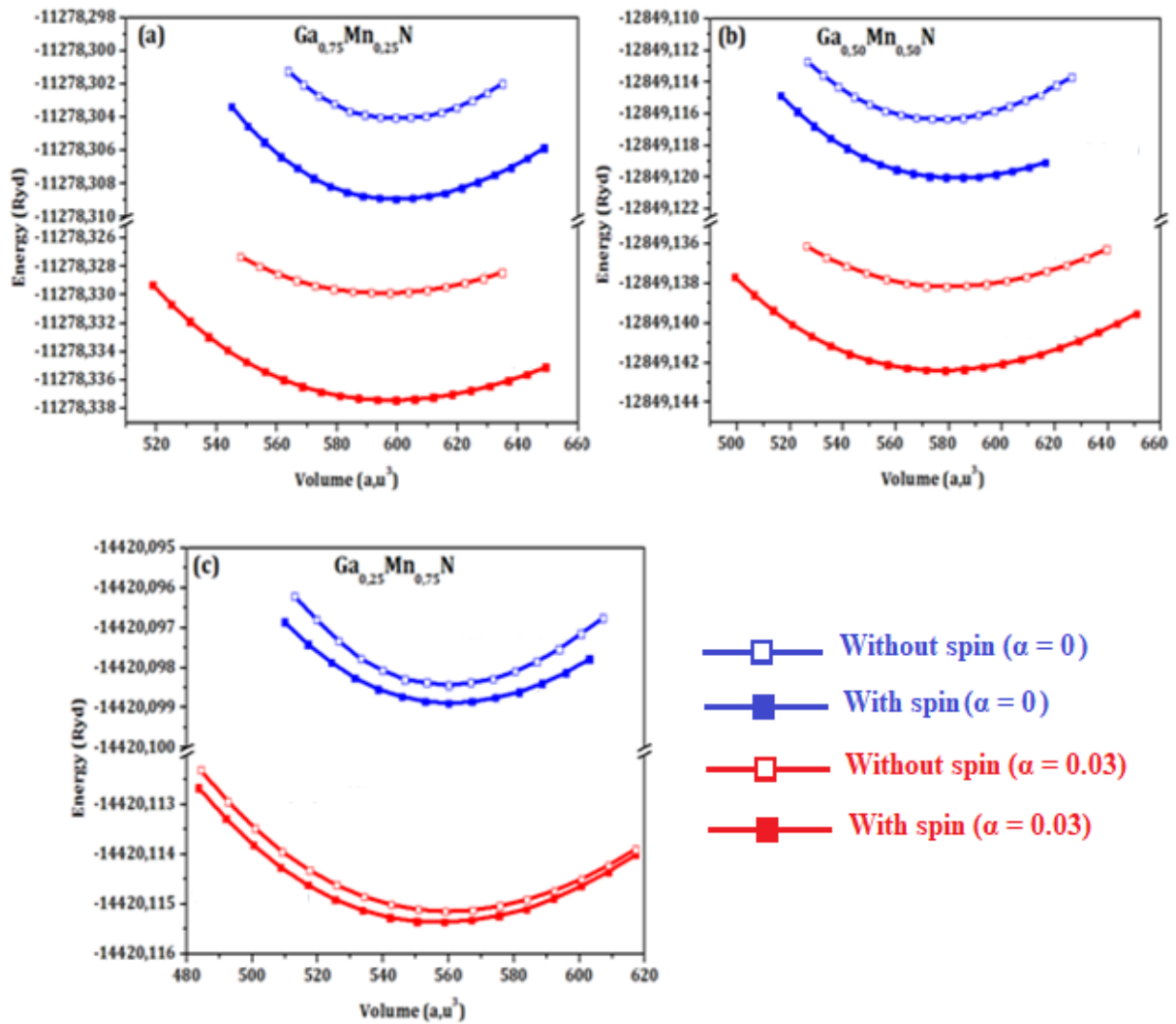


Fig. III.9: Variation of the total energy as a function of volume calculated using the PBE+E method of $\text{Ga}_{1-x}\text{Mn}_x\text{N}$.

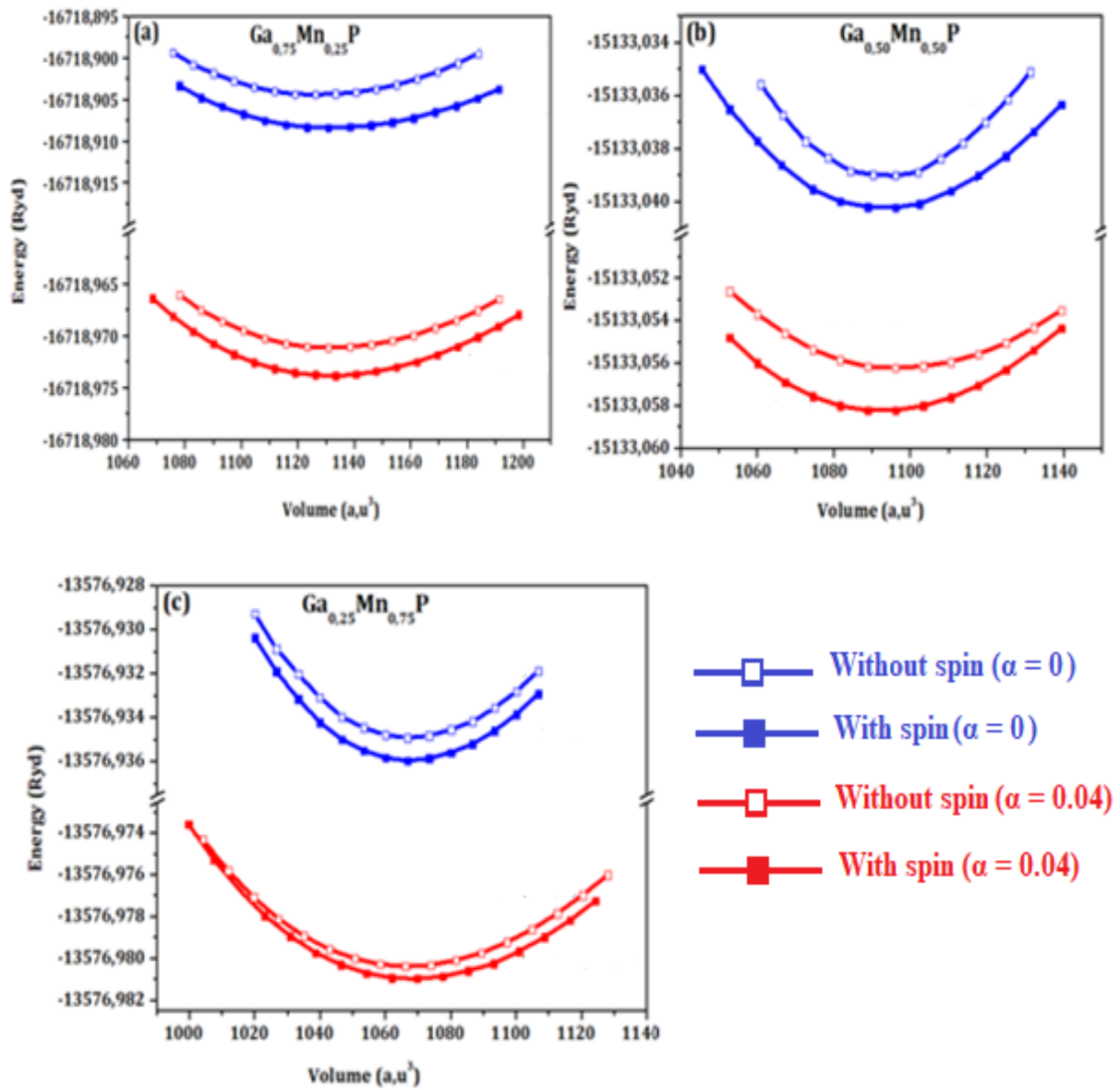


Fig. III.10: Variation of the total energy as a function of volume calculated using the PBE+E method of $\text{Ga}_{1-x}\text{Mn}_x\text{P}$.

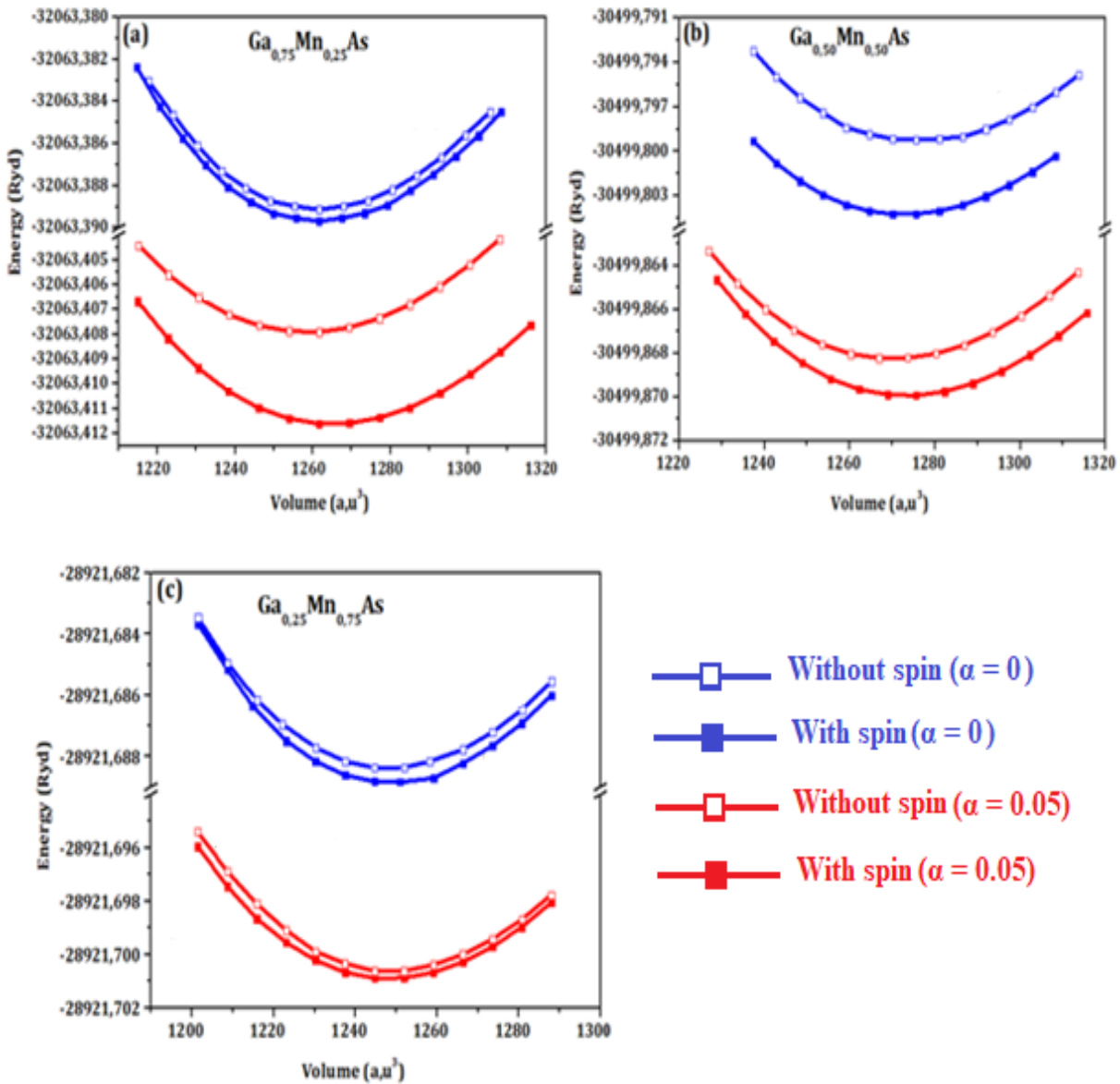


Fig. III.11: Variation of the total energy as a function of volume calculated using the PBE+E method of $\text{Ga}_{1-x}\text{Mn}_x\text{As}$.

In the provided **Figures (III.9, III.10 and III.11)**, the stability of various phases within the alloy system is evaluated by comparing their total energies. A lower total energy indicates a more stable phase, indicating a configuration of atoms and spins that is energetically favorable. Specifically, we can assess the stability of different compositions by examining the trends in total energy across the range of α value.

The consistently minimal total energy observed at specific α values, such as $\alpha = 0.03$ for GaMnN, $\alpha = 0.04$ for GaMnP and $\alpha = 0.05$ for GaMnAs, across all three curves indicates that these compositions correspond to the most stable phases within their respective alloy systems. This observation suggests that these particular compositions exhibit energetically favorable configurations of atoms and spins, reinforcing the assertion of a ferromagnetic ground state for these compounds.

By identifying the α values associated with the lowest total energy for each alloy system, we can infer the most stable compositions within the GaMnN, GaMnP, and GaMnAs alloys systems. These findings provide valuable insights into the energetically preferred configurations of these alloy systems, supporting the understanding of their magnetic and structural properties.

This observation can be further analyzed in the context of phase diagrams, which depict the stable phases of a material system. The occurrence of a minimum in the total energy curve corresponds to a thermodynamically stable phase, indicating the prevalence of ferromagnetic behavior in the ground state of the alloy at this specific composition.

In the context of spin-polarized configurations, a ferromagnetic ground state indicates that the majority of spins are aligned in the same direction, resulting in a net magnetic moment and overall ferromagnetic behavior. The fact that α phase exhibits the lowest total energy suggests that this composition fosters the most favorable conditions for ferromagnetic ordering in the alloy system.

Table III.4 encompasses diverse structural parameters, including lattice constants (a) and (c), bulk modulus (B), and the derivative of the bulk modulus (B').

| Parameters | $\text{Ga}_{0.75}\text{Mn}_{0.25}\text{N}$ | | $\text{Ga}_{0.5}\text{Mn}_{0.5}\text{N}$ | | $\text{Ga}_{0.25}\text{Mn}_{0.75}\text{N}$ | |
|---------------|---|---------------------|---|---------------------------|---|---------------------------|
| | PBE+E ($\alpha = 0.03$) | Other works [20] | PBE+E ($\alpha = 0.03$) | Other works [21,22] | PBE+E ($\alpha = 0.03$) | Other works [21,22] |
| a(A°) | 4,46205 | 4.425 | 4.39096 | 4.401 | 4,35849 | 4.315 |
| B(GPa) | 205.735 | 213 | 229.99 | 125.564 | 210.18 | 916.618 |
| B' | 5.331 | 4.60 | 5.524 | 1.562 | 5.291 | 38.222 |
| E(Ryd) | -11278,33728 | / | -12849,14236 | / | -14420,11536 | / |
| | $\text{Ga}_{0.75}\text{Mn}_{0.25}\text{P}$ | | $\text{Ga}_{0.5}\text{Mn}_{0.5}\text{P}$ | | $\text{Ga}_{0.25}\text{Mn}_{0.75}\text{P}$ | |
| | PBE+E ($\alpha = 0.04$) | Other works [23] | PBE+E ($\alpha = 0.04$) | Other works [23] | PBE+E ($\alpha = 0.04$) | Other works [23] |
| a(A°) | 5.52719 | 5.49 | 5.45601 | 5.45 | 5.41186 | 5.42 |
| B(GPa) | 110.731 | 80.25 | 115.522 | 67.76 | 117.901 | 82.64 |
| B' | 5.113 | 5.00 | 5.320 | 5.00 | 5.455 | 5.00 |
| E(Ryd) | -16718,97583 | -16718.97382 | -15133,05821 | -7566.52912 | -13576,98092 | -13576.98096 |
| | $\text{Ga}_{0.75}\text{Mn}_{0.25}\text{As}$ | | $\text{Ga}_{0.5}\text{Mn}_{0.5}\text{As}$ | | $\text{Ga}_{0.25}\text{Mn}_{0.75}\text{As}$ | |
| | PBE+E ($\alpha = 0.05$) | Other works [23] | PBE+E ($\alpha = 0.05$) | Other works [23] | PBE+E ($\alpha = 0.05$) | Other works [23] |
| a(A°) | 5.71801 | 5.69 | 5.74897 | 5.73 | 5.69228 | 5.71 |
| B(GPa) | 119.155 | 76.98 | 129.997 | 53.03 | 110.184 | 67.58 |
| B' | 5.312 | 5.00 | 5.320 | 5.00 | 5.455 | 5.00 |
| E(Ryd) | -32063,41161 | -32063.40666 | -30499,86993 | -15249.93495 | -28921,70078 | -28921.70088 |

Tab. III.4: Structural properties of $\text{Ga}_{1-x}\text{Mn}_x\text{N}$, $\text{Ga}_{1-x}\text{Mn}_x\text{P}$ and $\text{Ga}_{1-x}\text{Mn}_x\text{As}$ with PBE+E method.

When Mn atoms are introduced into the crystal lattice of GaN, GaP or GaAs, they can substitute for Ga atoms in some of the lattice sites. This substitution occurs because Mn and Ga have similar chemical properties, allowing Mn to occupy some of the positions typically occupied by Ga atoms.

In these semiconductor materials, Ga typically occupies certain lattice sites within the crystal lattice structure. However, when Mn atoms are incorporated into the lattice, they can take the place of Ga atoms due to their smaller size.

Due to the smaller size of Mn atoms compared to Ga atoms, the effective size of the unit cell decreases as more Mn atoms are incorporated. This reduction in size leads to a decrease in the lattice constant.

When P atoms are substituted with As or N atoms in the crystal lattice, the smaller size of As or N atoms compared to P atoms leads to a decrease in the effective size of the unit cell. This substitution occurs because As or N atoms have a smaller atomic radius compared to P atoms, resulting in a tighter packing of atoms within the unit cell.

The decrease in lattice constant is a result of the reduced distance between neighboring atoms caused by the smaller size of manganese atoms, leading to a more compact arrangement of atoms within the crystal lattice.

The decrease in the Mn concentration in GaN, GaP and GaAs results in a reduction in the total energy of the system due to the energetically favorable arrangement of atoms in the crystal lattice. As the Mn concentration decreases, there are fewer lattice distortions caused by the size and bonding differences between Mn and Ga, leading to a more stable configuration and lower total energy.

III.7.2. Electronic Properties

III.7.2.1. Band Structure

The spin-polarized electronic band structures within the first Brillouin zone are crucial for understanding the electronic properties of alloy systems. In this analysis, we focus on the alloy system $\text{Ga}_{1-x}\text{Mn}_x\text{X}$, where X represents N, P or As. Specifically, we investigate three compositions: $\text{Ga}_{0.75}\text{Mn}_{0.25}\text{X}$, $\text{Ga}_{0.50}\text{Mn}_{0.50}\text{X}$, and $\text{Ga}_{0.25}\text{Mn}_{0.75}\text{X}$. Prototype electronic band structures for $\text{Ga}_{1-x}\text{Mn}_x\text{X}$ are presented in **Figures (III.12, III.13 and III.14)**.

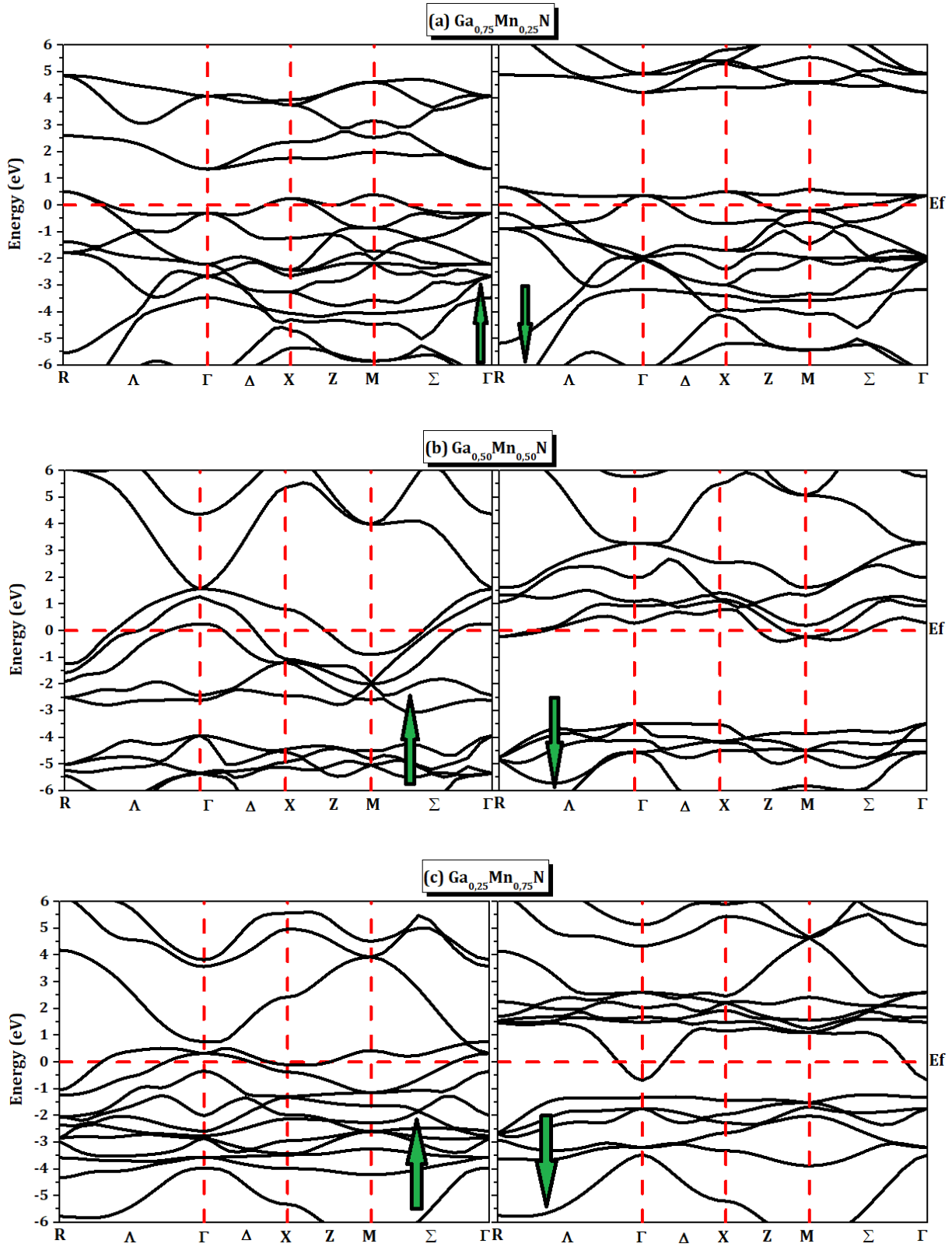


Fig. III.12: Calculated spin polarized band structure of (a) $\text{Ga}_{0.75}\text{Mn}_{0.25}\text{N}$, (b) $\text{Ga}_{0.50}\text{Mn}_{0.50}\text{N}$ and (c) $\text{Ga}_{0.25}\text{Mn}_{0.75}\text{N}$ with the PBE + E ($\alpha=0.05$).

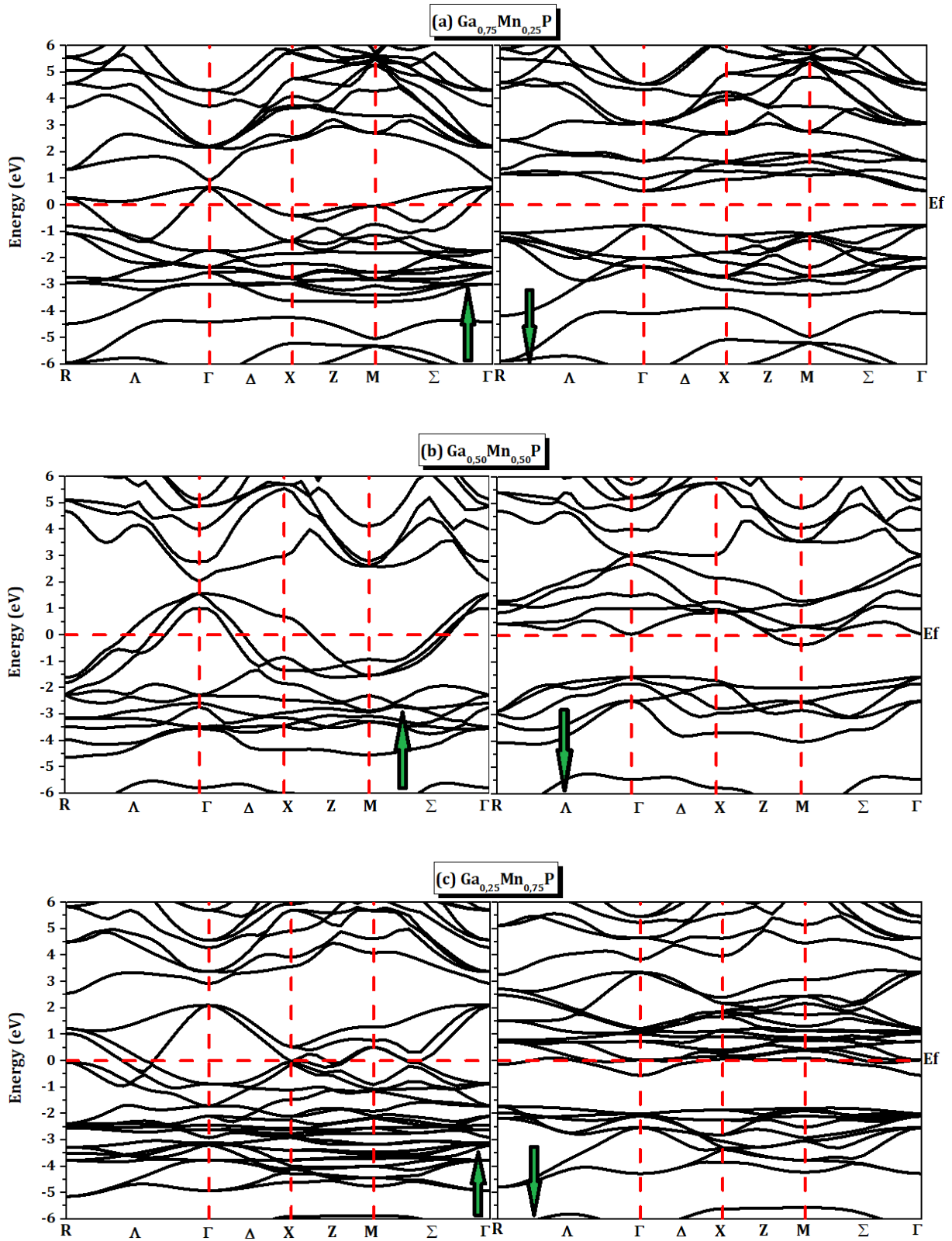


Fig. III.13: Calculated spin polarized band structure of (a) $\text{Ga}_{0.75}\text{Mn}_{0.25}\text{P}$, (b) $\text{Ga}_{0.50}\text{Mn}_{0.50}\text{P}$ and (c) $\text{Ga}_{0.25}\text{Mn}_{0.75}\text{P}$ with the PBE + E ($\alpha=0.04$).

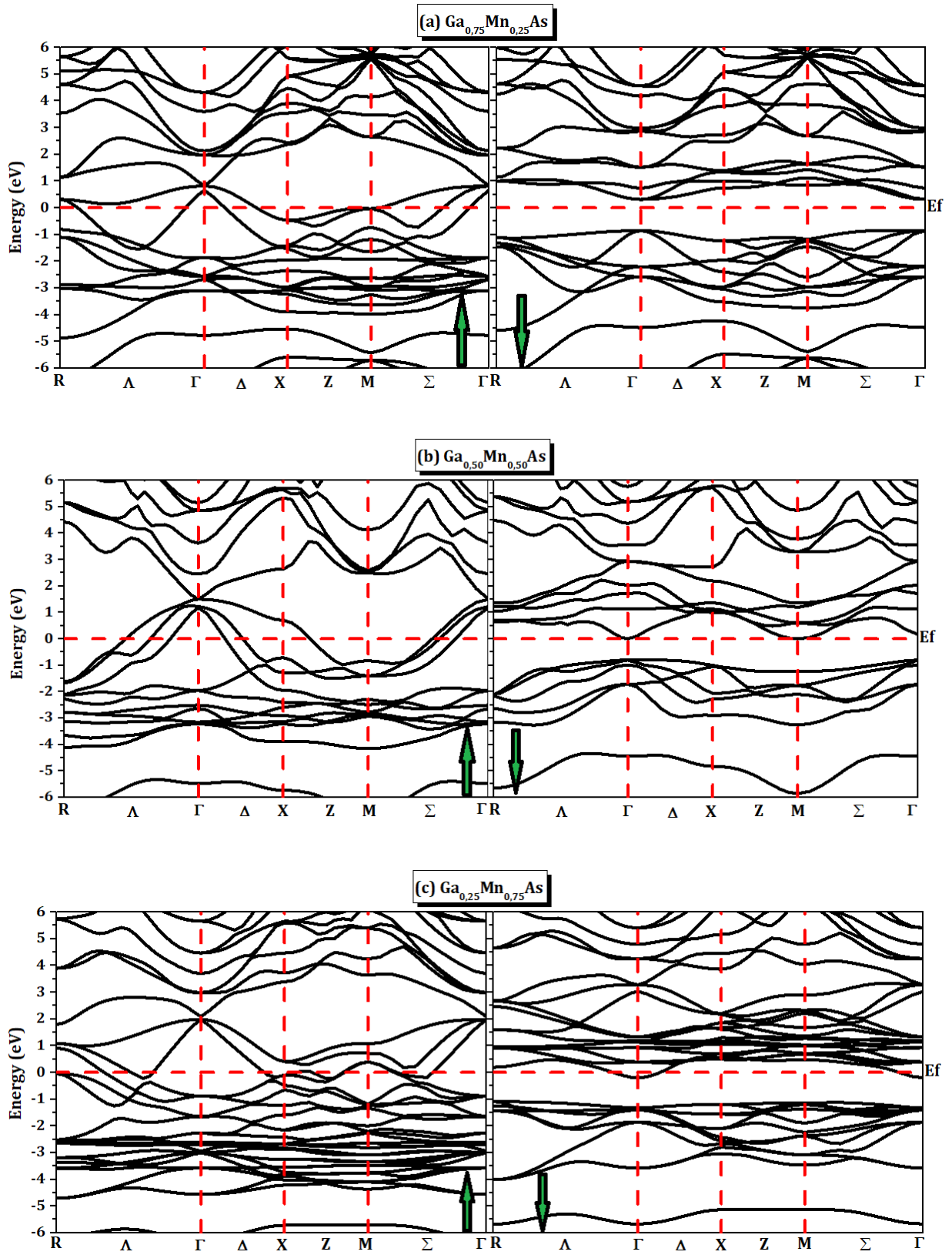


Fig. III.14: Calculated spin polarized band structure of (a) $\text{Ga}_{0.75}\text{Mn}_{0.25}\text{As}$, (b) $\text{Ga}_{0.50}\text{Mn}_{0.50}\text{As}$ and (c) $\text{Ga}_{0.25}\text{Mn}_{0.75}\text{As}$ with the PBE + E ($\alpha=0.05$).

Figure III.12 illustrates the band structures of three distinct alloys: $\text{Ga}_{0.75}\text{Mn}_{0.25}\text{N}$, $\text{Ga}_{0.50}\text{Mn}_{0.50}\text{N}$ and $\text{Ga}_{0.25}\text{Mn}_{0.75}\text{N}$. In both the spin-down and spin-up states of $\text{Ga}_{0.75}\text{Mn}_{0.25}\text{N}$, the band structures display similarities, particularly with certain valence bands intersecting the Fermi level and extending into the conduction band, indicative of metallic behavior. Conversely, in the spin-up configurations of $\text{Ga}_{0.50}\text{Mn}_{0.50}\text{N}$ and $\text{Ga}_{0.25}\text{Mn}_{0.75}\text{N}$, certain conduction bands intersect the Fermi level and extend into the valence band.

An important characteristic observed in these alloys is the conspicuous absence of a band gap near the Fermi level in the spin-up and spin down configurations. This absence of a band gap, which is a typical feature of metals, suggests that these alloys exhibit metallic behavior rather than semiconductor behavior, where a band gap would usually be present.

In **Figure III.13**, the band structure of the $\text{Ga}_{0.75}\text{Mn}_{0.25}\text{P}$ alloy shows different behaviors in spin-down and spin-up states. In the spin-down state, a band gap around the Fermi level indicates semiconductor behavior. In contrast, the spin-up state has valence bands crossing the Fermi level into the conduction band, indicating metallic behavior and suggesting half-metallicity. Both $\text{Ga}_{0.50}\text{Mn}_{0.50}\text{P}$ and $\text{Ga}_{0.25}\text{Mn}_{0.75}\text{P}$ exhibit metallic behavior in the spin-down state, with conduction bands intersecting the Fermi level. However, in the spin-up state, $\text{Ga}_{0.50}\text{Mn}_{0.50}\text{P}$ shows valence bands crossing into the conduction band, while $\text{Ga}_{0.25}\text{Mn}_{0.75}\text{P}$ displays an overlap between valence and conduction bands at the Fermi level.

In the **Figure III.14**, the behavior observed in both $\text{Ga}_{0.75}\text{Mn}_{0.25}\text{As}$ and $\text{Ga}_{0.50}\text{Mn}_{0.50}\text{As}$ alloys is consistent with the presence of half-metallicity. Specifically, the spin-down state manifests a distinct band gap around the Fermi level, characteristic of semiconductor behavior. However, in the spin-up state of these alloys, certain valence bands extend into the conduction band, crossing the Fermi level and exhibiting an overlap between their bands, indicative of metallic behavior. This transition from semiconductor to metallic behavior in different spin configurations underscores the presence of half-metallicity in these alloys, consistent with findings reported in references [23-25]. Additionally, $\text{Ga}_{0.25}\text{Mn}_{0.75}\text{P}$ exhibits metallic behavior because, in the spin-down state, certain conduction bands intersect the Fermi level and extend into the valence band. However, in the spin-up state, an overlap is observed between valence bands and conduction bands at the Fermi level.

The analysis of **Figures (III.12, III.13 and III.14)** reveals several key findings regarding the electronic properties of the studied alloy systems; in all considered alloys, the spin-up (\uparrow) state consistently exhibits a higher electron occupancy compared to the spin-down (\downarrow) state. This asymmetry in the electronic occupation suggests a spin polarization effect, indicating the presence of magnetic ordering in the systems.

The calculated band gaps are summarized in **Table III.5**, it includes conduction band minimum of spin down state and spin up state ($E_{\text{CBM}}^{\text{up}}, E_{\text{dn}}^{\text{CBM}}$), valence band maximum of spin down state and spin up state ($E_{\text{VBM}}^{\text{up}}, E_{\text{dn}}^{\text{VBM}}$), the band edge spin splitting (ΔE_c) for the conduction band minimum and the band edge spin splitting (ΔE_v) for the valence band maximum are determined using specific formulas:

$$\Delta E_c = E_{\text{CBM}}^{\text{up}} - E_{\text{dn}}^{\text{CBM}}, \quad (3)$$

$$\Delta E_v = E_{\text{VBM}}^{\text{up}} - E_{\text{dn}}^{\text{VBM}}, \quad (4)$$

| Materials | Eg (eV) | $E_{\text{VBM}}^{\text{up}}$ (eV) | $E_{\text{dn}}^{\text{VBM}}$ (eV) | $E_{\text{CBM}}^{\text{up}}$ (eV) | $E_{\text{dn}}^{\text{CBM}}$ (eV) | Behavior |
|---|---------------------|-----------------------------------|-----------------------------------|-----------------------------------|-----------------------------------|------------|
| Ga_{0.75}Mn_{0.25}N | 0 | 0 | 0 | 0 | 0 | Metal |
| Ga_{0.50}Mn_{0.50}N | 0 | 0 | 0 | 0 | 0 | Metal |
| Ga_{0.25}Mn_{0.75}N | 0 | 0 | 0 | 0 | 0 | Metal |
| Ga_{0.75}Mn_{0.25}P | 1,20127 1.2 [23] | 0 | -0,78953 | 0 | 0,41174 | Half-metal |
| Ga_{0.50}Mn_{0.50}P | 0 | 0 | 0 | 0 | 0 | Metal |
| Ga_{0.25}Mn_{0.75}P | 0 | 0 | 0 | 0 | 0 | Metal |
| Ga_{0.75}Mn_{0.25}As | 1,36242 1.4 [23] | 0 | -0,95072 | 0 | 0,41177 | Half-metal |
| Ga_{0.50}Mn_{0.50}As | 0,80165 1.6 [23] | 0 | -0,80165 | 0 | 0 | Half-metal |
| Ga_{0.25}Mn_{0.75}As | 0 | 0 | 0 | 0 | 0 | Metal |

Tab. III.5: Electronic properties of ofGa_{1-x}Mn_xN, Ga_{1-x}Mn_xP and Ga_{1-x}Mn_xAs with PBE+E method.

In **Table III.5**, the observed decrease in the band gaps of GaP and GaAs can be attributed to the presence of local strain and electric fields associated with Mn atoms in the alloy lattice [26]. These local effects influence the electronic structure of the material, leading to modifications in its band gap properties.

For the spin-down state, $\text{Ga}_{0.75}\text{Mn}_{0.25}\text{As}$, $\text{Ga}_{0.50}\text{Mn}_{0.50}\text{As}$ and $\text{Ga}_{0.75}\text{Mn}_{0.25}\text{P}$ alloys exhibit characteristics of direct band gap semiconductors. Specifically, the bottom of the conduction band and the top of the valence band occur at the Γ symmetry point. This direct band gap nature enhances the potential for efficient electronic transitions, which is beneficial for various applications.

The transition from an indirect band gap in GaP to a direct band gap in Mn-doped GaP suggests enhanced optical activity in the doped material. This modification implies that Mn doping can significantly improve the material's optoelectronic properties, making it more suitable for applications such as light-emitting diodes, laser diodes, and other devices that rely on direct band gap materials for efficient light emission.

III.7.2.2. Density of States

Figures (III.15, III.16, and III.17) visually represent the spin-dependent total and partial density of states for $\text{Ga}_{1-x}\text{Mn}_x\text{X}$ ($\text{X} = \text{N}, \text{P}, \text{and As}$) alloys with compositions $x = 0.25, 0.50,$ and 0.75 . These figures offer valuable insights into the electronic structure and magnetic properties of the studied compounds. The total density of states shows the overall distribution of electronic states, while the partial reveals the contributions from specific atomic orbitals.

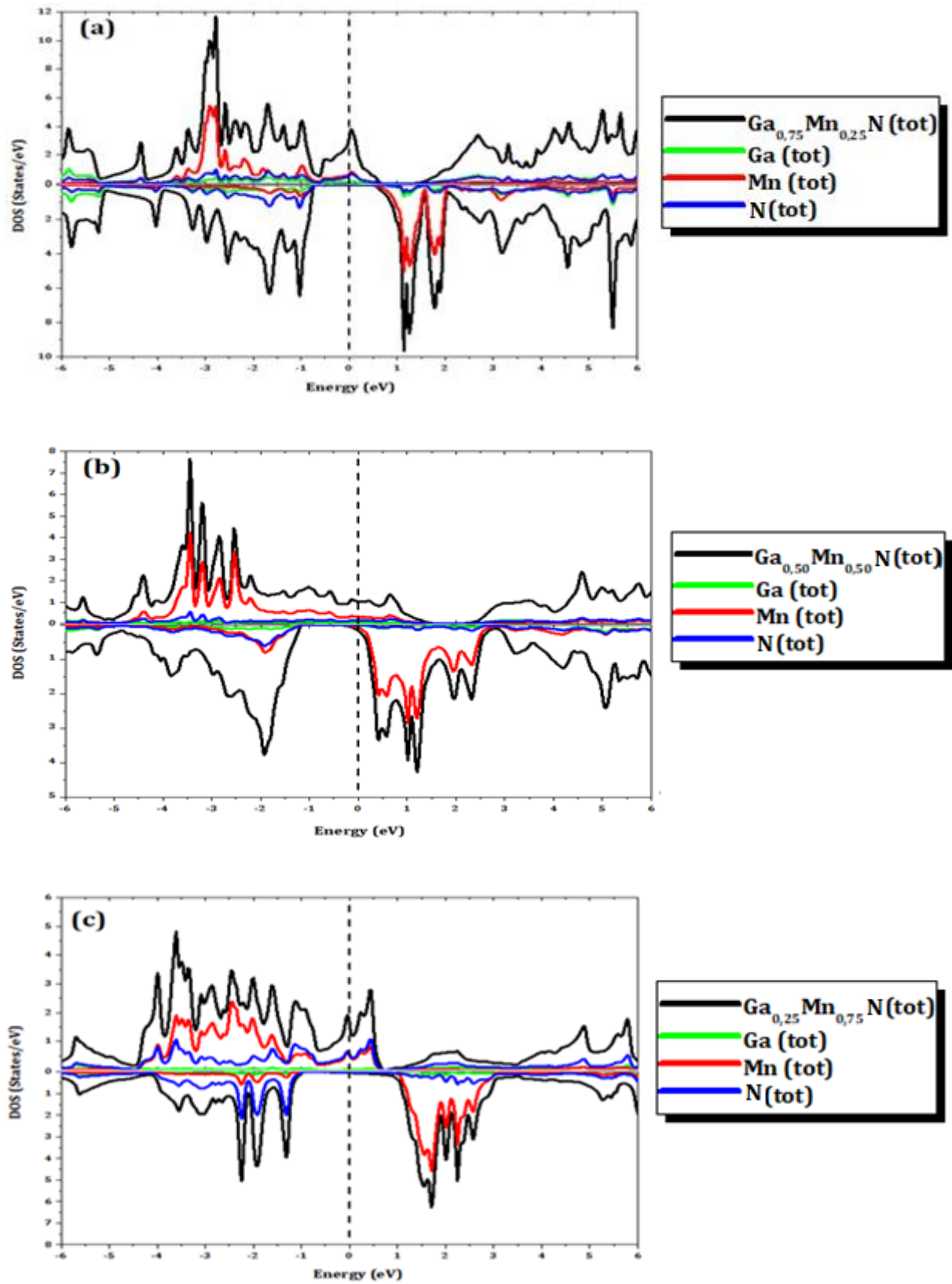


Fig. III.15: Calculated spin polarized total and partial density of states of (a) $\text{Ga}_{0.75}\text{Mn}_{0.25}\text{N}$, (b) $\text{Ga}_{0.50}\text{Mn}_{0.50}\text{N}$ and (c) $\text{Ga}_{0.25}\text{Mn}_{0.75}\text{N}$ with the PBE + E ($\alpha=0.03$).

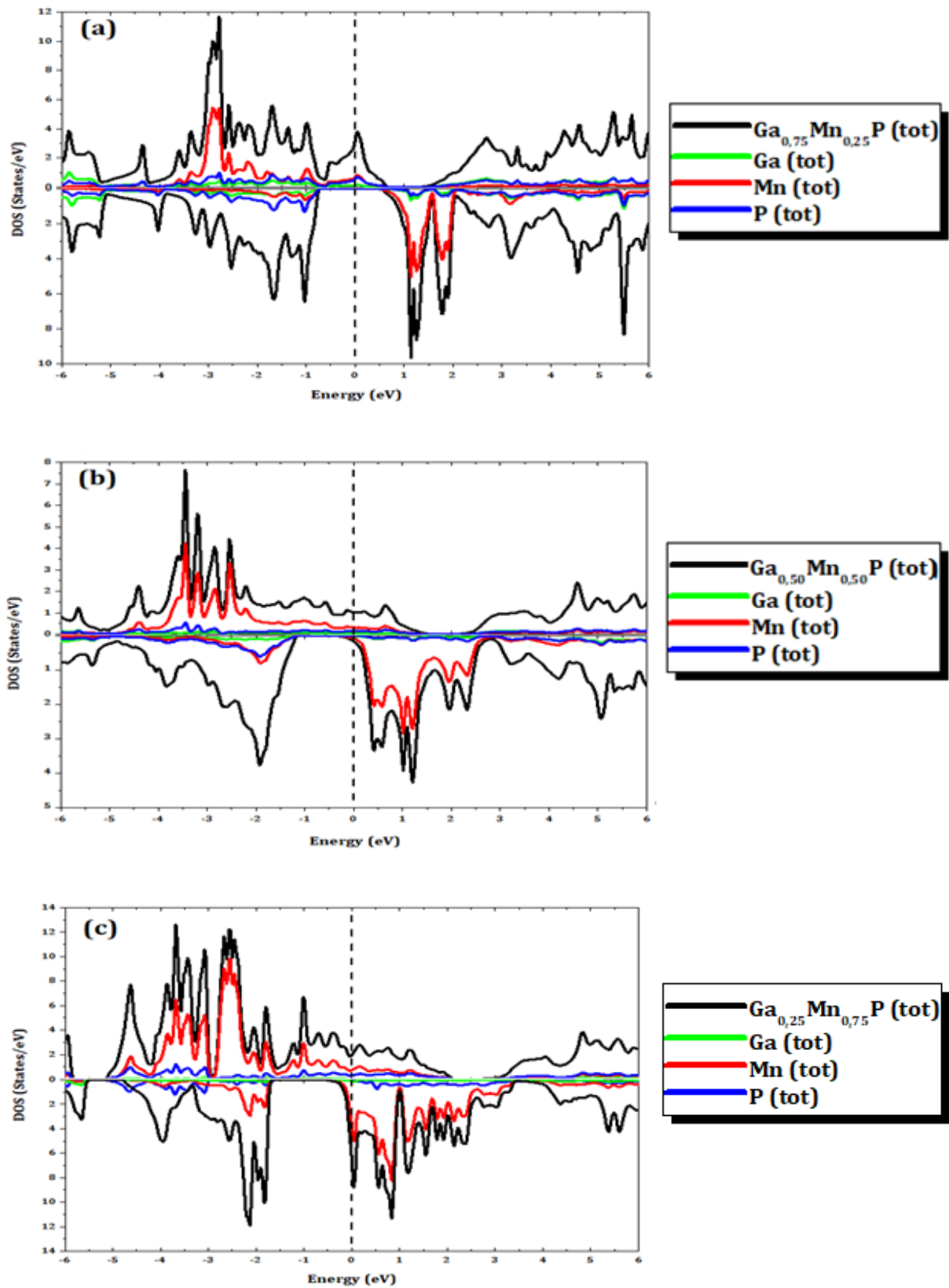


Fig. III.16: Calculated spin polarized total and partial density of states of (a) $\text{Ga}_{0.75}\text{Mn}_{0.25}\text{P}$, (b) $\text{Ga}_{0.50}\text{Mn}_{0.50}\text{P}$ and (c) $\text{Ga}_{0.25}\text{Mn}_{0.75}\text{P}$ with the PBE + E ($\alpha=0.04$).

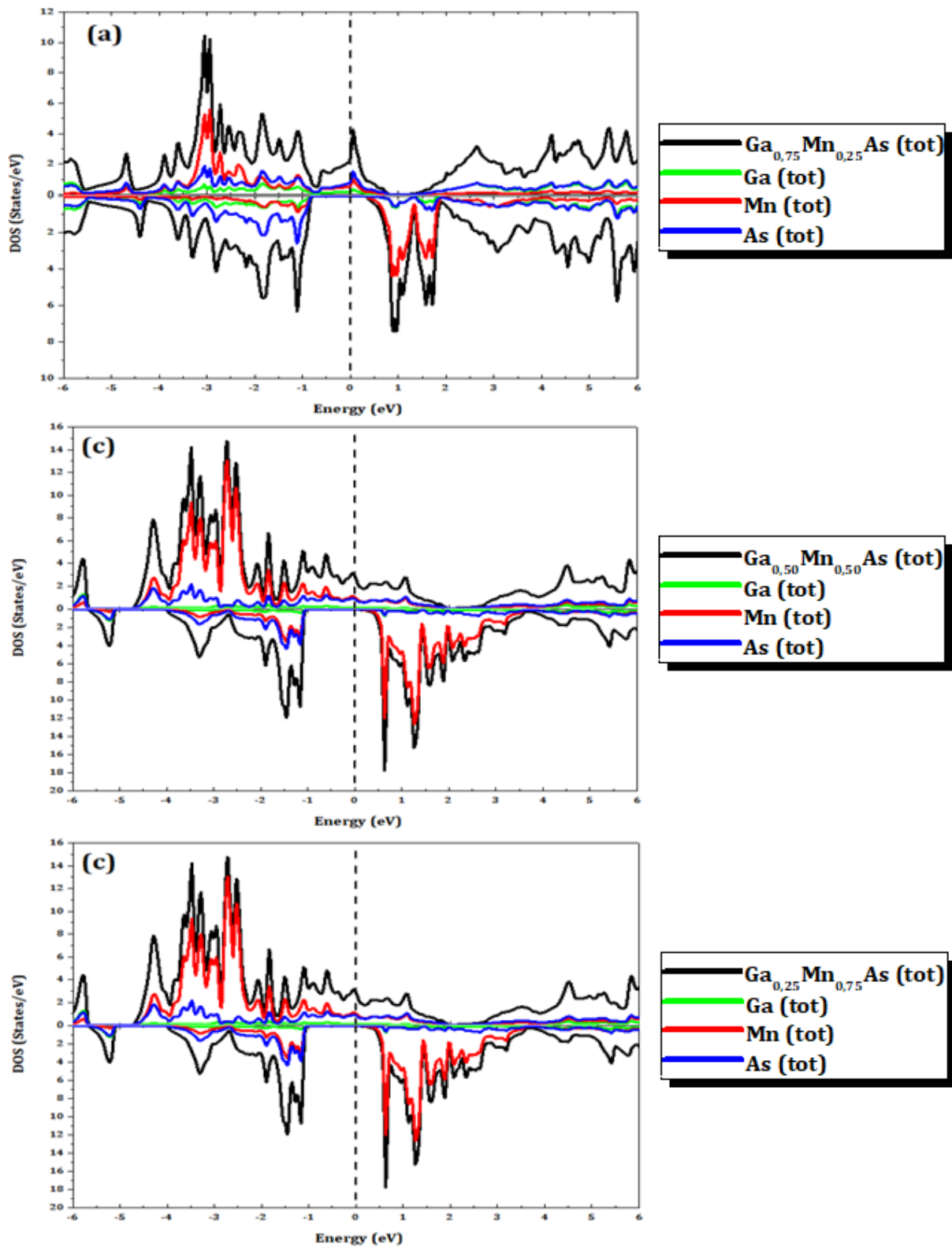


Fig. III.17: Calculated spin polarized total and partial density of states of (a) $\text{Ga}_{0.75}\text{Mn}_{0.25}\text{As}$, (b) $\text{Ga}_{0.50}\text{Mn}_{0.50}\text{As}$ and (c) $\text{Ga}_{0.25}\text{Mn}_{0.75}\text{As}$ with the PBE + E ($\alpha=0.05$).

In the **Figures (III.15, III.16, III.17)**, the partial density of states (PDOS) aids in understanding the origin of states in $\text{Ga}_{1-x}\text{Mn}_x\text{X}$ ($\text{X}=\text{N}, \text{P}$ and As) alloys, in these alloys, the PDOS provides valuable insights into the origin of states near the Fermi level. The Fermi level represents the energy level at which the probability of finding an electron is 50%, and it plays a crucial role in determining the electrical and magnetic properties of materials.

The PDOS analysis reveals that the bands near the Fermi level primarily arise from Mn-d states, indicating the significant contribution of Mn to the electronic structure. However, there is also a noticeable but limited contribution from the X-p states.

When considering the spin-up state, which represents the majority spin direction, the valence band is heavily influenced by both Mn-d and X-p states. This suggests a strong interaction between these states within the electronic structure. In this state, the Fermi level is fully occupied by electrons.

In contrast, the spin-down state, representing the minority spin direction, shows a different electronic structure. In this state, the valence band primarily originates from the X-p states, indicating that the contribution of manganese to the valence band is less significant. However, the conduction band, responsible for carrying electrical current, originates exclusively from the Mn-d states. Importantly, the Fermi level in these alloys is empty in the spin-down state.

This spin polarization, where the electronic structure differs significantly between spin-up and spin-down states, is primarily attributed to the spd-hybridization of Mn-d and X-p states. This hybridization refers to the mixing of electron orbitals from different elements, leading to unique electronic properties.

Overall, these observations highlight the intricate relationship between Mn-d and X-p states in determining the electronic structure of GaMnX compounds. This understanding is crucial for harnessing the unique magnetic and electronic properties of these materials in various technological applications

III.7.3. Magnetic Properties

Upon substituting Ga atoms with Mn in GaX (X=N/P/As), the resulting GaMnN(P/As) alloys exhibit magnetic properties attributed to Mn-d. The coupling between the d orbital of Mn and the p orbital of P atoms results in the emergence of small local magnetic moments in both Ga and P atoms. This observation leads to the conclusion that Ga_{1-x}Mn_xX (X = N, P and As) are ferromagnetic. This finding aligns well with experimental reports that have confirmed the presence of ferromagnetism in these compounds [27-29].

Table III.6 presents the calculated total magnetic moments of the compounds as well as partial magnetic moments at interstitial and anti-sites.

| | | $M^{int}(\mu B)$ | $M^{Mn}(\mu B)$ | $M^{Ga}(\mu B)$ | $M^{N/P/As}(\mu B)$ | $M^{Tot}(\mu B)$ |
|---|---|------------------|-----------------|-----------------|---------------------|------------------|
| Ga_{0.75}Mn_{0.25}N | BPE+E ($\alpha=0.03$) | 0.34182 | 3.38992 | 0.02909 | -0.0020 | 4.00125 |
| | Other works [30] | 0.577 | 3.313 | 0.028 | 0.002 | 3.98 |
| Ga_{0.50}Mn_{0.50}N | BPE+E ($\alpha=0.03$) | 0.36943 | 3.28034 | 0.03880 | -0.00829 | 7.04421 |
| | [30] | 1.160 | 3.345 | 0.057 | 0.008 | 8.00 |
| Ga_{0.25}Mn_{0.75}N | BPE+E ($\alpha=0.03$) | 0.51941 | 3.01116 | 0.03061 | -0.00242 | 4.00089 |
| | [30] | 0.340 | 1.641 | 0.022 | -0.002 | 5.25 |
| Ga_{0.75}Mn_{0.25}P | BPE+E ($\alpha=0.04$) | 0.41078 | 3.6477 | 0.03201 | -0.03691 | 4.00068 |
| | [23] | 0.41405 | 3.61285 | 0.03203 | -0.0306 | 4.00045 |
| Ga_{0.50}Mn_{0.50}P | BPE+E ($\alpha=0.04$) | 0.38196 | 3.47248 | 0.06160 | -0.05519 | 3.90065 |
| | [23] | 0.39427 | 3.52194 | 0.06612 | -0.0419 | 3.89862 |
| Ga_{0.25}Mn_{0.75}P | BPE+E ($\alpha=0.04$) | 0.70111 | 3.60744 | 0.07232 | -0.09001 | 11.65127 |
| | [23] | 0.8005 | 3.44312 | 0.08581 | -0.0908 | 10.8526 |
| Ga_{0.75}Mn_{0.25}As | BPE+E ($\alpha=0.05$) | 0.34949 | 3.6615 | 0.03413 | -0.04333 | 4.00042 |
| | [23] | 0.32683 | 3.74437 | 0.02977 | -0.040 | 4.00055 |
| Ga_{0.50}Mn_{0.50}As | BPE+E ($\alpha=0.05$) | 0.27885 | 3.89318 | 0.05012 | -0.06590 | 4.00015 |
| | [23] | 0.27494 | 3.81485 | 0.06311 | -0.0763 | 4.00025 |
| Ga_{0.25}Mn_{0.75}As | BPE+E ($\alpha=0.05$) | 0.79695 | 3.92007 | 0.09331 | 0.09988 | 11.96219 |
| | [23] | 0.78318 | 3.82311 | 0.09938 | -0.1001 | 11.9517 |

Tab. III.6: Magnetic properties of of Ga_{1-x}Mn_xN, Ga_{1-x}Mn_xP and Ga_{1-x}Mn_xAs with PBE+E method.

The observed magnetic moments at anti-sites (N, P and As) in the studied compounds exhibit distinct behaviors. In anti-ferromagnetic interactions, the magnetic moments of neighboring atoms align in opposite directions, leading to a cancellation of net magnetic moments between adjacent atoms. This results in a negative magnetic moment at the anti-site (N, P and As), indicating an anti-parallel alignment with Mn atoms. On the other hand, in ferromagnetic interactions, the magnetic moments of neighboring atoms align in the same direction, reinforcing each other's magnetic moments. This results in a positive magnetic moment at the on-site (Ga), indicating a parallel alignment with Mn atoms. These interactions play a crucial role in determining the overall magnetic properties and stability of the materials.

The spd-hybridization phenomenon results in a reduction of the local magnetic moment of manganese (Mn) from its free space magnetic moment. This reduction occurs due to the interaction and overlapping of Mn-d states with X-p states, leading to changes in the electronic structure and magnetic properties of Mn atoms within the compound. Despite this reduction in the local magnetic moment of Mn, the net magnetic moment for all studied compounds remains a whole number, specifically 4 μB . This observation is consistent with previous literature and theoretical predictions [31].

The $\text{Ga}_{0.75}\text{Mn}_{0.25}\text{As}$, $\text{Ga}_{0.50}\text{Mn}_{0.50}\text{As}$ and $\text{Ga}_{0.75}\text{Mn}_{0.25}\text{P}$ alloys exhibit characteristics of half-metallic ferromagnets, as indicated by their integer magnetic moment of 4 μB [32-34]. This consistency in the net magnetic moment across the studied compounds underscores the robustness and reliability of the theoretical calculations and supports the understanding of the magnetic properties of these materials. It also highlights the importance of considering electronic structure and hybridization effects in accurately predicting and interpreting the magnetic behavior of Mn-doped compounds.

III.8. Effect of exchange and correlation interactions

III.8.1. Lattice Parameter and Volume

Figure III.18 demonstrates that as exchange and correlation interactions increase, both the Lattice Parameter and Volume of the half-metallic behaviour of $\text{Ga}_{0.75}\text{Mn}_{0.25}\text{As}$, $\text{Ga}_{0.50}\text{Mn}_{0.50}\text{As}$ and $\text{Ga}_{0.75}\text{Mn}_{0.25}\text{P}$ increase. This indicates significant influence of these interactions on the unit cell size. Specifically, exchange and correlation interactions directly

affect the equilibrium positions of atoms and their bonding behavior within the unit cell, ultimately leading to an expansion of the unit cell size.

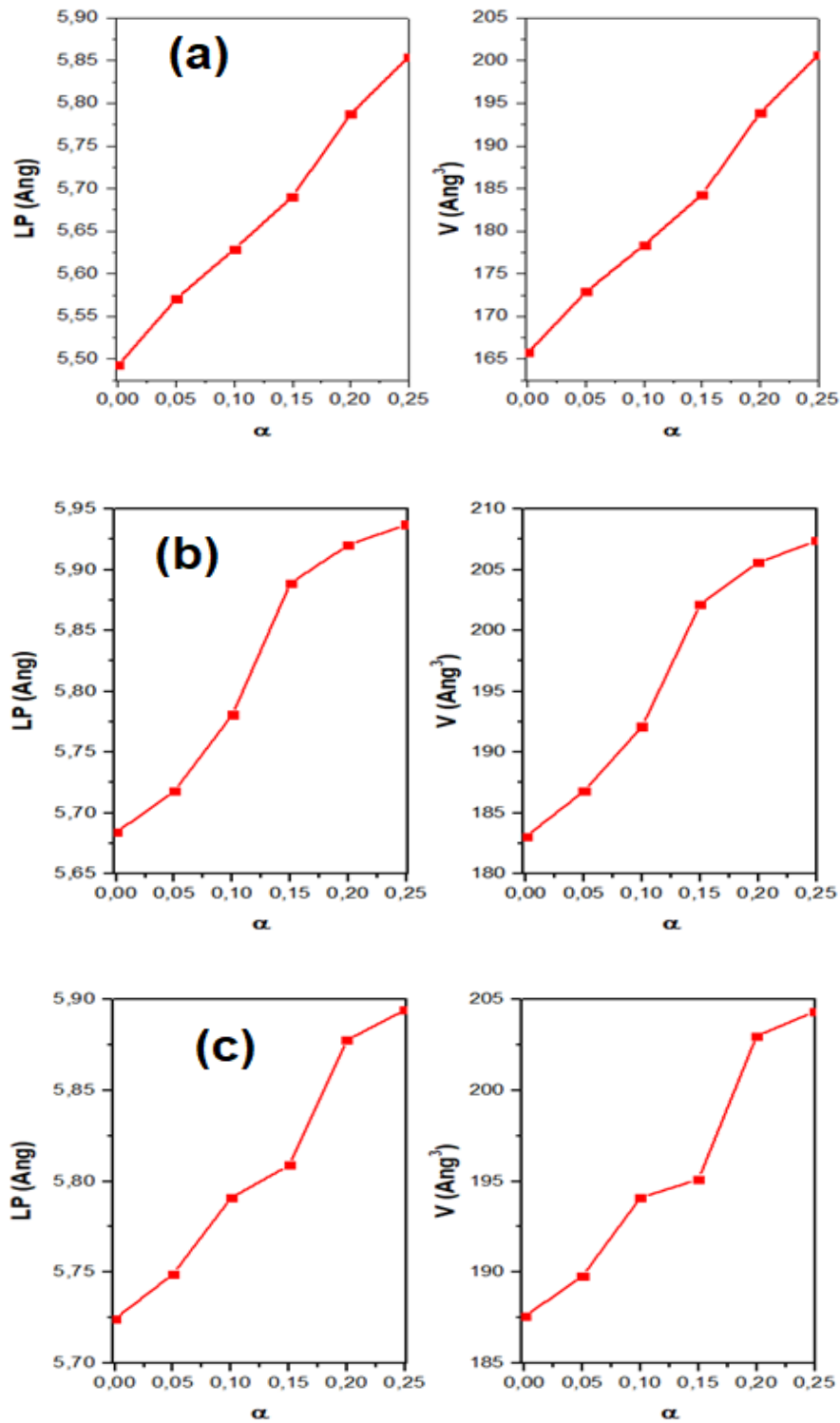


Fig. III.18: Influence of exchange and correlation interactions on lattice parameter (LP) and volume (V) of (a) Ga_{0.75}Mn_{0.25}P, (b) Ga_{0.75}Mn_{0.25}As and (c) Ga_{0.50}Mn_{0.50}As.

III.8.2. Total Energy

Figure III.19 shows that increasing exchange and correlation interactions lead to a significant decrease in total energy of the half-metallic behavior of $\text{Ga}_{0.75}\text{Mn}_{0.25}\text{As}$, $\text{Ga}_{0.50}\text{Mn}_{0.50}\text{As}$ and $\text{Ga}_{0.75}\text{Mn}_{0.25}\text{P}$. These interactions strongly influence the electronic properties by modifying the distribution and behavior of electrons, resulting in a pronounced reduction in total energy.

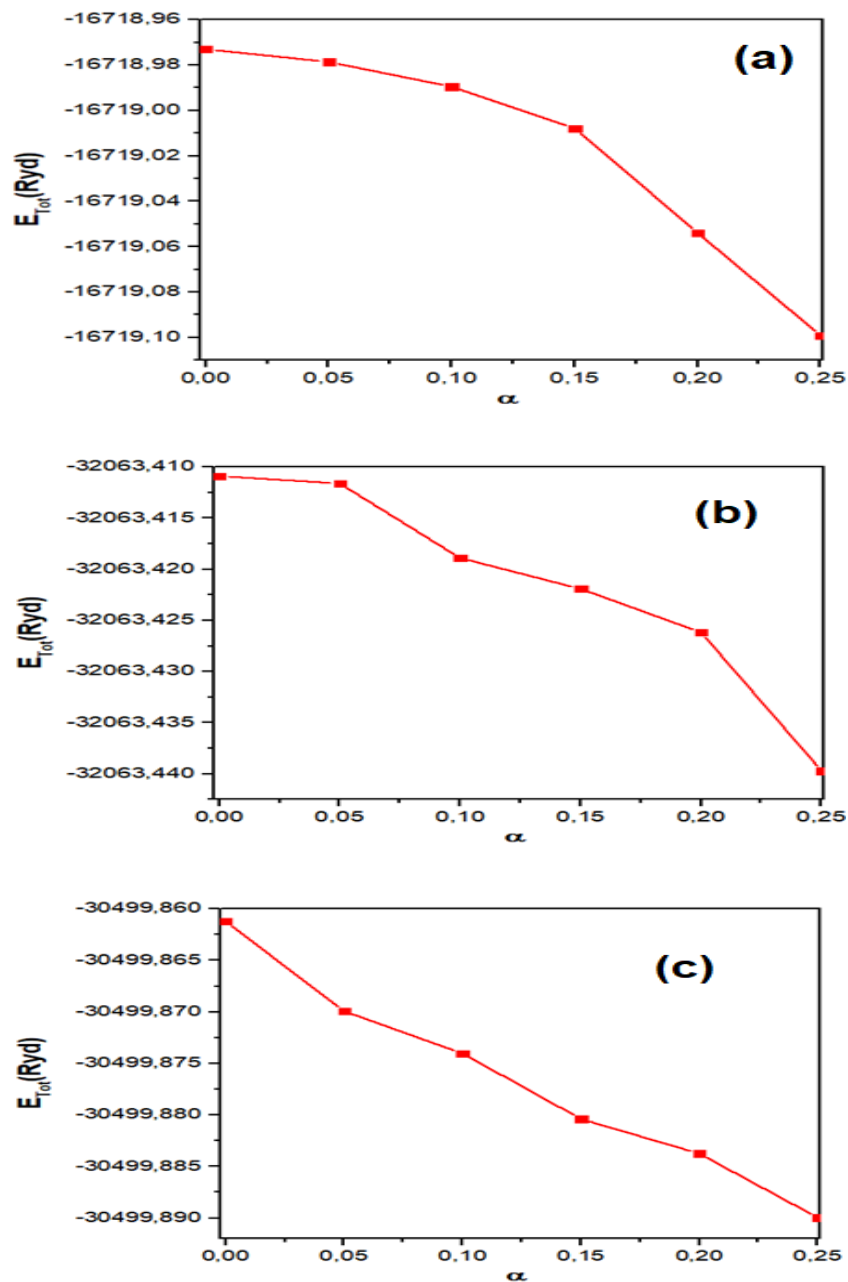


Fig. III.19: Influence of exchange and correlation interactions on total energy (E_{Tot}) of (a) $\text{Ga}_{0.75}\text{Mn}_{0.25}\text{P}$, (b) $\text{Ga}_{0.75}\text{Mn}_{0.25}\text{As}$ and (c) $\text{Ga}_{0.50}\text{Mn}_{0.50}\text{As}$.

III.8.3. Band Gap Energy

In the **Figure III.20**, the calculated band structures of the half-metallic behavior of $\text{Ga}_{0.75}\text{Mn}_{0.25}\text{As}$, $\text{Ga}_{0.50}\text{Mn}_{0.50}\text{As}$ and $\text{Ga}_{0.75}\text{Mn}_{0.25}\text{P}$ highlight a noticeable increase in the forbidden energy gap (E_g) for spin down state. This increase is attributed to significant changes in the maximum of the conduction band and the minimum of the valence band, resulting from the increasing exchange and correlation interactions.

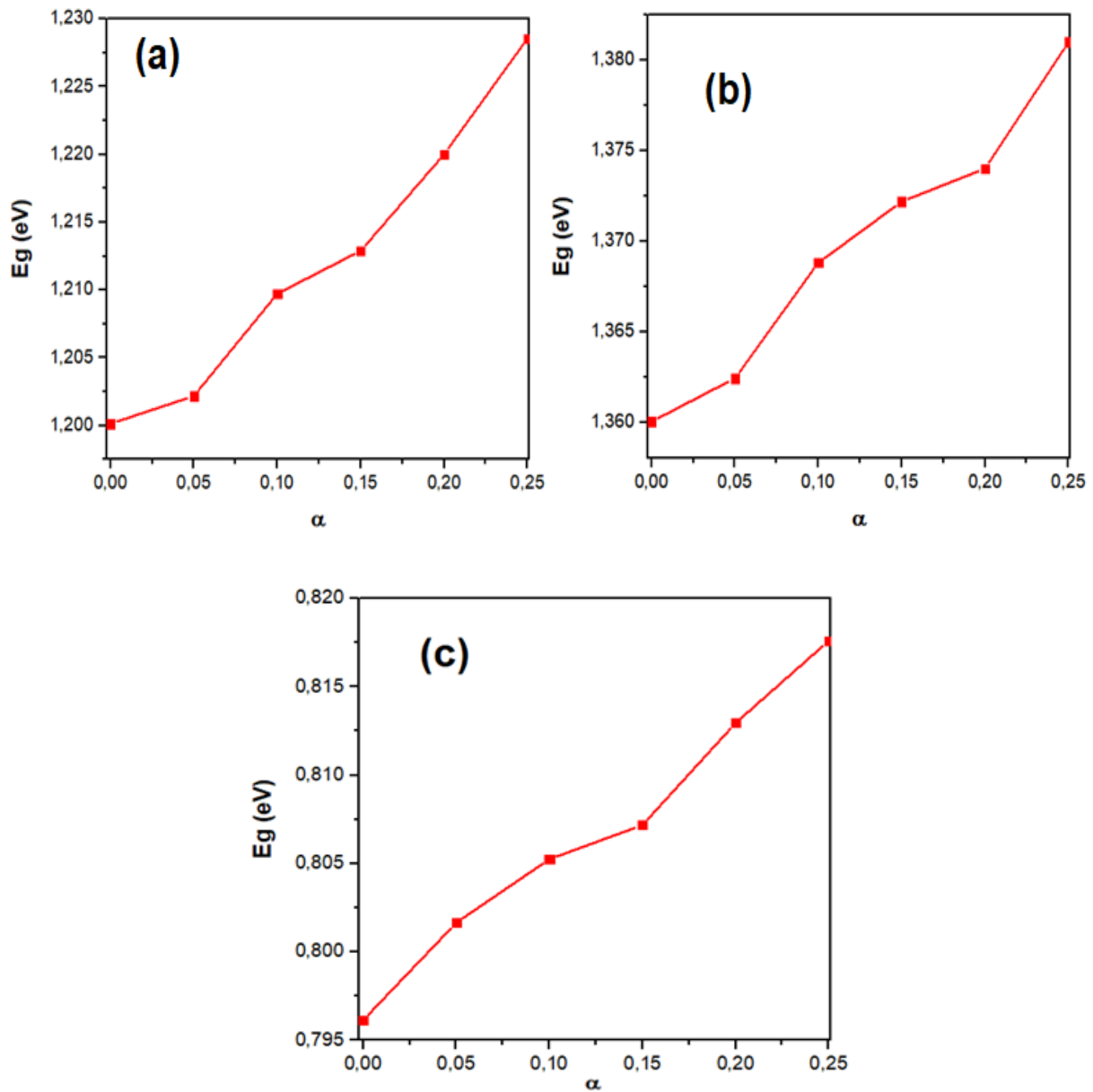


Fig. III.20: Influence of exchange and correlation interactions on band gap energy (E_g) of (a) $\text{Ga}_{0.75}\text{Mn}_{0.25}\text{P}$, (b) $\text{Ga}_{0.75}\text{Mn}_{0.25}\text{As}$ and (c) $\text{Ga}_{0.50}\text{Mn}_{0.50}\text{As}$.

III.8.4. Magnetic Moment

Upon substituting Ga atoms with Mn in GaP, GaN and GaAs the resulting GaMnN(P/As) compounds exhibit magnetic properties attributed to Mn-d. The coupling between the d orbital of Mn and the p orbital of N, P and As atoms result in the emergence of small local magnetic moments in both Ga and N/P/As atoms. Notably, for $\text{Ga}_{0.75}\text{Mn}_{0.25}\text{As}$, $\text{Ga}_{0.50}\text{Mn}_{0.50}\text{As}$ and $\text{Ga}_{0.75}\text{Mn}_{0.25}\text{P}$, the local magnetic moment of N/P/As exhibit a negative value, indicating an anti-parallel alignment with the Mn spin, whereas the positive value observed on Ga signifies a parallel alignment.

Figure III.21 illustrates the variation of the both local and total magnetic moments of $\text{Ga}_{0.75}\text{Mn}_{0.25}\text{As}$, $\text{Ga}_{0.50}\text{Mn}_{0.50}\text{As}$ and $\text{Ga}_{0.75}\text{Mn}_{0.25}\text{P}$ under the influence of exchange and correlation interactions. As the interactions increase, the total magnetic moment remains constant at 4.00 μB . Nonetheless, the magnetic moment of Mn atom increases, whereas the local magnetic moments at N/P/As and Ga atoms decrease.

III.8.5. Spin Polarized Band Structures

The spin polarized band structures of half-metallic behavior of $\text{Ga}_{0.75}\text{Mn}_{0.25}\text{As}$, $\text{Ga}_{0.50}\text{Mn}_{0.50}\text{As}$ and $\text{Ga}_{0.75}\text{Mn}_{0.25}\text{P}$ have been computed within the first Brillouin zone. **Figure III.22** depicts that the electrons in the spin up (\uparrow) state outnumber those in the spin down (\downarrow) state. There is a band gap present around the Fermi level (E_f) for spin down state, while a few valence bands in the spin up state intersect the Fermi level and transition into the conduction band. Consequently, based on the occurred interactions range of 0 to 25%, these alloys are predicted to exhibit metallic behaviors for spin up state and semiconductor behaviors for the spin down state. Further investigation indicates that these alloys are a half metallic ferromagnetic material.

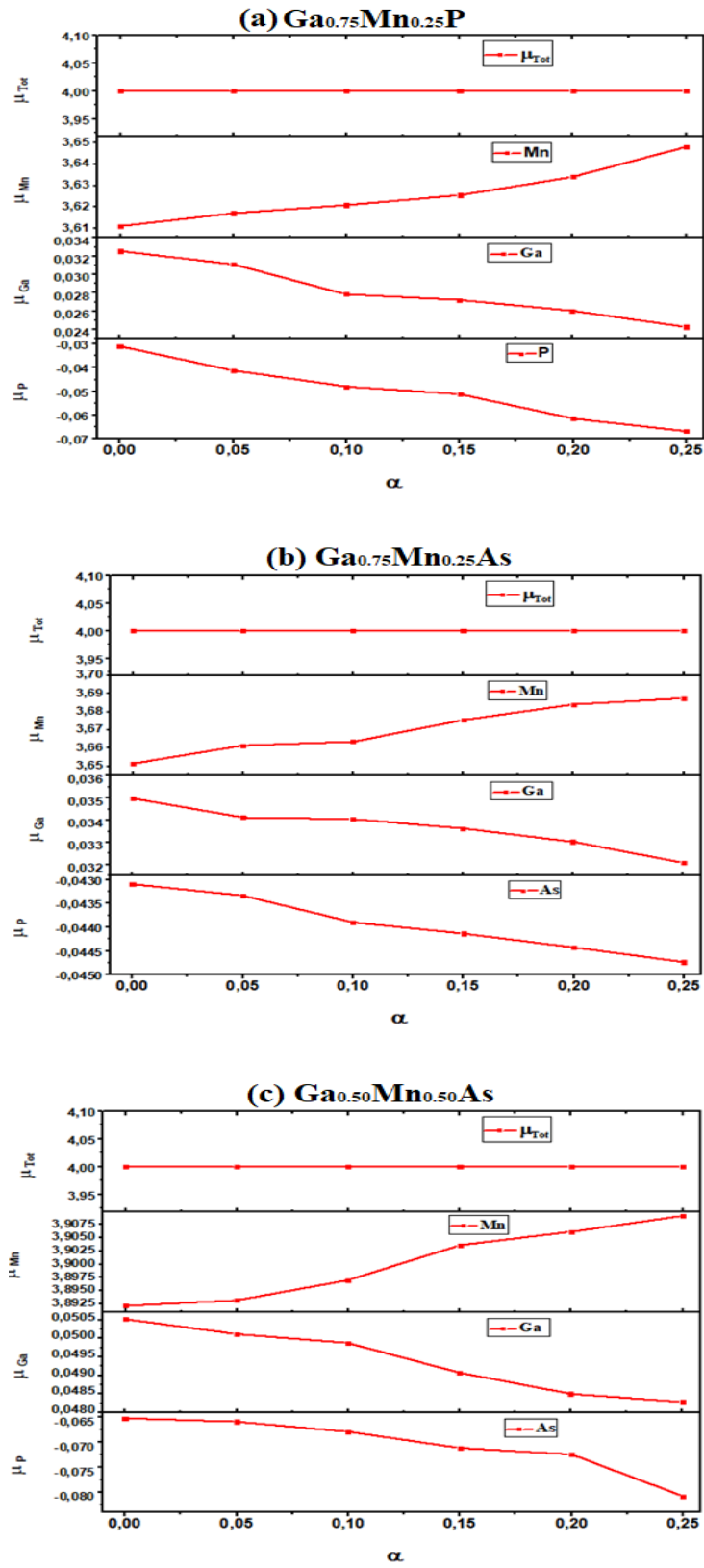


Fig. III.21: Influence of exchange and correlation interactions on magnetic moment μ_{Tot} , μ_{Mn} , μ_{Ga} and $\mu_{\text{N/P/As}}$ of (a) $\text{Ga}_{0.75}\text{Mn}_{0.25}\text{P}$, (b) $\text{Ga}_{0.75}\text{Mn}_{0.25}\text{As}$ and (c) $\text{Ga}_{0.50}\text{Mn}_{0.50}\text{As}$.

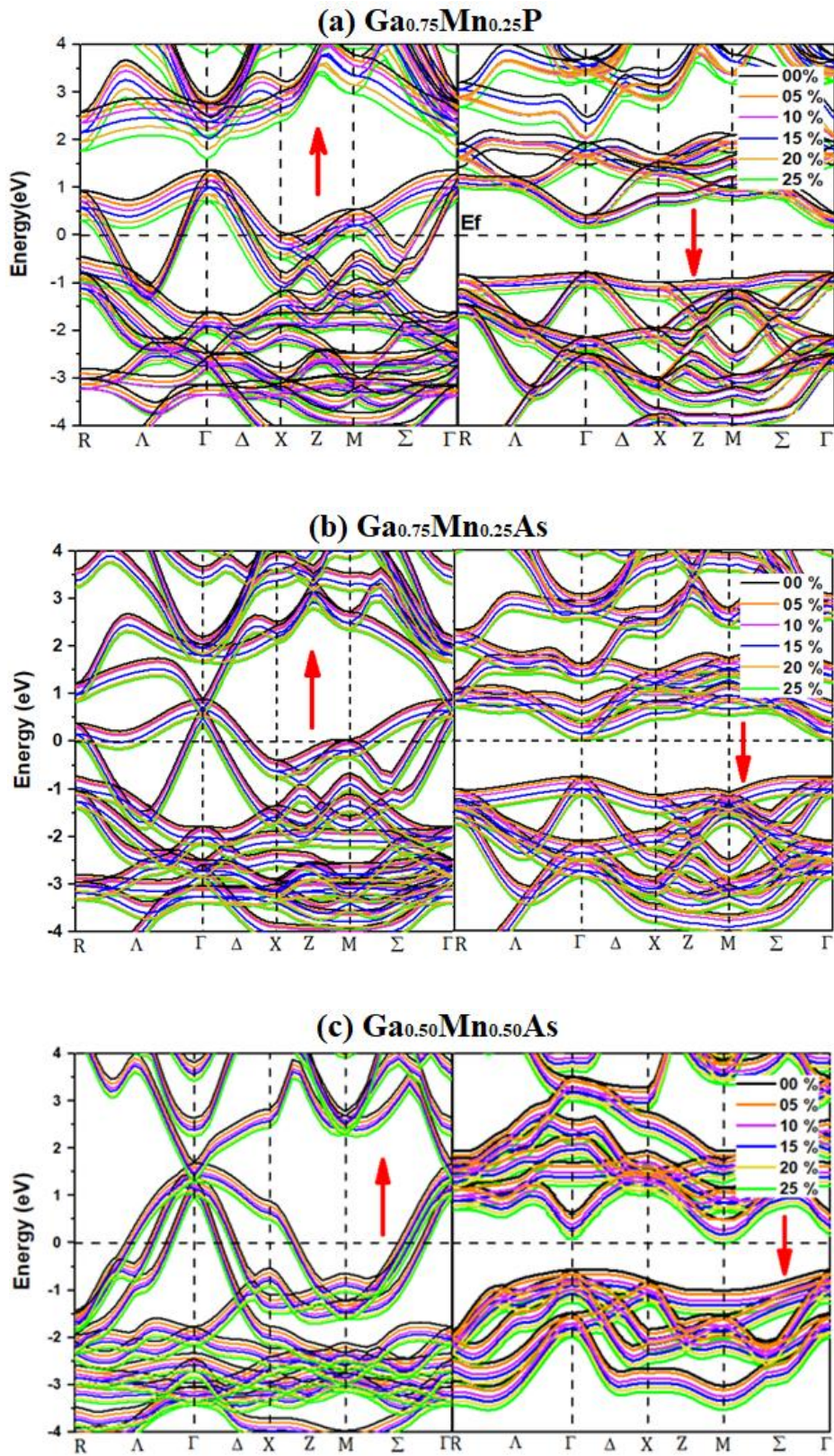


Fig. III.22: Influence of exchange and correlation interactions on spin polarized band structures of (a) $\text{Ga}_{0.75}\text{Mn}_{0.25}\text{P}$, (b) $\text{Ga}_{0.75}\text{Mn}_{0.25}\text{As}$ and (c) $\text{Ga}_{0.50}\text{Mn}_{0.50}\text{As}$.

In the **Figure III.22**, the calculated band structures of the half-metallic behavior of $\text{Ga}_{0.75}\text{Mn}_{0.25}\text{As}$, $\text{Ga}_{0.50}\text{Mn}_{0.50}\text{As}$ and $\text{Ga}_{0.75}\text{Mn}_{0.25}\text{P}$ highlight a noticeable increase in the forbidden energy gap (E_g) for spin down state. This increase is attributed to significant changes in the maximum of the conduction band and the minimum of the valence band, resulting from the increasing exchange and correlation interactions.

The resulting values for various structural, electronic and magnetic properties demonstrating the half-metallic behavior of $\text{Ga}_{0.75}\text{Mn}_{0.25}\text{As}$, $\text{Ga}_{0.50}\text{Mn}_{0.50}\text{As}$ and $\text{Ga}_{0.75}\text{Mn}_{0.25}\text{P}$ alloys are presented in the **Tables (III.7, III.8 and III.9)**.

| α | 0.05 | 0.10 | 0.15 | 0.20 | 0.25 |
|--------------------------------|--------------|--------------|--------------|--------------|-------------|
| $a(\text{Å}^\circ)$ | 5.571 | 5.629 | 5.690 | 5.787 | 5.854 |
| $V(\text{Å}^3)$ | 172.882 | 178.364 | 184.301 | 193.854 | 200.687 |
| $E_{\text{Tot}} (\text{Ryd})$ | -16718,97859 | -16718,98954 | -16719,00784 | -16719,05385 | -16719,0992 |
| $E_g (\text{eV})$ | 1,20218 | 1,20973 | 1.21289 | 1,22001 | 1,22857 |
| $M^{\text{Mn}} (\mu\text{B})$ | 3,61718 | 3,62101 | 3,62559 | 3,63412 | 3,64813 |
| $M^{\text{Ga}} (\mu\text{B})$ | 0,03112 | 0,02784 | 0,02723 | 0,02603 | 0,02428 |
| $M^{\text{P}} (\mu\text{B})$ | -0,04114 | -0,0479 | -0,05113 | -0,06142 | -0,06673 |
| $M^{\text{Tot}} (\mu\text{B})$ | 4,00068 | 4,00068 | 4,00068 | 4,00068 | 4,00068 |

Tab. III.7: Structural, electronic and magnetic properties of $\text{Ga}_{0.75}\text{Mn}_{0.25}\text{P}$ compound at different values of HF exchange parameter (α).

| α | 0.05 | 0.10 | 0.15 | 0.20 | 0.25 |
|-------------------------------|--------------|--------------|--------------|--------------|-------------|
| $a(\text{Å}^\circ)$ | 5.718 | 5,7808 | 5,889 | 5,9205 | 5,9372 |
| $V(\text{Å}^3)$ | 186,806 | 192,100 | 202,159 | 205,588 | 207,369 |
| $E_{\text{Tot}}(\text{Ryd})$ | -32063,41161 | -16718,98954 | -16719,00784 | -16719,05385 | -16719,0992 |
| $E_g(\text{eV})$ | 1,36242 | 1,36881 | 1,37219 | 1,37402 | 1,38101 |
| $M^{\text{Mn}}(\mu\text{B})$ | 3.6615 | 3,66361 | 3,67559 | 3,68412 | 3,68753 |
| $M^{\text{Ga}}(\mu\text{B})$ | 0.03413 | 0,03405 | 0,03363 | 0,03303 | 0,03208 |
| $M^{\text{As}}(\mu\text{B})$ | -0.04333 | -0,0439 | -0,04413 | -0,04442 | -0,04473 |
| $M^{\text{Tot}}(\mu\text{B})$ | 4.00042 | 4.00042 | 4.00042 | 4.00042 | 4.00042 |

Tab. III.8: Structural, electronic and magnetic properties of $\text{Ga}_{0.75}\text{Mn}_{0.25}\text{As}$ compound at different values of HF exchange parameter (α).

| α | 0.05 | 0.10 | 0.15 | 0.20 | 0.25 |
|-------------------------------|--------------|--------------|--------------|--------------|--------------|
| $a(\text{Å}^\circ)$ | 5.749 | 5,789 | 5,807 | 5,879 | 5,895 |
| $V(\text{Å}^3)$ | 189,803 | 194,104 | 195,120 | 202,986 | 204,336 |
| $E_{\text{Tot}}(\text{Ryd})$ | -30499,86993 | -30499,87403 | -30499,88039 | -30499,88375 | -30499,88997 |
| $E_g(\text{eV})$ | 0,80165 | 0.80529 | 0.80724 | 0.81302 | 0.81757 |
| $M^{\text{Mn}}(\mu\text{B})$ | 3,89318 | 3,89701 | 3,90359 | 3,90612 | 3,90913 |
| $M^{\text{Ga}}(\mu\text{B})$ | 0,05012 | 0,04988 | 0,04908 | 0,04851 | 0,04829 |
| $M^{\text{As}}(\mu\text{B})$ | -0,0659 | -0,06789 | -0,07113 | -0,07242 | -0,0808 |
| $M^{\text{Tot}}(\mu\text{B})$ | 4,00015 | 4,00015 | 4,00015 | 4,00015 | 4,00015 |

Tab. III.9: Structural, electronic and magnetic properties of $\text{Ga}_{0.50}\text{Mn}_{0.50}\text{As}$ compound at different values of HF exchange parameter (α).

III.9. Conclusion

The PBE+E calculations revealed that Mn-doped III–V semiconductors exhibit distinct electronic and magnetic properties. Specifically, $\text{Ga}_{0.75}\text{Mn}_{0.25}\text{As}$, $\text{Ga}_{0.50}\text{Mn}_{0.50}\text{As}$ and $\text{Ga}_{0.75}\text{Mn}_{0.25}\text{P}$ alloys display half-metallic behavior with a direct band gap for the spin down state, while $\text{Ga}_{1-x}\text{Mn}_x\text{N}$ ($x = 0.25, 0.50, 0.75$), $\text{Ga}_{0.25}\text{Mn}_{0.75}\text{P}$, $\text{Ga}_{0.25}\text{Mn}_{0.75}\text{As}$ and $\text{Ga}_{0.50}\text{Mn}_{0.50}\text{P}$ alloys are metallic for both spin up and spin down states.

Furthermore, the ferromagnetic states were found to be energetically more stable than the nonmagnetic states. Additionally, replacing Ga with Mn in the alloys resulted in a decrease in the lattice constant, attributed to the different atomic sizes of Ga and Mn.

Moreover, spd-hybridization between the electronic cloud of N/P/As-p states and the transition metal Mn-d states played a crucial role in determining the electronic and magnetic properties of the Mn-doped III–V semiconductors.

References

- [1] A.H. Reshak and M. Jamal. "Calculation of the lattice constant of hexagonal compounds with two dimensional search of equation of state and with semilocal functionals a new package (2D-optimize)". *Journal of Alloys and Compounds*, 555, 362–366 (2013).
- [2] P. Novák, J. Kuneš, L. Chaput and W.E. Pickett. "Exact exchange for correlated electrons". *Physica Status Solidi (b)*, 243(3), 563–572 (2006).
- [3] O. A. Vydrov, J. Heyd, A. V. Krukau and G. E. Scuseria. "Importance of short-range versus long-range Hartree-Fock exchange for the performance of hybrid density functionals". *The Journal of Chemical Physics*, 125(7) (2006).
- [4] A.D. Becke. "A new mixing of Hartree-Fock and local density- functional theories". *The Journal of Chemical Physics*, 98(2), 1372-1377 (1993).
- [5] M. Ernzerhof and G. E. Scuseria. "Assessment of the Perdew-Burke-Ernzerhof exchange-correlation functional". *The Journal of Chemical Physics*, 110(11), 5029-5036 (1999).
- [6] C. Adamo and V. Barone. "Toward reliable density functional methods without adjustable parameters: The PBE0 model". *The Journal of Chemical Physics*, 110(13), 6158-6170 (1999).
- [7] M. Krause and F. Bechstedt. "Structural and magnetic properties of MnTe phases from ab initio calculations". *J. Supercond. Novel Magn.* 26, 1963, (2013).
- [8] F.D. Murnaghan. "The compressibility of media under external pressures". *Proceeding of National Academy of Sciences*, 30(9), 244-247 (1944).
- [9] H. Qin, T. Kuang, Xinghe Luan, Wangyun Li, Jing Xiao, Ping Zhang, Daoguo Yang, Guoqi Zhang. "Mechanical, Thermodynamic and Electronic Properties of Wurtzite and Zinc-Blende GaN Crystals". (2010).
- [10] S.S. Parashari, S. Kumar and S. Auluck. "Calculated structural, electronic and optical properties of Ga-based semiconductors under pressure". *Phys. Rev B* 403, 3077-3088, (2008).
- [11] A. Rashid, S. J. Hashemifar, H. Akbarzadeh and A. Maqsood. "Ab initio study of structural and electronic properties of III-arsenide binary compounds". *Com. Mat.* 39(3) 580-586, (2007).
- [12] I. Vurgaftman, J. R. Meyer and L. R. Ram-Mohan "Band parameters for III–V compound semiconductors and their alloys". *Journal of applied physics* volume 89, number 11, (2001).
- [13] H. Xia, Q. Xia and A.L. Ruoff. "High-pressure structure of gallium nitride: Wurtzite-to-rocksalt phase transition". *Phys. Rev. B*, 47, 12925–12928, (1993).
- [14] Y.K. Yoğurtçu, A.J. Miller and G.A. Saunders. "Pressure dependence of elastic behaviour and force constants of GaP", *J. Phys. Chem. Solids* 42, 49-56, (1981).
- [15] D.L. Smith. "Strain-generated electric fields in [111] growth axis strained-layer superlattices". *Solid State Commun*, 57, 919-921, (1986).

- [16] H. Landolt and R. Börnstein, "Landolt-Börnstein numerical data and functional relationships in science and technology". Crystal and solid state physics. Vol. 17, (1982).
- [17] B. Daoudi, M. Sehil, A. Boukraa, H. Abid. "FP-LAPW calculations of ground state properties for AlN, GaN and InN compounds". J. Nanoelectronics and Materials. (2008).
- [18] A. Rani and R. Kumar. "Structural and electronic properties of GaAs and GaP semiconductors". Proceedings of International Conference on Condensed Matter Physics. (2014).
- [19] A. Rashid, S. J. Hashemifar, A. Hadi, A. Maqsood, A. Fazal. "Ab-initio study of structural and electronic properties of III-arsenide binary compounds". Computational Materials Science. 39, 580-586, (2007).
- [20] I.Vurgaftmana, J.R.Meyer, L.R.Ram-Mohan. "Band parameters for III–V compound semiconductors and their alloys". J. Appl. Phys. Vol 89. N°11, (2001).
- [21] B. Doumi, A. Tadjer, F. Dahmane, D. Mesri, H. Aourag. "Investigations of Structural, Electronic, and Half-metallic Ferromagnetic Properties in $(Al, Ga, In)_{1-x}M_xN$ ($M = Fe, Mn$) Diluted Magnetic Semiconductors". J. Supercond.Nov.Magn, 26, 515-525, (2013).
- [22] A. Alsaad, M. Bani Yassein, I. A. Qattan, A. A. Ahmad, S. Malkawi. "Structural and magnetic properties of MnN and ScN binaries and their ScN: Mn diluted magnetic semiconductors and $Mn_xSc_{1-x}N$ alloys". 405(5):1408-1414, (2010).
- [23] H. Ullah, K. Inayat, S.A. Khan, S. Mohammad, A. Ali, Z.A. Alahmed, A.H. Reshak, "First-principles calculation on dilute magnetic alloys in zinc blend crystal structure". Journal of Magnetism and Magnetic Materials, 385, 27-31 (2015).
- [24] E. Kulatov, H. Nakayama, H. Mariette, H. Ohta, Y.A. Uspenskii. "Electronic structure, magnetic ordering, and optical properties of GaN and GaAs doped with Mn". Phys. Rev. B 66, 045203, (2002).
- [25] L.M. Sandratskii, P. Bruno, J. Kudrnovsky. "On-site Coulomb interaction and the magnetism of $(GaMn)N$ and $(GaMn)As$ ". Phys. Rev. B 69,195203, (2004).
- [26] D. Khanin, S. Kulkova. "Electronic properties of III–V semiconductors". Russian Physics Journal, 48, 70, (2005).
- [27] M. Kaminska, A. Twardowski, D. Wasik. "Mn and other magnetic impurities in GaN and other III–V semiconductors – perspective for spintronics application". J. Mater. Sci: Mater. Electron. (19), 828-834 (2008).
- [28] S.J. Pearton, M.E. Overberg, G.T. Thaler, C.R. Abernathy, J. Kim, F. Ren, N. Theodoropoulou, A.F. Hebard, Y.D. Park. "Room temperature ferromagnetism in $GaMnN$ and $GaMnP$ ". Phys. Status Solidi A 195 222–227, (2003).
- [29] M.E. Overberg, K.H. Baik, G.T. Thaler, C.R. Abernathy, S.J. Pertion, J. Kelly, R. Rairigh, A.F. Hebard, W. Tang, M. Stavola, J.M. Zavada. "Hydrogenation Effects on Magnetic Properties of $GaMnP$ ". Electrochem Solid state Lett. 6 (2003) 131.

- [30] A. Boukra, A. Zaoui, and M. Ferhat. "Magnetic trends in $\text{Ga}_x\text{Mn}_{1-x}\text{N}$, $\text{Al}_x\text{Mn}_{1-x}\text{N}$ and $\text{In}_x\text{Mn}_{1-x}\text{N}$ ternary systems: A first-principles study". *J. Appl. Phys.* 108, 123904 (2010).
- [31] T. Ogawa, M. Shirai, N. Suzuki, I. Kitagawa. "First-principles calculations of electronic structures of diluted magnetic semiconductors (Ga,Mn)As". *J. Magn. Mater.* 196, 428–429, (1999).
- [32] M. Zhang, E. Bruk, F.R.D. Boer, G. Wu. "Half-metallic ferromagnetism in hypothetical wurtzite MBi (M=V, Cr, Mn)". *J. Appl. Phys.* 97, 10C306, (2005).
- [33] L. Adamowicz, M. Wierzbicki. "Symmetry induced half-metallic alkaline earth ferromagnetic". *Acta Phys. Pol. A* 115 217, (2009).
- [34] G.Y. Gao, K.L. Yao, E. Sasioglu, L.M. Sandratskii, Z.L. Liu, J.L. Jiang. "Half-metallic ferromagnetism in zinc-blende CaC, SrC, and BaC from first principles". *Phys. B* 75, 174442, (2007).

Conclusion

Spintronics is a discipline that offers a vast array of attractive possibilities for innovative and high-performance applications. One current technological barrier involves the injection of spin into III-V semiconductors, particularly GaN, GaP and GaAs. This project focuses on studying the structural, electronic and magnetic properties of GaX ($X = \text{N/P/As}$) doped with Mn for spintronics. Indeed, this material shows great potential as a ferromagnetic semiconductor for spintronic applications.

The PBE+E methodology was employed to analyze the GaX doped Mn series and compare the three compounds. It was found that the ground magnetic state corresponds to non-magnetism before doping, but after doping, the alloys exhibit a ferromagnetic phase across various concentrations of Mn. Additionally, electronic property analysis indicates that GaP and GaAs exhibit semi-metallic behavior at specific Mn concentrations, such as $\text{Ga}_{0.75}\text{Mn}_{0.25}\text{As}$, $\text{Ga}_{0.50}\text{Mn}_{0.50}\text{As}$ and $\text{Ga}_{0.75}\text{Mn}_{0.25}\text{P}$, whereas GaN displays complete metallic behavior at 0.25, 0.50 and 0.75 of Mn concentrations.

The main difference between GaP, GaAs and GaN lies in the hybridization of Mn-d orbitals. Specifically, Mn-d orbitals are extensively hybridized in the valence band of both GaP and GaAs. This does not exclude the presence of strong correlation effects, but their influence on the density of states is much less pronounced. Furthermore, the magnetic moments of Mn are closer to $4 \mu\text{B}$ for GaP and GaAs compared to GaN.

These findings provide valuable insights into the most common use of spintronics, which is in devices exploiting the properties of half-metallic behavior. Materials exhibiting half-metallic behavior, such as $\text{Ga}_{0.75}\text{Mn}_{0.25}\text{P}$, $\text{Ga}_{0.75}\text{Mn}_{0.25}\text{As}$, and $\text{Ga}_{0.50}\text{Mn}_{0.50}\text{As}$, conduct electricity like metals for one spin direction (typically spin-up) while acting as semiconductors for the other spin direction (typically spin-down). This property is crucial for the development of Magneto-Electronic Devices such as Spin Valves, Spin Filters, Spin Torque Oscillators (STOs), Spin-FETs (Spin Field-Effect Transistors) and Spin-Polarized Light Emitters used in magnetic storage devices like Hard Disk Drives (HDDs) and Magneto-resistive Random-Access Memory (MRAM). Additionally, these materials find application in the Zero Instruction-Set

Computing Processor (ZIP), High-Density Information storage (HDI) and Ferroelectric Random-Access Memory (FeRAM), among others. The unique properties of these half-metallic materials hold promise for enhancing the performance and functionality of such devices.

In contrast, while metallic behavior in spintronics, exemplified by materials like $\text{Ga}_{1-x}\text{Mn}_x\text{N}$ (with $x=0.25, 0.50,$ and 0.75), $\text{Ga}_{0.25}\text{Mn}_{0.75}\text{P}$, $\text{Ga}_{0.50}\text{Mn}_{0.50}\text{P}$, and $\text{Ga}_{0.25}\text{Mn}_{0.75}\text{As}$, can also find applications in certain devices such as Spin Transistors, Spin-Based Logic Devices, Spin-Polarized Current Sources and Spin Hall Effect Devices (SHE). However, its utilization is less common compared to half-metallic behavior due to the specific requirements of spin polarization and control in many spintronic applications. This disparity in utilization underscores the greater relevance of GaAs and GaP in spintronics compared to GaN.

INFLUENCE OF EXCHANGE AND CORRELATION INTERACTIONS ON THE SPIN POLARIZED ELECTRONIC STRUCTURE AND MAGNETIC PROPERTIES OF $\text{Ga}_{0.75}\text{Mn}_{0.25}\text{P}$ IN THE B3 ZINC BLENDE STRUCTURE

 **Noureddine Bouteldja**^{a*},  **Mohamed Belabbas**^b, **Rachid Taleb**^c

^a *Laboratoire de Physique Théorique et de Physique des Matériaux (LTPM), Faculty of Exact Sciences and Informatics, Hassiba Benbouali University of Chlef, Algeria*

^b *Department of Physics, Faculty of Exact Sciences and Informatics, Hassiba Benbouali University of Chlef, Algeria*

^c *Laboratoire Génie Electrique et Energies Renouvelables (LGEER), Faculty of Technology, Hassiba Benbouali University of Chlef, Algeria*

*Corresponding Author e-mail: n.bouteldja@univ-chlef.dz

Received November 8, 2023; revised December 11, 2023; accepted December 20, 2023

This study focuses on investigating the influence of exchange and correlation interactions on the spin polarized electronic structure and magnetic properties of $\text{Ga}_{0.75}\text{Mn}_{0.25}\text{P}$ in the B3 Zinc Blende phase. First-principle calculations were performed by systematically varying the Hartree-Fock (HF) exchange (α) value from 0 to 25% using the onsite exact-exchange functional for the treatment of the correlated electrons. The electronic and magnetic properties unveil that $\text{Ga}_{0.75}\text{Mn}_{0.25}\text{P}$ manifests a half-metallic ferromagnetic behaviour at deferent values of HF exchange. Moreover, as the fraction (α) parameter increases, the band gap increases, leading to modifications in the spin polarized band structures. Additionally, our investigations indicate that exchange and correlation interactions cause an increase in the lattice parameter and volume of the compound. Furthermore, these interactions result in a decrease in the magnetic moments of P and Ga atoms, while the Mn moments increase. These findings provide valuable insights into the behavior of $\text{Ga}_{0.75}\text{Mn}_{0.25}\text{P}$ and offer potential applications in the design of spintronic devices.

Keywords: *HF Exchange; Correlated electrons; GaMnP; Magnetic material; Half-metallic; Spintronic*

PACS: 31.15.eg, 75.50.-y, 81.05.Ea, 85.75.-d

INTRODUCTION

Diluted Magnetic Semiconductors (DMS) and spintronics (spin-based electronics) are two fascinating fields of research in semiconductor physics that intersect through the study of materials like III-V (GaX , InX , AlX ,..... $\text{X} = \text{As}$, P , N ,....) or II-VI (CdX , ZnX , MgX ,..... $\text{X} = \text{S}$, Se , Te ,....) doped with magnetic ions having a 3d layer or a 4f layer of transition metals or rare earths (lanthanides). These materials have gained considerable interest for their potential in spintronics applications.

Spintronics seeks to exploit the charge and spin of electrons for the development of new functionalities and devices. Diluted Magnetic Semiconductors, specifically, Mn-doped III-V compounds, offer unique features that allow for precise modulation of carrier spin dynamics, a crucial aspect for the advancement of spintronic devices [1]. One prominent application of these materials is in the field of Magnetic Random Access Memory (MRAM), where they enable efficient spin injection and manipulation [2]. Mn-doped III-V compounds have also found applications in magneto resistive sensors, such as Tunnelling Magneto-Resistance (TMR) and Giant Magneto-Resistance (GMR) sensors to detect and amplify magnetic fields [3,4]. They also hold promise for advanced mass storage devices like hard disks, as they allow for precise spin orientations manipulation and detection [5].

Researchers are actively investigating GaMnP's potential for spin injection, spin manipulation and spin detection, which are fundamental components of spintronic systems. This exploration is focused on establishing the connection between DMS materials and spintronics. S.J. Pearton et al., [6] synthesized ferromagnetic GaMnN and GaMnP compounds at high temperatures to prevent amorphization and enhance their magnetic properties. Iftibhar Ahmed et al., [7] used the FP-LAPW method to investigate the spin polarization of GaMnP and GaMnAs at $x = 0.125$. Y. Yuang et al., [8] examined the structural transport and magnetic properties of GaMnP with varying Mn concentrations using pulsed laser annealing (PLA) and ion implantation. A. Laref et al., [9] conducted calculations on hexagonal $\text{GaN}_{1-x}\text{P}_x$, revealing direct energy gaps and strong polarization dependence in their optical properties, making them promising for solar-cell applications. Z. Young-Zhi et al., [10] found room temperature ferromagnetism in GaAs and GaP compounds doped with V, Cr and Mn atoms at a concentration 25%. J. Mašek et al., [11] focused an investigation the electronic structure of Mn doped Ga(P,As) and (Ga,Al)As materials in the ferromagnetic state. W. Sukkabet., [12] studied magnetism in GaP with transition metal doping using spin density functional calculations. Co and Fe dopants transformed GaP into metal while V retained semiconducting with a reduced band gap. K. Kirandish et al., [13] explored the effect of the pressure on the properties of $\text{Ga}_{0.75}\text{Cr}_{0.25}\text{P}$ utilizing the SIESTA code (Spanish Initiative for Electronic Simulations with Thousands of Atoms). P. Mahadevan et al., [14] delved into the inherent mechanism of ferromagnetism in GaAs, GaP, GaN and GaSb diluted magnetic alloys with Mn substitution focusing on the analysis of the electronic structure trends. N Benbouchi et al., [15] applied spin-dependent density functional theory to study Co doping in GaP,

revealing that Co-doped GaP for spin-based electronic applications due to their complete half-metallic properties and integer total magnetic moments.

Exchange and correlation interactions exert a substantial effect on the distinct properties and behaviors of semiconductors. The exchange interaction reflects the tendency of electrons to align their spins. Meanwhile, the correlation interaction refers to the influence of electrons on each other, impacting the electronic structure and transport characteristics.

This paper investigates the impact of these interactions on the spin polarization of $\text{Ga}_{0.75}\text{Mn}_{0.25}\text{P}$ electronic structure and magnetic properties in the B3 Zinc Blende phase. The study utilizes the Density Functional Theory (DFT) with onsite exact-exchange functional, incorporation variations in the HF exchange parameter (α) ranging from 0 to 25%.

METHOD OF CALCULATIONS

The calculations were conducted utilizing the WIEN2k computer package, employing the FP-LAPW method (Full Potential Linearized Augmented Plane Wave) [16,17]. For spin polarized calculations, the PBE+E parameterization was used, which combines for the PBE (Perdew, Burke and Ernzerhof [18]) method with an onsite exact-exchange treatment for correlated electrons. This approximation effectively considered the exchange and correlation effect. The onsite exact-exchange energy expression as defined by Novák et al [19] can be represented as:

$$E_{XC}^{DFT+E} = E_{XC}^{DFT+E}[\rho] + (\alpha E_{XC}^{HF}[\varphi] - E_{XC}^{DFT}[\rho]). \quad (1)$$

Where (ρ) represents the electron density, (φ) denotes the wave function and (α) signifies the fraction of HF exchange, which can take on either a short-range or long-range value [20]. The long-range value of HF exchange up to 50% is required to obtain acceptable thermo chemistry for the Local Spin Density Approximation (LSDA) [21]. In the Generalized Gradient Approximation (GGA) of PBE, typically uses a short-range value of $\alpha=0.25$ it has been theoretically deduced and this choice has proven notable success [22,23].

The wave functions and potential are expanded using Muffin-tin approach with a cutoff $I_{\max} = 9$. For the Interstitial Region (IR), a cutoff $R_{\min} = 8$ is employed. The chosen cut-off energy is 10^{-3} Ryd which separates core states from valence states. For first-consistent results, 1000 k-points are used in the first Brillouin zone.

The crystal structure of $\text{Ga}_{0.75}\text{Mn}_{0.25}\text{P}$ was generated using eight atoms super cell with dimensions $1 \times 1 \times 1$. Specifically, the Mn atom replaced the Ga atom located at the position (0,0,0). The atomic spheres radii for Ga, Mn and P were set to 1.95, 1.99 and 1.55 respectively. The total energy was optimized by adjusting the volume of the super cell utilizing the Package of Two-Dimensional Optimize [24].

RESULTS AND DISCUSSION

Structural properties

To determine the ground state of the $\text{Ga}_{0.75}\text{Mn}_{0.25}\text{P}$ compound, The Murnaghan's equation of state [25] is employed for the purpose of fitting to calculate the total energy in term of its volume. This calculation is performed for ferromagnetic state using PBE+E approximation.

The resulting values for various structural parameters of $\text{Ga}_{0.75}\text{Mn}_{0.25}\text{P}$ such like the Lattice Parameter (LP), the Volume (V), the Bulk modulus (B), derivative of bulk modulus (B') and the Total Energy (E_{Tot}) show observable convergence with other data [26-28] presented in Table 1.

Table 1. Structural properties of $\text{Ga}_{0.75}\text{Mn}_{0.25}\text{P}$ at different values of HF exchange parameter (α)

| α | LP (Ang) | V (Ang ³) | B (GPa) | B' | E_{Tot} (Ryd) |
|-------------|-------------------------------|-----------------------|--------------------------------|-------------------------------|--|
| 0 | 5.493 5.49 ^[26] | 165.719 | 79.03 88.61 ^[26] | 4.894 4.68 ^[27] | -16718,973 -16718.97441 ^[28] |
| 0.05 | 5.571 | 172.882 | 76.86 | 4.487 | -16718,97859 |
| 0.10 | 5.629 | 178.364 | 53.64 | 5.257 | -16718,98954 |
| 0.15 | 5.690 | 184.301 | 67.58 | 5.201 | -16719,00784 |
| 0.20 | 5.787 | 193.854 | 70.18 | 4.733 | -16719,05385 |
| 0.25 | 5.854 | 200.687 | 82.46 | 5.051 | -16719,0992 |

Figure 1 demonstrates that as exchange and correlation interactions increase, both the LP and Volume of $\text{Ga}_{0.75}\text{Mn}_{0.25}\text{P}$ increase. This indicates significant influence of these interactions on the unit cell size. Specifically, exchange and correlation interactions directly affect the equilibrium positions of atoms and their bonding behavior within the unit cell, ultimately leading to an expansion of the unit cell size.

Figure 2 shows that increasing exchange and correlation interactions lead to a significant decrease in total energy of $\text{Ga}_{0.75}\text{Mn}_{0.25}\text{P}$. These interactions strongly influence the electronic properties by modifying the distribution and behavior of electrons, resulting in a pronounced reduction in total energy.

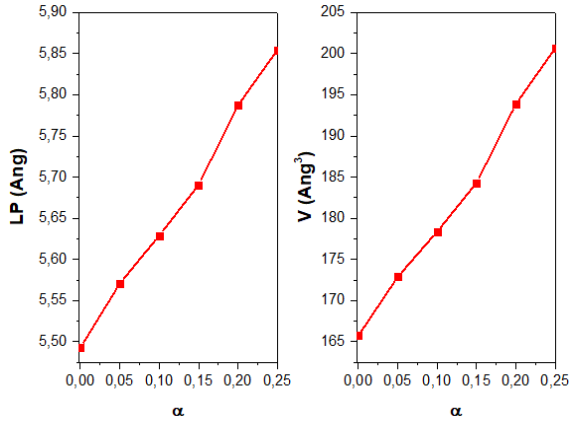


Figure 1. Influence of exchange and correlation interactions on lattice parameter (LP) and volume (V) of Ga_{0.75}Mn_{0.25}P

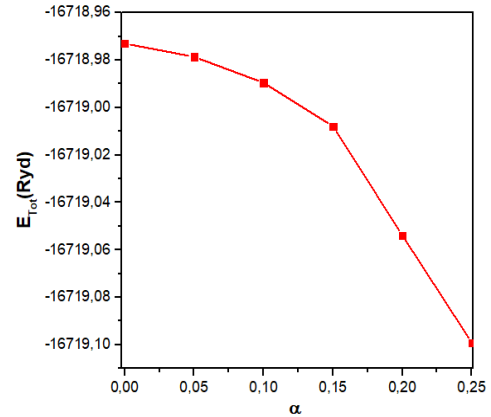


Figure 2. Influence of exchange and correlation interactions on total energy (E_{Tot}) of Ga_{0.75}Mn_{0.25}P

Electronic properties

The spin polarized band structures of Ga_{0.75}Mn_{0.25}P have been computed within the first Brillouin zone. Figure 3 depicts that the electrons in the spin up (\uparrow) state outnumber those in the spin down (\downarrow) state. There is a band gap present around the Fermi level (E_f) for spin down state, while a few valence bands in the spin up state intersect the Fermi level and transition into the conduction band. Consequently, based on the occurred interactions range of 0 to 25%, Ga_{0.75}Mn_{0.25}P compound is predicted to exhibit metallic behavior for spin up state and semiconductor behavior for the spin down state. Further investigation indicates that this compound is a half metallic ferromagnetic material.

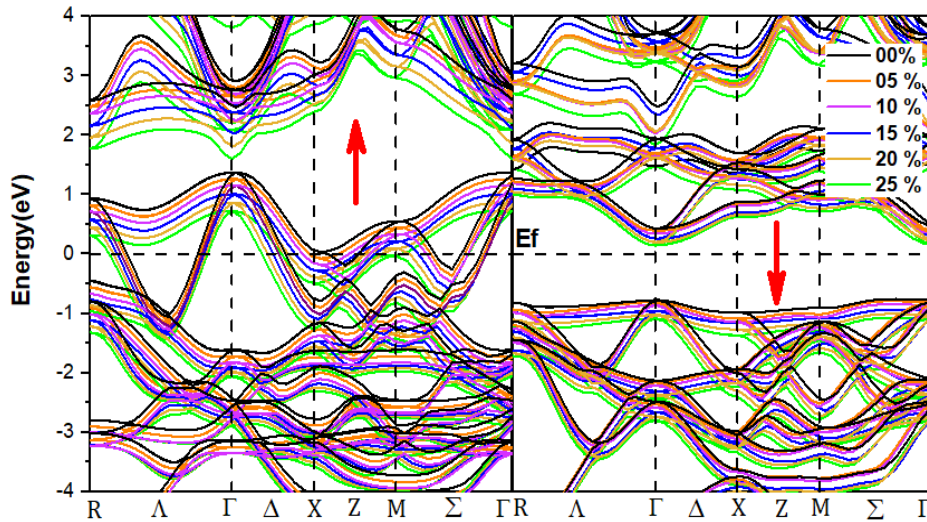


Figure 3. Influence of exchange and correlation interactions on spin polarized band structures of Ga_{0.75}Mn_{0.25}P

In the Figure 4, the calculated band structures highlight a noticeable increase in the forbidden energy gap (E_g) for spin down state. This increase is attributed to significant changes in the maximum of the conduction band and the minimum of the valence band, resulting from the increasing exchange and correlation interactions.

The calculated electronic properties are summarized in Table 2, it includes conduction band minimum of spin down state and spin up state ($E_{CBM}^{up}, E_{dn}^{CBM}$), valence band maximum of spin down state and spin up state ($E_{VBM}^{up}, E_{dn}^{VBM}$), the band edge spin splitting (ΔE_c) for the conduction band minimum and the band edge spin splitting (ΔE_v) for the valence band maximum are determined using specific formulas:

$$\Delta E_c = E_{CBM}^{up} - E_{dn}^{CBM}, \quad (2)$$

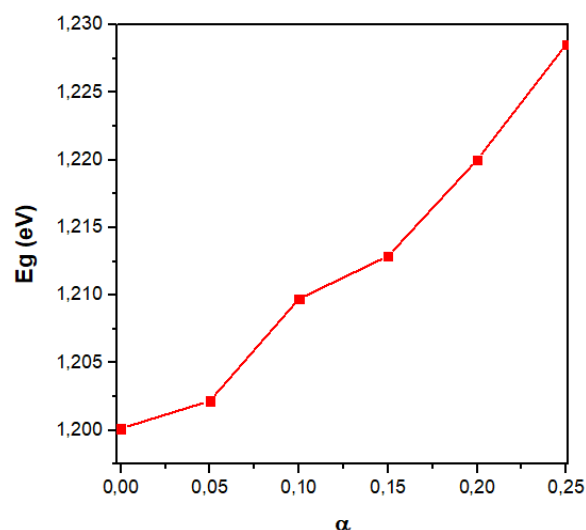
$$\Delta E_v = E_{VBM}^{up} - E_{dn}^{VBM}. \quad (3)$$

These formulas are commonly used to analyze band structure and determine various properties of electronic states at (Γ) symmetry point.

In the Figure 4, the calculated band structures highlight a noticeable increase in the forbidden energy gap (E_g) for spin down state. This increase is attributed to significant changes in the maximum of the conduction band and the minimum of the valence band, resulting from the increasing exchange and correlation interactions.

Table 2. Electronic properties of $\text{Ga}_{0.75}\text{Mn}_{0.25}\text{P}$ at different values of HF exchange parameter (α)

| α | 0 | 0.05 | 0.10 | 0.15 | 0.20 | 0.25 |
|-----------------------------------|---------------------------------|----------|----------|----------|----------|----------|
| E_{gdn} (eV) | 1.20013 1.20 ^[28] | 1,20218 | 1,20973 | 1.21289 | 1,22001 | 1,22857 |
| $E_{\text{VBM}}^{\text{up}}$ (eV) | 0 | 0 | 0 | 0 | 0 | 0 |
| $E_{\text{dn}}^{\text{VBM}}$ (eV) | -0,77277 | -0,80629 | -0.86033 | -0,95136 | -1,02482 | -1.08531 |
| $E_{\text{CBM}}^{\text{up}}$ (eV) | 0 | 0 | 0 | 0 | 0 | 0 |
| $E_{\text{dn}}^{\text{CBM}}$ (eV) | 0,42736 | 0,39589 | 0.3494 | 0,26153 | 0,19519 | 0.14326 |
| ΔE_{v} (eV) | 0,77277 | 0,80629 | 0.86033 | 0,95136 | 1,02482 | 1.08531 |
| ΔE_{c} (eV) | -0,42736 | -0,39589 | -0.3494 | -0,26153 | -0,19519 | -0.14326 |

**Figure 4.** Influence of exchange and correlation interactions on band gap energy (E_{g}) of $\text{Ga}_{0.75}\text{Mn}_{0.25}\text{P}$

Magnetic properties

Upon substituting Ga atoms with Mn in GaP, the resulting GaMnP compound exhibits magnetic properties attributed to Mn-3d. The coupling between the 3d orbital of Mn and the 3p orbital of P atoms results in the emergence of small local magnetic moments in both Ga and P atoms. Notably, for $\text{Ga}_{0.75}\text{Mn}_{0.25}\text{P}$, the local magnetic moment of P exhibits a negative value, indicating an anti-parallel alignment with the Mn spin, whereas the positive value observed on Ga signifies a parallel alignment.

Figure 5 illustrates the variation of the both local and total magnetic moments of $\text{Ga}_{0.75}\text{Mn}_{0.25}\text{P}$ under the influence of exchange and correlation interactions. As the interactions increase, the total magnetic moment remains constant at 4.00 μ_{B} . Nonetheless, the magnetic moment of Mn atom increases, whereas the local magnetic moments at P and Ga atoms decrease. These findings are in agreement with other data [29] presented in Table 3.

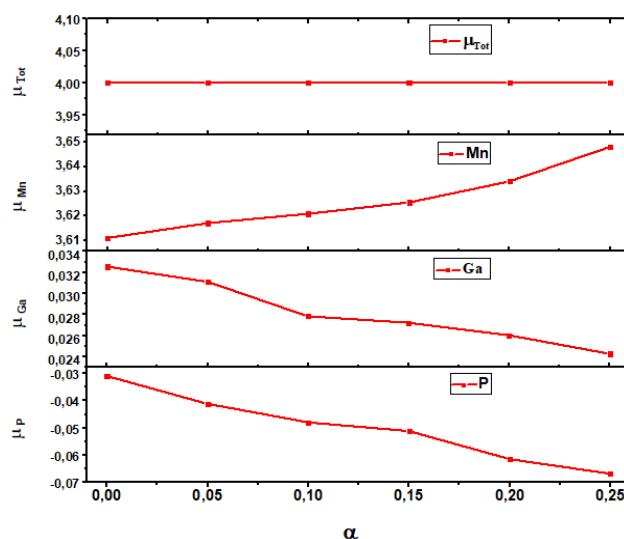
**Figure 5.** Influence of exchange and correlation interactions on magnetic moment μ_{Tot} , μ_{Mn} , μ_{Ga} and μ_{P} of $\text{Ga}_{0.75}\text{Mn}_{0.25}\text{P}$.

Table 3. Magnetic properties of Ga_{0.75}Mn_{0.25}P at different values of HF exchange parameter (α)

| α | μ_{Mn} (μB) | μ_{Ga} (μB) | μ_P (μB) | μ_{Tot} (μB) |
|----------|----------------------------------|----------------------------------|------------------------------------|---------------------------------|
| 0 | 3,61121 3,382 ^[29] | 0,03255 0,023 ^[29] | -0,03091 -0,039 ^[29] | 4,00042 4,05 ^[29] |
| 0.05 | 3,61718 | 0,03112 | -0,04114 | 4,00068 |
| 0.10 | 3,62101 | 0,02784 | -0,0479 | 4,00068 |
| 0.15 | 3,62559 | 0,02723 | -0,05113 | 4,00068 |
| 0.20 | 3,63412 | 0,02603 | -0,06142 | 4,00068 |
| 0.25 | 3,64813 | 0,02428 | -0,06673 | 4,00068 |

CONCLUSIONS

The interactions studied affect the structural properties of Ga_{0.75}Mn_{0.25}P by increasing the lattice parameter and volume, and decreasing the total energy. The electronic structures show a downward shift of the valence and conduction bands, resulting in an increased band gap. The compounds exhibit half metallic ferromagnetism within the range of 0 to 25% of HF exchange. The magnetic properties indicate a noteworthy phenomenon in which the coupling between the 3d orbital of Mn and the 3p orbital of P atoms induces local magnetic moments in the Ga and P atoms. Moreover, as the interactions strength intensifies, the magnetic moment of Mn atom increases, while it decreases on Ga and P atoms. However, it is important to note that despite these changes, the total magnetic moment remains unchanged.

ORCID

©Noureddine Bouteldja, <https://orcid.org/0000-0002-9356-7238>; ©Mohamed Belabbas, <https://orcid.org/0000-0003-1325-8011>

REFERENCES

- [1] G. Zho, Z. Deng, and C. Jin, Journal of semiconductors, **40**(8), 081505 (2019). <https://doi.org/10.1088/1674-4926/40/8/081505>
- [2] I.A. Iusipova, Semiconductors, **52**, 1982 (2018). <https://doi.org/10.1134/S10637826181>
- [3] A. Doll, S. Lecurieux-Lafayette, J. Moulin, C. Chopin, G. Jasmin-Lebras, M. Pannetier-Lecoer, A. Solignac, and C. Fermon, Proc. SPIE, Spintronics XII, **11090**, 110903M, 146 (2019). <https://doi.org/10.1117/12.2529246>
- [4] M. Oogane, K. Fujiwara, A. Kanno, T. Nakano, H. Wagatsuma, T. Arimoto, and S. Mizukami, Applied Physics Express, **14**(12), 123002 (2021). <https://doi.org/10.35848/1882-0786/ac3809>
- [5] Z. Guo, J. Yin, Y. Bin, D. Zhu, K. Shi, G. Wang, K. Cao, and W. Zho, Proceedings of the IEEE, **109**(8), 1398 (2021). <https://doi.org/10.1109/JPROC.2021.3084997>
- [6] S.J. Pearton, M.E. Overberg, G.T. Thaler, C.R. Abernathy, J. Kim, F. Ren, and N. Theodoropoulou, Physica Status Solidi (a), **195**(1), 222 (2003). <https://doi.org/10.1002/pssa.200306283>
- [7] I. Ahmad, and B. Amin, Computational Materials Science, **68**, 55 (2013). <https://doi.org/10.1016/j.commatsci.2012.07.037>
- [8] Y. Yang, Y. Wang, M. Khalid, K. Gao, S. Prucnal, O.D. Gordan, and G. Salvan, IEEE Transactions on Magnetics, **50**(11), 1 (2014). <https://doi.org/10.1109/TMAG.2014.2322332>
- [9] A. Laref, Z. Hussain, S. Laref, J.T. Yang, Y.C. Xiong, and S.J. Luo, Journal of Physics and Chemistry of Solids, **115**, 355 (2018). <https://doi.org/10.1016/j.jpcs.2017.12.002>
- [10] Z. Young-Zhi, and H. Mei-Chun, Chinese Physics Letters, **21**(8), 1632 (2004). <https://doi.org/10.1088/0256-307X/21/8/061>
- [11] J. Mašek, J. Kudrnovský, F. Máca, J. Sinova, A.H. MacDonald, R.P. Campion, B.L. Gallagher, and T. Jungwirth, Physical Review B, **75**(4), 045202 (2007). <https://doi.org/10.1103/PhysRevB.75.045202>
- [12] W. Sukkabot, Chemical Physics, **523**, 57 (2019). <https://doi.org/10.1016/j.chemphys.2019.04.007>
- [13] K. Kaur, and S. Sharma, in: *Proceedings of the International Conference on integrated interdisciplinary. Innovations in Engineering*, (Panjab, India, 2020), pp. 1033.
- [14] P. Mahandevan, and A. Zunger, Applied Physics Letters, **85**(14), 2860 (2004). <https://doi.org/10.1063/1.1799245>
- [15] N. Benbouchi, E.A. Mohammed-Mounir, F.Z. Dahou, A. Bahnes, and A. Laref, Results in Physics, **24**, 104118 (2021). <https://doi.org/10.1016/j.rinp.2021.104118>
- [16] P. Blaha, K. Schwarz, G.K.H. Madsen, D. Kvasnicka, and J. Luitz, in: *WIEN2K. An Augmented Plane Wave Plus Local Orbitals Program for Calculating Crystal Properties*, edited by K. Schwarz (Techn. Universität Wien, Austria, 2001).
- [17] F. Tran, P. Blaha, K. Schwarz and P. Novák, Physical Review B, **74**(15), 155108 (2006). <https://doi.org/10.1103/PhysRevB.74.155108>
- [18] J.P. Perdew, K. Burke, and M. Ernzerhof, Physical Review Letters, **77**(18), 3865 (1996). <https://doi.org/10.1103/PhysRevLett.77.3865>
- [19] P. Novák, J. Kuneš, L. Chaput, and W.E. Pickett, Physica Status Solidi (b), **243**(3), 563 (2006). <https://doi.org/10.1002/pssb.200541371>
- [20] O.A. Vydrov, J. Heyd, A.V. Krukau, and G.E. Scuseria, The Journal of Chemical Physics, **125**(7) (2006). <https://doi.org/10.1063/1.2244560>
- [21] A.D. Becke, The Journal of Chemical Physics, **98**(2), 1372 (1993). <https://doi.org/10.1063/1.464304>
- [22] M. Ernzerhof, and G. E. Scuseria, The Journal of Chemical Physics, **110**(11), 5029 (1999). <https://doi.org/10.1063/1.478401>
- [23] C. Adamo, and V. Barone, The Journal of Chemical Physics, **110**(13), 6158 (1999). <https://doi.org/10.1063/1.478522>
- [24] A.H. Reshak, and M. Jamal, Journal of Alloys and Compounds, **555**, 362 (2013). <https://doi.org/10.1016/j.jallcom.2012.12.028>
- [25] F.D. Murnaghan, Proceeding of National Academy of Sciences, **30**(9), 244 (1944). <https://doi.org/10.1073/pnas.30.9.244>

- [26] K. Kaur, and A. Rani, Applied Physics A, **123**(12), 791 (2017). <https://doi.org/10.1007/s00339-017-1398-z>
- [27] B. Doumi, A. Mokaddem, A. Sayede, M. Boutab, A. Tadjer, and F. Dahmane, Journal of Superconductivity and Novel Magnetism, **28**, 3163 (2015). <https://doi.org/10.1007/S10948-015-3148-9>
- [28] H. Ullah, K. Inayat, S.A. Khan, S. Mohammad, A. Ali, Z.A. Alahmed, and A.H. Reshak, Journal of Magnetism and Magnetic Materials, **385**, 27 (2015). <https://doi.org/10.1016/j.jmmm.2015.02.069>
- [29] A. Djedid, B. Doumi, S. Méçabih, and B. Abbar, Journal of Materials Science, **48**, 6074 (2013). <https://doi.org/10.1007/s10853-013-7405-7>

ВПЛИВ ОБМІННОЇ ТА КОРЕЛЯЦІЙНОЇ ВЗАЄМОДІЇ НА СПІНОВУ ПОЛЯРИЗОВАНУ ЕЛЕКТРОННУ СТРУКТУРУ ТА МАГНІТНІ ВЛАСТИВОСТІ $Ga_{0.75}Mn_{0.25}P$ У СТРУКТУРІ ЦИНКОВОЇ ОБМАНКИ ВЗ

Нуреддін Бутелджа^a, Мохамед Белаббас^b, Рашид Талеб^c

^a *Лабораторія теоретичної фізики та фізики матеріалів (LTPM), Факультет точних наук та інформатики, Університет Хасіба Бенбуалі, Члефі, Алжир*

^b *Кафедра фізики, Факультет точних наук та інформатики, Університет Хасіба Бенбуалі, Члефі, Алжир*

^c *Лабораторія електротехніки та відновлюваної енергії (LGEER), Технологічний факультет, Університет Хасіба Бенбуалі, Члефі, Алжир*

Це дослідження зосереджено на вивченні впливу обмінних і кореляційних взаємодій на спін-поляризовану електронну структуру та магнітні властивості $Ga_{0.75}Mn_{0.25}P$ у фазі ВЗ Zinc Blende. Розрахунки першого принципу були виконані шляхом систематичної зміни значення обміну Хартрі-Фока (HF) (α) від 0 до 25% з використанням локального функціоналу точного обміну для обрахунку поведінки корельованих електронів. Електронні та магнітні властивості показують, що $Ga_{0.75}Mn_{0.25}P$ демонструє напівметалеву феромагнітну поведінку при різних значеннях HF-обміну. Крім того, зі збільшенням параметра фракції (α) ширина забороненої зони збільшується, що призводить до модифікацій у спін-поляризованих зонах структурах. Крім того, наші дослідження показують, що обмінні та кореляційні взаємодії викликають збільшення параметра решітки та об'єму сполуки. Крім того, ці взаємодії призводять до зменшення магнітних моментів атомів P і Ga, тоді як моменти Mn збільшуються. Ці висновки дають цінну інформацію про поведінку $Ga_{0.75}Mn_{0.25}P$ для потенційних застосувань в дизайні спінтронних пристроїв.

Ключові слова: ВЧ-обмін; корельовані електрони; GaMnP; магнітний матеріал; напівметалічний; спінтроніка